INVESTIGATION OF PROTOPORPHYRIN IX AND COPPER CYSTEAMINE NANOPARTICLES TO IMPROVE CURRENT CANCER TREATMENT METHODS

By

LALIT CHUDAL

Presented to the Faculty of the Graduate School of

The University of Texas at Arlington in Partial Fulfillment

of the Requirements for the Degree of

DOCTOR OF PHILOSOPHY

THE UNIVERSITY OF TEXAS AT ARLINGTON

August 2020

Supervising Committee:

Dr. Wei Chen, Supervising Professor

Dr. Alexander Weiss

Dr. Zui Pan

Dr. Mingwu Jin

Dr. Yujie Chi

Dedicated to:

My parents Bhanu Bhakta and Laxmi Devi

ACKNOWLEDGMENTS

I would like to thank my advisor, Dr. Wei Chen, for his support throughout my dissertation work. This work would not have been possible without his guidance, support, and patience.

I would also like to thank Dr. Alex Weiss, Dr. Zui Pan, Dr. Mingwu Jin, and Dr. Yujie Chi for taking their time to serve as a committee member in my defense, Dr. Michael Antosh (The University of Rhodes Island) for agreeing to collaborate in one of the dissertation projects, and all current and past lab members of the Nano-Bio Physics lab for direct or indirect contribution to achieving my research goals.

I would like to express the most profound gratitude towards my parents Bhanu Bhakta Chudal and Laxmi Devi Chudal, who motivated and guided me in the right direction since childhood. Thanks to my brothers Ramesh, Sanjeev, Naresh, and Sudip, who always supported me throughout my academic journey. I want to thank all the teachers who taught me through class 1 to M.Sc. in Nepal. Finally, without the support of my wife, Anusha, this journey would be arduous. She was always there to drive me with positive energy at difficult times and to celebrate at good times. Finally, I want to thank my kids Aadesh and Aarya, for being a constant source of motivation in this journey.

July 22, 2020

ABSTRACT

INVESTIGATION OF PROTOPORPHYRIN IX AND COPPER CYSTEAMINE NANOPARTICLES TO IMPROVE CURRENT CANCER TREATMENT METHODS

Lalit Chudal, Ph.D.

The University of Texas at Arlington, 2020

This research is focused on using nanotechnology to improve current cancer treatment methods, particularly photodynamic therapy and chemotherapy. Photodynamic therapy, being a local treatment method with low systemic toxicity, has a great deal of potential for cancer treatment. However, due to the lack of oxygen (hypoxia) in the tumor microenvironment and PDT's intrinsic dependence on oxygen to generate reactive oxygen species, the performance of PDT severely affected in solid tumors. Accordingly, we fabricated a nano-platform that can supply oxygen in cancer cells and subsequently improve the PDT under hypoxic conditions. Protoporphyrin IX, an FDA approved sensitizer, was encapsulated into a liposomal bilayer, and the liposomal surface was coated with MnO_2 nanoparticles, which can generate a sufficient level of oxygen by reacting with elevated levels of H_2O_2 in cancer cells. The nanosystem was well characterized and successfully demonstrated to enhance PDT efficacy by alleviating tumor hypoxia.

Another disadvantage of photodynamic therapy is the occurrence of phototoxic effects in PDT treated patients for a prolonged period, particularly if exposed to bright light. This phenomenon can be attributed to the fact that the traditional photosensitizers are easily activatable by visible

light. Accordingly, new types of sensitizers that are free of phototoxic effects are desirable. One of the most promising ways to achieve this goal is to develop the sensitizers that are activatable by excitation sources other than visible light. Copper cysteamine nanoparticle that is invented by our group in 2014 meets this criterion as it can be activated by UV light, X-ray, microwave, and ultrasound but not by visible light. Therefore, we anticipate Cu-Cy NPs to have very low phototoxicity due to sunlight irradiation. To validate this hypothesis, a systematic study was conducted to compare the phototoxic effect of Cu-Cy NPs with an FDA approved photosensitizer. The result demonstrated that Cu-Cy NPs caused minimal phototoxic effects when compared to the Protoporphyrin IX, an FDA approved photosensitizer.

Current chemotherapeutic drugs lack selectivity, leading to a number of side effects. Fabricating tumor microenvironment responsive drugs is a reliable approach to improve the current chemotherapy for cancer treatment. Due to the existence of Cu^{1+} on its surface, Cu-Cy NPs may be an excellent heterogeneous Fenton-like catalyst for cancer treatment. Considering the elevated level of H_2O_2 and low pH conditions, Cu-Cy may produce a significantly higher level of ROS in tumor cell and microenvironment, thereby causing a highly selective cancer-killing effect. Therefore, the third part of this dissertation explores Cu-Cy NPs as a heterogeneous Fenton-like catalyst for highly selective cancer treatment. The result demonstrated that, with IC-50 value of 11 µg/mL (lowest among reported heterogeneous Fenton system) and high selectivity index of 4.5 against cancer cells. Overall, Cu-Cy NPs could be a highly selective chemodynamic drug with low systemic toxicity.

Lalit Chudal, PhD

The University of Texas at Arlington, 2020

Table of Contents

Contents

LIST OF FIGURES

luminescence of the assay in cobalt chloride treated cells indicates the successful induction of hypoxia. (Scale bar: 50 μm).

Figure 2.9 Study of PDT effect of PPIX-Lipo and PPIX-Lipo-M under (a) normoxia, (b) hypoxia, and (c)IC-50.

Figure S2.1 MnO_2 nanoparticles disintegrate in the presence of GSH or H_2O_2.

Figure S2.2 Photoluminescence of PPIX-Lipo with or without 3mM GSH. There is no change in intensity, showing that GSH does not react with PPIX-Lipo.

Figure S2.3 Change in PL intensity of PPIX-Lipo and PPIX-Lipo-M in the presence of 100 μM H_2O_2. The change in PL intensity was expressed as a ratio with corresponding initial PL intensity. PL intensity of PPIX-Lipo decreases over time while PPIX-Lipo-M decreases initially and then start to increase. The increase in PL intensity could be due to the disintegration of MnO_2 by H_2O_2 and hence regain in initially quenched luminescence.

Figure S2.4 Cellular uptake of bare PPIX mixed in DI water. Large PPIX aggregates can be seen on the top of cells indicating that naked PPIX has poor cellular uptake. Scale bar: 50μM

Figure S2.5 Confocal imaging to confirm cellular uptake of PPIX-Lipo into MCF7 cell lines. A. bright-field image B. merged image of HOECHT and PPIX Channel. C. Merged image of HOECHT (blue), PPIX(red), and brightfield image. D. 3D image showing PPIX inside the MCF7 cell lines. Scale bar: 25μm

Figure 3.1 (A) Absorption and (B) photoluminescence (Excitation wavelength = 420 nm and Emission wavelength= 630 nm) spectra of PPIX.

Figure 3.2 Absorption and photoluminescence spectra (excitation wavelength = 365 nm, emission wavelength= 607 nm) of copper cysteamine nanoparticles.

Figure 3.3 (A) Evaluation of dark toxicity and (B) sunlight toxicity of Cu-Cy and PPIX towards healthy cell lines (HDF and HET1A) using MTT assay.

Figure 3.4 Evaluation of dark toxicity of Cu-Cy and PPIX towards HET1A and HDF using Live/Dead assay. Green color represents calcein-positive (live cells), and the red color represents Ethidium homodimer-1 (dead cells). (scale bar= 100 μM).

Figure 3.5 Evaluation of sunlight toxicity of Cu-Cy and PPIX using Live/Dead assay. Green and red colors represent live and dead cells, respectively. (Scale bar =100 μM)

Figure 4.1 (A) Absorption spectrum of Cu-Cy NPs dispersed in DI water. (B) Photoluminescence spectra of Cu-Cy with excitation and emission peaks taken at 365 nm and 607 nm, respectively. (C) Image of Cu-Cy dispersed in DI water under ambient light (Left) and UV light (Right). (D) XRD pattern of Cu-Cy powders. (E) HRTEM image of Cu-Cy NPs. (F) A representative TEM image of Cu-Cy NPs used in this study.

Figure 4.2 Measurement of hydroxyl radical generated by Cu-Cy/H_2O_2 using coumarin as a probe. The $^{\bullet}OH$ produced by (A) Cu-Cy (0-300 µg/mL) and H_2O_2 (100 µM) and (B) Cu-Cy (100 µg/mL) and (0-1mM H_2O_2) at various time intervals. (C) The $^{\bullet}OH$ generated by Cu-Cy (100 µg/mL)+ H_2O_2 (100 µM) at different pH conditions and (D) statistical analysis of $^{\bullet}OH$ production after 6h of (C).

Figure 4.3 Stability test of Cu-Cy following the Fenton-like reaction. (A) The PL intensity change of Cu-Cy following the incubation with H_2O_2 up to 24 h. (B) Free Cu^{2+} detected in the supernatant of the Cu-Cy (1 mg/ mL) following the incubation with H_2O_2 (100 µM) up to 24 h. (C) FTIR spectra and (D) XRD patterns of Cu-Cy before and after Fenton-like reaction for 24 h.

Figure 4.4 Intracellular $^{\bullet}OH$ detection using DCFH-DA. (A) Representative images (B) Quantification of ROS level. The cells pre-incubated with or without Cu-Cy for 12h were treated with 20 µM DCFH-DA for 1 h. The green luminescence of DCF was imaged using a 495/515 nm filter of Olympus IX-71 and quantified using imageJ. (* $p< 0.01$)

Figure 4.5 Oxygen consumption rate assay of **(A)** HET1A **(B)** KYSE-30 at various concentrations of Cu-Cy (0-45 mg/L). **(C-D)** Normalized **(C)** ATP and **(D)** Basal respiration at various concentrations of Cu-Cy. Normalization was done with respect to control (without Cu-Cy). * $p< 0.05$ ** $p<0.01$.

Figure 4.6 Live/dead assay to assess the toxicity of Cu-Cy to cancer (DM6 and KYSE-30) and normal (HDF and HET1A) cell lines: Green and red channels are from calcein-AM (Live) and Ethidium homodimer (Dead), respectively. **(B)** Quantification for the cell viability and early apoptosis using imageJ. **(C)** Bright-field imaging to observe morphological changes of the Cu-Cy (15 µg/mL) treated normal and cancer cell lines: **(a)** HET1A, **(b)** HDF, **(c)** KYSE-30, and **(d)** DM6. Scale bar: 100 µm.

Figure 4.7 Evaluation of cytotoxicity of Cu-Cy to different cell lines using MTT assay. (A) Cell viability of different cell lines with Cu-Cy treatment. (B) IC-50 value of Cu-Cy towards normal and cancerous cells. (* $p < 0.05$, ** $p < 0.01$)

Figure 4.8 Schematic of Cu-Cy mediated Fenton-like reaction for selective cancer treatment. Cu-Cy NPs can undergo Fenton-like reaction with overproduced H_2O_2 in cancer cells resulting in ROS levels that is above the safe ROS level, causing cell death. On the other hand, owing to the lower level of H_2O_2, Cu-Cy is harmless to normal cells.

Figure S4.1 Hydroxyl radical(·OH)measurement using coumarin as a probe. The PLspectraof coumarin monitored after 6h of the reaction with the mixture of **(A)** various doses(0-300µg/mL) of Cu-Cywith100 µMH_2O_2. **(B)**Various doses of H_2O_2(10µM-1mM) with Cu-Cy(100 µg/mL),and **(C)**Cu-Cy(100 µg/mL) andH_2O_2(100 µM).The excitation wavelength was 332 nm.

Figure S4.2 Figure S2. A spectrophotometric method to detect free Cu^{2+} in aqueous solution. A calibration curve was obtained using $CuCl_2.2H_2O$ as a source of free Cu^{2+}. Inset shows the calibrated equation to determine the free Cu^{2+} concentration in an aqueous solution.

Figure S4.3 Intracellular ROS measurement in MCF-7 cell lines using DCFH-DA. FL-intensity of DCF on MCF-7 cell lines incubated (A) without Cu-Cy (control), (B) with Cu-Cy (30 µg/ mL) for 12 h, and (C) quantification of DCF intensity using imageJ. (*) indicates $p<0.01$.

Figure S4.4 (A) Cell viability of different cell lines with Cu-Cy treatment. (B) Cell viability and IC-50 value of MCF-7 cell line.

Figure S4.5 Oxygen consumption rate assay on Cu-Cy treated DM6 cell line. (A) OCR spectra, (B) basal respiration rate, and (C) ATP turnover rate with respect to the control (without Cu-Cy). (D) Comparison of proton-leak of HET1A, KYSE-30, and DM6 cell lines.

Figure S4.6: Flow-chart for Live/dead assay quantification using ImageJ.

Chapter:1

INTRODUCTION

Cancer is the second major leading cause of death in the United States.[1] Estimated 1,762,450 new cancer cases and 606,880 cancer deaths were projected to occur in the United States in 2019.[1] Although death rates of most cancer types are dropping in the past years, overall cancer-related deaths are on the rise each year. [1,2] Major clinical cancer treatment options include surgery, chemotherapy, and radiotherapy. However, most of the conventional cancer drugs lack selectivity, leading to the toxic effects on healthy cells resulting in many side effects. Several novel approaches have been explored to find new and safe treatment modalities in the past decade.

1.1. PHOTODYNAMIC THERAPY: DEFINITION

Photodynamic therapy (PDT) refers to a suitable combination of light, photosensitizer, and oxygen to destroy the tumor by generating highly reactive oxygen species.[3] PDT can be used either on its own or as a complementary to chemotherapy or radiotherapy.[4] The three essential components components of PDT are light, photosensitizer, and oxygen. None of these are individually toxic, but together they initiate series of photochemical reaction that generates a highly reactive products, namely singlet oxygen ($^1O_2$) and other reactive oxygen species (ROS) such as superoxide anion, hydroxyl radical, hydrogn peroxide etc. The ROS can produce significant toxicity leading to cell death via apoptosis or necrosis [4–6]. PDT has some notable advantages over traditional cancer treatment modalities: (1) PDT uses combinations of light, photosensitizers, and oxygen to produce reactive oxygen species. The photosensitizer is ideally non-toxic in the absence of light, ensuring lower systemic toxicity. (2) Being a localized treatment, PDT has fewer side effects than chemotherapy. (3) Furthermore, unlike surgery, PDT is a non-

invasive cancer treatment modality. (4) PDT needs the light of a low dose to activate the photosensitizer; therefore, it is unlikely to cause the occurrence of secondary cancer, which is one of the main concerns of existing radiotherapy.

A typical PDT carried out in multiple steps, as illustrated in **Figure 1**. In the first step, a photosensitizer is injected and then allowed them to accumulate in the tumor for a few hours. Then, the tumor site is illuminated with light of a suitable wavelength to destroy the tumor.

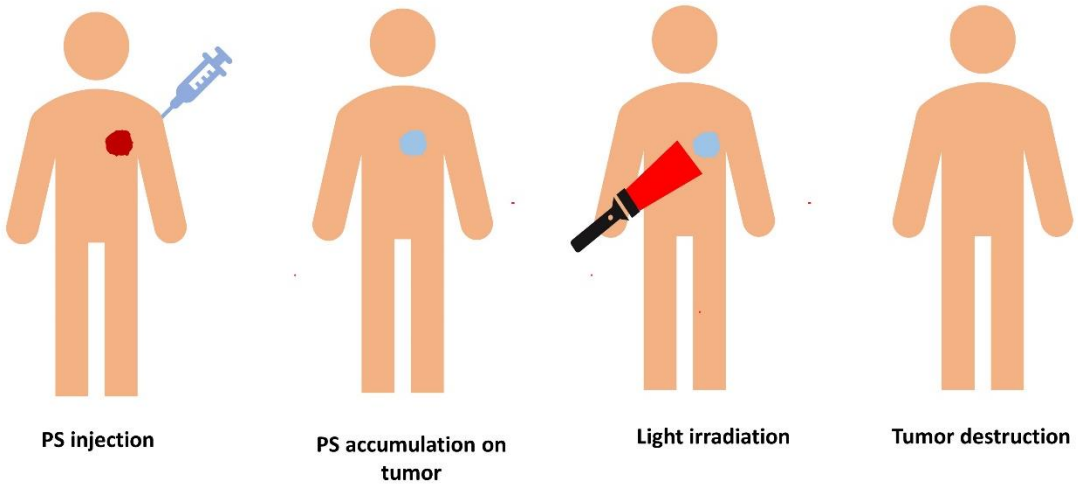

Figure 1. Schematic of photodynamic therapy representing various steps involved in photodynamic therapy.

1.2. A BRIEF HISTORY OF PHOTODYNAMIC THERAPY

In Indian and eastern cultures, light has been used for medicinal purposes since ancient times. In fact, the sun is worshipped as a god in eastern culture, such as Indian culture and Greek culture. In the late 19th century, Finsen used light therapy for the treatment of Ricketts and was awarded Nobel prize in 1903. In the meantime, Oscar Raab, a medical student, discovered that the paramecia killing ability of eosin positively depend upon the light intensity.[7] This is the first

time that light was found to activate a molecule, thereby leading to the discovery of photosensitizer. The Nobel prize-winning work by Fisher in the early 20th century investigated the roles of certain components of blood, called porphyria, for the occurrence of a skin disease porphyria.[8] His work, for the first time, shed light on the possibility of porphyrin as a photosensitizer but was not realized in practice explicitly at that time. During the 1950-60s, Schwartz et al. investigated hematoporphyrin as a potential sensitizer for radiation therapy.[9] The result showed that porphyrin might increase tumor destruction ability of X-ray radiation alone.

Modern photodynamic therapy was born when Thomas Dougherty, also referred to as the father of photodynamic therapy, observed the photodynamic activity of fluorescein while working as a chemist in Roswell Park Cancer Institute.[10] He was responsible for developing dyes and investigating their radiation toxicity in cancer cells. He was advised to protect the dye treated tumor cells from light, as the light used to kill tumor cells before the radiation was given. Out of curiosity, he intentionally exposed fluorescein diacetate treated tumor cells to light and observed that most of the cells were dead. Later, he investigated the photodynamic activity of hematoporphyrin. However, it was impure and less efficient due to which leads to its failure in the clinical trial due to safety concerns.[10] Doughtery obtained a pure form of porphyrin by using chromatography and patented under the name of Photofrin®, which was subsequently approved by the FDA as a first-ever photosensitizer.[10] The photofrin®, also called the first-generation photosensitizer, has approvals in several countries, including the USA, Japan, Canada, for the treatments of esophageal cancer, prostate cancer, and some skin cancers.[11,12] Photofrin can remain in the body for over two months, and patients are required to avoid bright light for several weeks after the treatment.[13,14] Some other problems associated with photofrins are its tendency

to accumulate both in healthy cells and cancerous cells, slow clearance rate, and poor sensitivity.[12] Then, researchers focused on finding new photosensitizers with better purity, longer excitation wavelengths, selectivity, and sensitivity. Some of the FDA approved photosensitizers developed over the last couple of decades Motexafin lutetium, Temoporfin, Palladium bacteriopheophohorbide, porphyrin, Veteporfin, and PPIX precursors.

Temoporfin (Foscan; Biolitec) is a second-generation photosensitizing agent used for the treatment of head, neck, breast, and pancreatic cancer (**Figure 3**). [15–19] Foscan can be excited at 652 nm (longer wavelength as compared to 633 nm of Photofrin) and therefore has better efficacy owing to higher penetration. Furthermore, 0.1-0.15 mg/kg was an effective dose for Foscan in contrast to 2-5 mg/kg for photofrin. In addition, the phototoxicity issue is much shorter (4 weeks) as compared to several months for Photofrin.

Lutex (Motexafin Lutetium, Phamacyclics Inc) is a porphyrin-based second-generation photosensitizer. The Lutex has activation wavelength in the range 730 - 750 nm, and a phase I clinical trial for prostate cancer treatment was completed in 2008. The results revealed that 2 mg/kg dose was very effective for prostate cancer treatment. Motexafin-Gadolinium, a metal complex of Motexafin, was investigated as a potent radiosensitizer for the treatment of brain and lung cancer. However, a phase II clinical trial for the treatment of brain cancer on children failed on account of its failure to improve the survival of the patients.[20]

Palladium bacteriopheoporbide, also called Tookad, is another second-generation PS used in the treatment of prostate cancer (See **Figure 3** for its structure) . [21,22] This drug, with an excitation wavelength of 762 nm, targets vasculature of tumors rather than tumors directly. Tookad was used in a clinical trial for low-risk prostate cancer treatment. [21,22] The phase I-III clinical results revealed that Tookad has rapid clearance from the body leading to minimal systemic toxicity.

Furthermore, the treatment was well tolerated by the body keeping the urinary function, erectile function, and bowel movement intact. [21,22] Besides, Tookad also showed reduced photosensitivity as compared to other porphyrin-based photosensitizers.[21,23] Despite apparent success in clinical trials, Tookad failed to receive FDA approval.

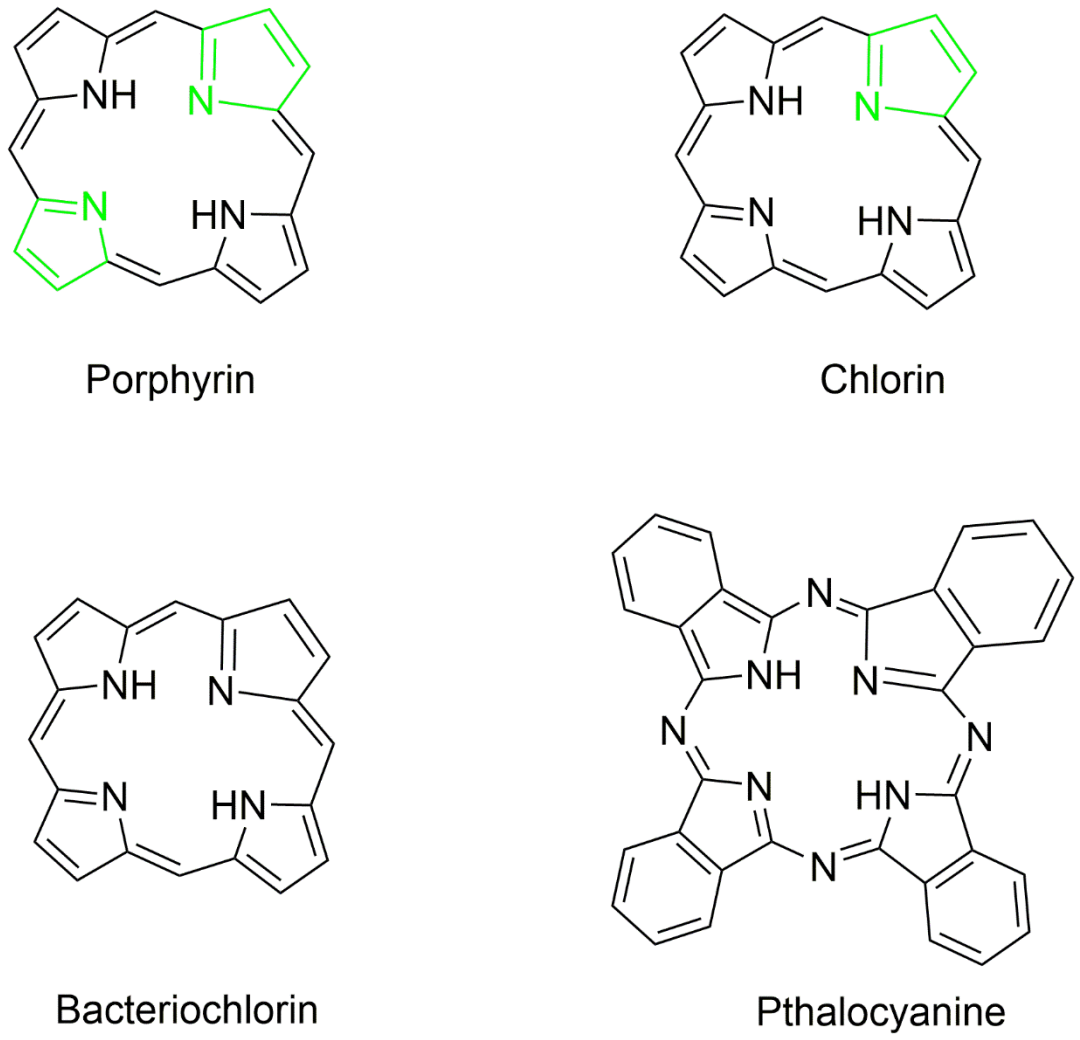

Figure 2 : Structures of a) Porphyrin (Exi: 407 nm, Emi: 620 nm), b) Chlorin (Exi:405 nm, Emi 670 nm), c) Bacteriochlorin (Exi 374 nm, Emi 795 nm), d) Phthalocyanine (Exi: 635 nm, Emi: 700 nm).

5-Aminolevulinic acid (ALA) is a second-generation photosensitizer that converts into PPIX endogenously. The US FDA has approved ALA induced PPIX for non-oncological treatment of

actinic keratosis in 1999.[24] It has also shown potential for PDT treatment to some other diseases including Bowen's disease and basal cell carcinoma.[25,26]

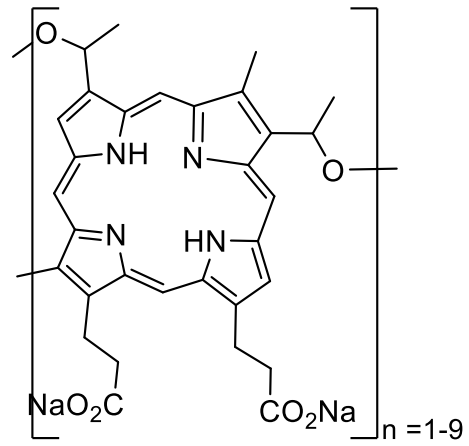

Photofrin

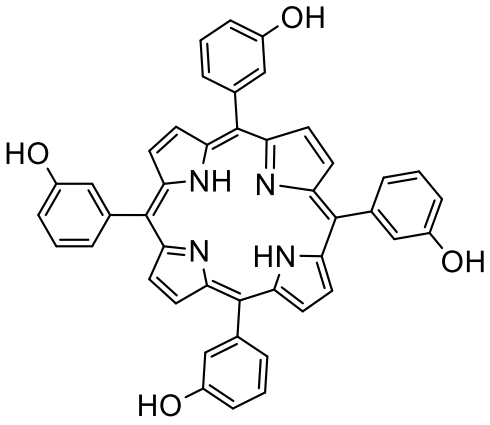

Foscan

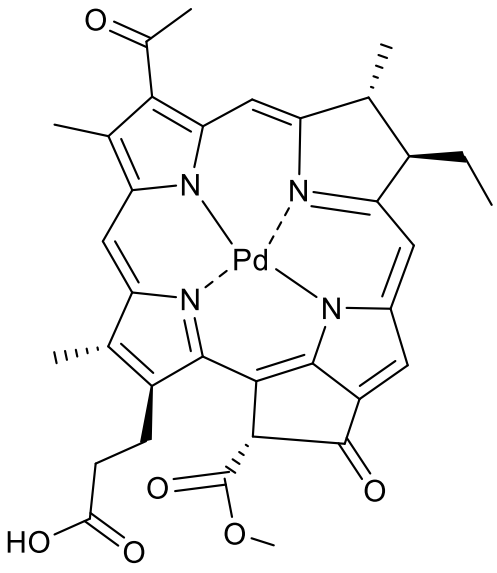

Tookad

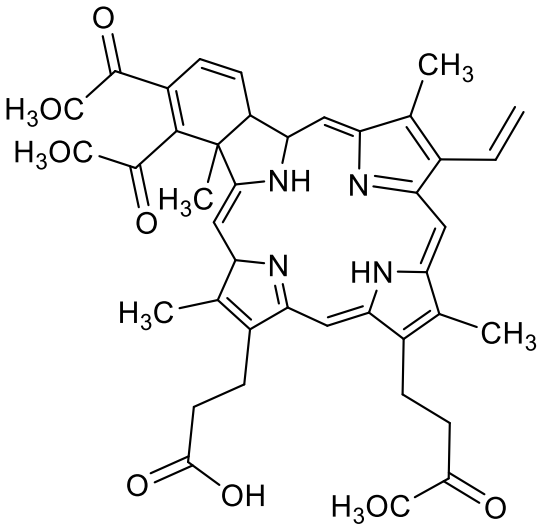

Visudyne

Figure 3 Structures of (a) Photofrin (b) Foscan (c) Bacteriochlorin (d) Phthalocyanine.

1.3. MECHANISM OF PHOTODYNAMIC THERAPY

In the typical photodynamic process, sensitizer absorbs light of a suitable wavelength and get excited from the ground state to the first excited state (S_1). The S_1 then undergoes intersystem crossing to the long-lived triplet state (T_1). The excited T_1 state then undergoes two types of reactions: type 1 and type 2.

1.3.1. Type 1 reaction

The excited sensitizer can undergo an electron transfer with an adjacent sensitizer molecule. The resultant molecule can react with molecular oxygen to produce reactive oxygen species such as superoxide anion, hydrogen peroxide, and hydroxyl radical.[25] The detailed reaction scheme is presented below.

$^3PS^* + {}^1PS \rightarrow PS^{-\bullet} + PS^{+\bullet}$

$^3PS^* + D \rightarrow PS^{-\bullet} + D^+$

$PS^- + O_2 \rightarrow {}^1PS + O_2^{-\bullet}$

$^3PS^* + O_2 \rightarrow O_2 + H_2O_2$

$2O_2^{-\bullet} + 2H^+ \rightarrow PS^{-*} + PS^{+*}$

$^3PS^* + {}^1PS \rightarrow PS^{-*} + PS^{+*}$

$Fe^{3+} + O_2^{-\bullet} \rightarrow Fe^{2+} + O_2$

$Fe^{2+} + H_2O_2 \rightarrow O_2 + OH^- + OH^{\bullet}$

1.3.2. Type 2 reaction

The energy from T_1 transferred to molecular oxygen to convert it to singlet oxygen, as presented below. An important condition for Type 2 reaction is that both of the reactants must be in the triplet state. The condition is easily met as molecular oxygen is in the triplet state.[25,27]

$^3PS^* + {}^3O_2 \rightarrow {}^1PS + {}^1O_2$

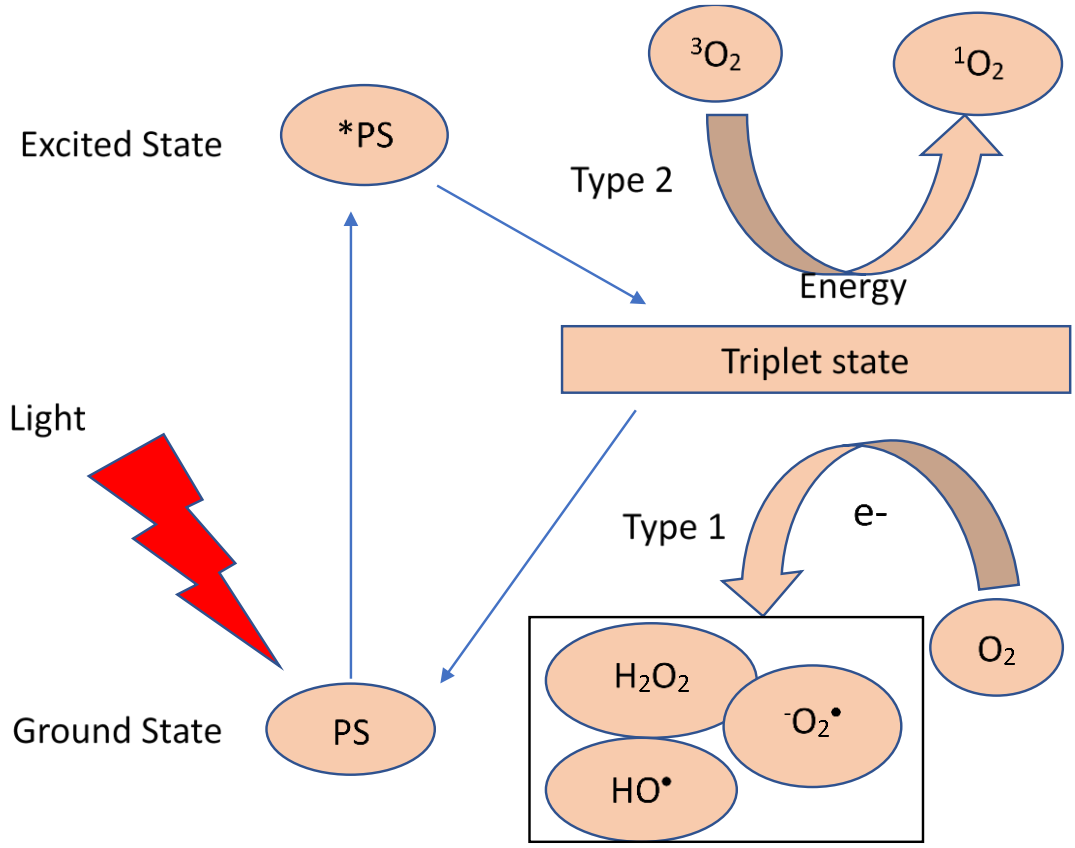

Figure 2. Schematic presentation of photosensitization mechanism.

1.4. LIMITATIONS OF PHOTODYNAMIC THERAPY

1.4.1. Tumor hypoxia

One of the major limitations of PDT originates from its intrinsic dependence on molecular oxygen to produce reactive oxygen species. The lack of oxygen, also called hypoxia, in tumor microenvironments (TMEs) leads to less than optimal performance of PDT. It has also been

reported that hypoxia in solid tumor cells leads to reduced radiotherapy efficacy.[28] The median oxygen levels in healthy cells lie between 40-60 mmHg, whereas they are in the range of 5-10 mmHg in tumor cells [29]. Therefore, it is essential to design smart strategies to supply adequate oxygen to improve the PDT efficacy in the hypoxic tumor microenvironment. Developing a tumor microenvironment's stimuli-responsive oxygen generating nanosystem is the central theme of current research in the area. It is well known that most tumor cells and microenvironments are characterized by the elevated level of H_2O_2 as a result of the Warburg effect.[30,31] In this direction, many nanosystems consisting of an oxygen supplying agent and a photosensitizer were fabricated and explored for their potential in combating tumor hypoxia both in vitro and in vivo.[32–35] In particular, researchers exploited the catalase that can convert H_2O_2 into O_2 or red blood cells (RBC) as natural oxygen supplier to develop catalase-based [36] or RBC based [32,37] nanosystems to combat tumor hypoxia.

Recently, MnO_2 involved smart strategies are drawing a great deal of attention owing to their catalase-like activity and biocompatibility.[38–42] MnO2 can convert H_2O_2 into O_2 under slightly acidic pH, cancer-specific conditions. Due to this reason, a nano-platform that consists of an FDA approved sensitizer (Protoporphyrin IX) encapsulated into the bilayer of liposome and then coated with MnO_2 nanoparticles by physical mixing.[43] The detailed investigation will be presented in chapter 2.

1.4.2. Issue of Photosensitivity

Unwanted photosensitivity is another major disadvantage of photosensitizer used in photodynamic therapy. [14,44–46] Since conventional photosensitizer is excitable by the full visible wavelength spectrum, PDT treated patients may experience severe photosensitivity for a considerable amount

of time following the treatment. The photosensitizers take up to several weeks to get cleared from the body and can accumulate in superficial organs, such as underneath dermal skin layers and eyes for a prolonged period. Accordingly, PDT treated patients are strongly recommended to avoid sunlight exposure for few weeks after the treatment. However, reports suggested that, despite the compliance with the guidance by the hospital, a significant number of patients experience the phototoxic effects.[14,47] The extent and length of photosensitivity influenced by drugs being used and varies patients to patients depending upon several factors, such as age, sex, skin color, etc.

Photofrin, the first-generation photosensitizer with approval in the USA and many other countries, is reported to cause cutaneous photosensitivity that can last up to 3 months.[48–50]. A significant level of photosensitivity issue has also been reported in Foscan, a second-generation photosensitizer, for a prolonged period. [45,50] Although some improvements have been reported in more recent sensitizers, photosensitivity remains as one of the limitations of photodynamic therapy.[44] Besides, photosensitivity is not only the problem of photosensitizers but also of many other drugs[51], demanding the detailed evaluation of phototoxicity of any new drugs. As an example, in-vivo experiments showed that topically administered hypericin acetate showed mild phototoxicity in mice.[52]

The primary mechanism responsible for photosensitivity is the ROS-mediated damage of vital cell organelles, including lipid, DNA, and protein. Alternatively, the formation of a stable photo-adduct between DNA and photosensitizer could be responsible for observed phototoxicity.[53] The common symptoms of phototoxicity are pain, edema, burn, and painful blistering.

In 2014, our lab invented copper-cysteamine nanoparticles that are activatable with various excitation sources such as X-ray,[54–58] MW,[59,60], ultrasound,[61] UV light,[62,63] and acidic pH/H_2O_2 (cancer-specific condition).[64] Unlike traditional photosensitizers that have multiple excitation wavelengths in the UV-NIR region, the Cu-Cy NPs have a single photoluminescence excitation peak at 365 nm. Due to this reason, we anticipated that Cu-Cy NPs are new photosensitizers with low sunlight toxicity. In the third chapter of this dissertation, a detailed investigation will be carried out to compare photosensitivity of Cu-Cy NPs to an FDA approved photosensitizer (Protoporphyrin IX).

1.5. CHEMOTHERAPY AND ITS LIMITATIONS

Chemotherapy is the second line of cancer treatment method after surgery. However, chemotherapeutic drugs suffer from various side effects due to lack of targetability, specific accumulation, and responsiveness towards cancer-specific biomarkers. Therefore, the primary focus of current cancer research is to develop highly targeted and selective drugs that are safe and yet effective in treating cancer. Fabricating drugs that are responsive to tumor or tumor microenvironment specific stimuli is one of the most effective ways to improve the selectivity of cancer drugs.[65,66] Hypoxia,[29] mild acidity,[67] elevated level of H_2O_2,[30] reduced catalase activity,[31] and elevated levels of GSH[68] are major hallmarks of the tumor microenvironment (TME). The unique TME, despite its roles in tumor proliferation and metastasis, can be exploited to develop efficient and highly selective cancer treatment methods. In fact, in the past few years, several cancer treatment modalities that can respond to the unique TME have been reported.[43,65,66,69,70] Nanomaterials are touted as next-generation cancer medicine on account of their numerous advantages over existing chemotherapeutic drugs.[71–74] In particular, nanoparticles can be programmed to selectively accumulate in tumors and avoid multi-drug

resistance to yield safe and yet effective treatment options over existing chemotherapeutics. Nanoparticles based platforms are primarily explored as a drug carrier for remote-controlled delivery.[73,74] Few nanocarriers have already received FDA approval and believed to improve the pharmacokinetics and thereby to improve the overall performance of the existing chemotherapeutic drugs such as doxorubicin.

Copper and its complexes have been studied extensively as an anti-cancer and anti-microbial agent.[75] Cu is an essential element to our body and helps in various metabolism. Moreover, Cu plays an important role in scavenging free radical superoxide catalase.[76,77] However, defect in Cu homeostasis is believed to produce various health hazards, especially in liver and brain functions.[76] Therefore, care should be taken while designing Cu-based nanoparticles to ensure the effective dose is at a safe level. It is desirable to design efficient Cu complexes so that even in its safe limits, Cu- complexes produce a desirable result.

Fenton reaction was first proposed in 1894 by H.J.H. Fenton [78]. He was first to report that ferrous ions strongly promote the oxidation of maleic acid by H_2O_2. He later suggested that a mixture of ferrous salts and H_2O_2 was an effective oxidant of various organic compounds. The Fenton reaction was assigned specific to ferrous salts and H_2O_2, whereas the reaction of H_2O_2 and other cations such as Fe^{3+}, Co^{2+}, Cu^{2+}, Fe^{2+} are called “Fenton-like reaction”. [79] Fenton based reactions are in wide use for wastewater treatment. In recent years, many researchers are investigating the possibility of Fenton and Fenton-like reactions for cancer treatment.[80,81] Mainly Fe and Fe-based systems are being investigated extensively for cancer therapy. However, Fe based Fenton reaction proceeds efficiently only at pH 2-3, which is physiologically irrelevant, and hence realization of Fe based Fenton therapy in cancer treatment seems almost impossible. On the other hand, Cu based Fenton-like reaction is physiologically more relevant than the Fe-based Fenton

reaction as Cu induced Fenton like reaction can proceeds efficiently in the circumneutral pH range (pH= 5-7).[82] In recent years, several copper-based Fenton-like systems have been reported for the cancer treatment both in vitro and in vivo. [83–87] It has been reported that Cu^{1+} has a 22 times faster reaction rate with H_2O_2 than that of Cu^{2+}. Unfortunately, as Cu^{1+} has a natural tendency to oxidize, most of the current Cu-based Fenton system exists in Cu^{2+}, leading to poor efficiency and therefore requires a higher dose for efficient performance. In this direction, we synthesized copper-cysteamine nanoparticles having Cu^{1+} instead of Cu^{2+} and investigated it for Fenton-reaction facilitated highly selective cancer treatment. Owing to the faster reaction rate of Cu^{1+} with H_2O_2, we anticipated Cu-Cy to be capable of generating substantial levels of •OH by reacting with endogenous H_2O_2 of cancerous cells and kill them with high selectivity. In the fourth chapter of this dissertation, a recently published study on Cu-Cy NPs as a heterogeneous Fenton-like catalyst for a selective cancer treatment method is presented.[64]

Chapter 2:
(Published in Material Science and Engineering C)

INVESTIGATION OF PPIX-LIPO-MnO_2 TO ENHANCE PHOTODYNAMIC THERAPY BY IMPROVING TUMOR HYPOXIA

Lalit Chudal[1], Nil Kanatha Pandey[1], Jonathan Phan[1], Omar Johnson[1], Xiuying Li[2], Wei Chen[1]*

1 Nano-Biophysics Lab, Department of Physics, University of Texas at Arlington, TX 76019, USA

2 Department of Mechanical Engineering, University of Texas at Dallas, TX, 75080, USA

**Corresponding author:* weichen@uta.edu

The author has permission to use in the dissertation.

Chudal L, Pandey NK, Phan J, Johnson O, Li X, Chen W. Investigation of PPIX-Lipo-MnO2 to enhance photodynamic therapy by improving tumor hypoxia. Materials Science and Engineering: C. 2019 Nov 1;104:109979.

ABSTRACT

The efficacy of photodynamic therapy (PDT) is reduced in the context of hypoxic environments. This is problematic, considering that hypoxia is exhibited in the vast majority of malignant tumors. Thus, increasing the concentration of oxygen in malignant tumors improves PDT treatment outcomes. Studies show that MnO_2 nanoparticles can produce oxygen when it reacts with endogenous H_2O_2. Herein, we encapsulated Protoporphyrin IX (PPIX) in the liposome bilayer (PPIX-Lipo), which was then coated with MnO_2 nanoparticles to construct PPIX-Lipo-MnO_2 (PPIX-Lipo-M) in order to enhance PDT efficacy under tumor hypoxia. The PDT results show that PPIX-Lipo-M was more cytotoxic to breast cancer cells than PPIX-Lipo while under hypoxic conditions, indicating that the production of oxygen gas in hypoxic conditions improved treatment outcomes. Upon encapsulating PPIX into the liposome, the aqueous solubility of PPIX significantly improved. Consequently, the cellular uptake of both PPIX-Lipo and PPIX-Lipo-M also increased significantly compared to that of bare PPIX. Overall, PPIX-Lipo-M has the capacity to act as a therapeutic agent that relieves hypoxia and hence improve PDT efficacy.

Keywords:

Photodynamic Therapy, Protoporphyrin IX, MnO_2, Liposome, Hypoxia, Normoxia, Nanoparticles, Cobalt Chloride, MTT Assay

2.1. INTRODUCTION

Photodynamic therapy (PDT) is a promising cancer treatment modality that can be used either on its own, or in addition to radiotherapy or chemotherapy[4]. PDT consists of three essential components: a photosensitizer, light and oxygen. When applied in conjunction to one another, they

initiate a photochemical reaction with oxygen that generate highly reactive products called singlet oxygen ($^1O_2$), along with other reactive oxygen species (ROS). ROS can cause significant cytotoxicity upon reaching an intracellular threshold concentration that leads to cell death via apoptosis or necrosis.[4–6] Light has extremely poor penetration, and therefore photodynamic therapy is unsuitable for deeply seated cancers. In this direction, considerable progress has been made in recent years. For instance, our group has recently reported a radio-photosensitizer that can be activated not only by UV light,[55,62] but also by X-rays,[55,88] microwaves,[60] and ultrasound.[61]

Most tumors suffer from a lack of oxygen (hypoxia). It has been reported that a lack of dissolved oxygen in tumor cells may be responsible for poor radiotherapy efficacy.[28] The median values of partial oxygen pressure in normal cells lie between 40 mm to 60 mmHg, whereas in tumor cells, they are less than 10 mmHg.[29] To enhance the PDT efficacy, it is necessary to develop effective strategies to supply adequate oxygen to reduce hypoxia.

Recently, MnO_2 involved strategies have been extensively investigated to combat the problem of hypoxia.[38,42,89,90] Two important characteristics MnO_2 possess to enhance the PDT effect of photosensitizers are: 1) high specificity and reactivity toward H_2O_2, producing O_2 and H_2O while simultaneously consuming protons[38] and 2) effectively reduce glutathione levels in the cancerous cells.[91] Due to these reasons, MnO_2 stands as an excellent candidate to improve the tumor hypoxia conditions for PDT.

Protoporphyrin IX (PPIX) is an FDA approved photosensitizer with the ability to accumulate in tumors.[25,92,93] Because of its amphiphilic nature, PPIX aggregates in the aqueous environment either via π-π stacking or intermolecular interactions between hydrophilic -COOH groups and the hydrophobic porphyrin core.[93] It has been shown that the aqueous solubility of the PPIX could

be improved by conjugating it to APTES[15] and poly(styrene-co- 4 vinyl pyridine).[94] However, naked PPIX might lead to unwanted toxicity; liposomes, on the other hand, offer improved biocompatibility[95–97] and are an accepted vehicle for drug delivery.[98–101] It can also be further functionalized to add targetability and controlled release.[102–104]

In the present study, we designed a liposome based nanosystem to combat tumor hypoxia for PDT. Initially, to construct this system, we encapsulated water insoluble PPIX into liposomes (PPIX-Lipo) to improve biocompatibility and drug delivery. Then, the PPIX-Lipo was reacted with MnO_2 coated with bovine serum albumin (BSA) to fabricate a PPIX-Lipo-MnO_2 (PPIX-Lipo-M) nanosystem. As-synthesized PPIX-Lipo and PPIX-Lipo-M were not only highly soluble in aqueous media, but also improved PDT by increasing the oxygen level in cancer cells.

2.2. MATERIAL AND METHODS

2.2.1. Materials

Cholesterol (Chol) and Dipalmitoyl phosphatidylcholine (DPPC) were bought from Avanti polar lipids. PPIX, $KMnO_4$, 3-(4,5-Dimethylthiazol-2-Yl)-2,5-Diphenyltetrazolium Bromide (MTT assay), 4′,6-diamidino-2-phenylindole (HOECHST), Tetrahydrofuran and chloroform were bought from Sigma-Aldrich. A singlet oxygen green sensor (SOSG) was purchased from Invitrogen. An ROS-ID hypoxia assay was bought from Enzo-life sciences. The MCF-7 cell lines were purchased from ATTC (American Type Culture Collection) and grown in RPMI 1640 culture medium supplemented with 100 units/mL aqueous penicillin G, 100 µg/mL streptomycin, and 10 % fetal bovine serum.

2.2.2. Synthesis of PPIX-Lipo, BSA-MnO_2, and PPIX-Lipo-M

PPIX was encapsulated inside DPPC/Chol liposomes by using a lipid film hydration method.[27] 50 mg/mL DPPC in chloroform, 7 mg/mL Chol in chloroform, and 1 mg/mL PPIX solution in tetrahydrofuran (THF) were separately prepared. Then, 200 µL of the DPPC solution, 100 µL of the Chol solution, and 250 µL of the PPIX solution were mixed. The mixture was vortexed for about 1 minute to mix it homogeneously. The mixture was dried to a thin lipid film under a high vacuum using a rotatory evaporator for 2 hours. The thus-formed thin film was hydrated with DI water at 55 °C rotating at 150 rpm for 1 hour. In each 10-minute intervals of rotation, the mixture was vortexed for 1 minute to facilitate the liposome formation. The as-synthesized PPIX-Lipo was then stored in a fridge at 4 °C overnight to allow the completion of liposome formation. Unencapsulated PPIX was removed by allowing it to precipitate overnight. Unreacted chemicals were then removed by washing with DI water 3 times. The PPIX-Lipo was then sonicated for 15 minutes to obtain nano-sized liposomes. The as-synthesized PPIX-Lipo was stored in a fridge protected from light with aluminum foil until further use.

BSA-coated MnO_2 (here after MnO_2) was prepared using a previously reported method with minor modifications.[105] Briefly, 9 mg $KMnO_4$ was dispersed in 3 mL 1X PBS and stirred for 5 minutes. 50 mg BSA was dispersed in 3 mL of PBS and stirred for 20 minutes. Then, the $KMnO_4$ solution was added dropwise to the BSA solution and stirred for 2 hours at 37 °C. The obtained MnO_2 was purified by dialysis using a dialysis bag of 12 kDa cutoff molecular weight against DI water for 24 hours. Purified MnO_2 was stored at 4 °C for further use. As-synthesized MnO_2 was highly soluble and stable in aqueous media for several weeks.

MnO_2 was coated onto the liposome surface via physical interactions. PPIX-Lipo and MnO2 were mixed at a respective molar ratio 1:50, and moderately stirred for 3 hours at room temperature.

During the mixing process, the mixing flask was covered with aluminum foil to protect the mixture protected from incoming light.

2.2.3. Particle Size Analysis

The particle size distribution of MnO_2, PPIX-Lipo, and PPIX-Lipo-M were evaluated by a dynamic light scattering (DLS) method, using a ZetaPALS zeta potential analyzer (Brookhaven Instruments Inc., Holtsville, NY, USA). The morphological characteristics of particles were evaluated by a transmission electron microscope (TEM).

2.2.4. Absorption and Photoluminescence Measurement

The absorption and photoluminescence (PL) spectra were measured using a Shimadzu UV-2450 UV-Vis spectrophotometer and a Shimadzu RF-5301PC luminescence spectrophotometer, respectively. To measure absorption and the PL spectrum of MnO_2, PPIX-Lipo and PPIX-Lipo-M, samples were prepared in DI water such that both PPIX-Lipo and PPIX-Lipo-M had an equal concentration of PPIX, and both PPIX-Lipo-M and MnO_2 had an equal concentration of MnO_2. Typically, PPIX-Lipo and PPIX-Lipo-M had 3 μM PPIX. In PPIX-Lipo-M, the ratio of PPIX and MnO_2 was 1:50 for all further experiments.

To demonstrate that MnO_2 adsorbed onto the liposome surface luminescence quenching of PPIX in PPIX-Lipo-M with respect to PPIX-Lipo and the regain in luminescence following the addition of 3 mM glutathione (GSH) was measured. Photobleaching of PPIX-Lipo and PPIX-Lipo-M was measured after 5 minutes of UV-light exposure three times. The relative change in luminescence was plotted with UV-light treatment time.

2.2.5. Drug Loading Efficiency

To determine the encapslation efficiency of PPIX into liposomes, the luminescence of PPIX dissolved in DMSO was measured at various concentrations and a calibration curve was established by plotting the integrated PL intensity against its concentration. 2.8 mL of DMSO was added to 200 µL of PPIX-Lipo to disrupt the liposomes, and the PL integrated intensity was measured and plotted against corresponding concentration. The loading efficiency was calculated in percentage by comparing the slope of PPIX and PPIX-Lipo dissolved in DMSO.

2.2.6. In-vitro pH Measurement

To demonstrate that our nanosystem can react with H_2O_2 under acidic conditions, we measured the change in pH of acidic solutions. First, 100 µM H_2O_2 was dispersed in pH = 5.6 (HCl solution). Then, MnO_2 was added to the solution. The pH change was monitored in each 1 minute intervals by using a digital pH meter.

2.2.7. Singlet Oxygen Generation Measurement

Singlet oxygen produced by PPIX-Lipo and PPIX-Lipo-M with and without 100 µM H_2O_2 were measured in PBS (pH=7.4) buffers. The singlet oxygen green sensor (SOSG) was used as a luminescence-based singlet oxygen probe. UV light was excited for 5 minutes interval for 5 times, and luminescence intensity was monitored after each excitation. Integrated PL intensity was calculated at each concentration and plotted against the concentration.

2.2.8. Cellular Uptake Experiment

200,000 cells were cultured in a 35 mm petri-dish and incubated for 24 hours to allow cell attachment. Naked PPIX, PPIX-Lipo, and PPIX-Lipo-M were added and incubated for 24 hours. Old media were replenished with new media having 1 µM HOECHST dye to stain the nucleus. The Olympus IX71 fluorescence microscope was used to image the cells. Default DAPI filter (Emi/Exi at 457 nm/350 nm) was used to image the HOECHST dye, while PPIX was imaged using a Emi/Exi 617 nm/403 nm filter. Cellular uptake of PPIX-Lipo and PPIX-Lipo-M was confirmed by merging the HOECHST and PPIX channel.

2.2.9. Cell Viability Study

Cell viability or dark toxicity of the MnO_2, PPIX-Lipo, and PPIX-Lipo-M was studied using an MTT assay on MCF-7 cell lines. 10,000 cells/well were cultured in 96-well plates and were incubated for 24 hours for the completion of cell attachment. Then, MnO_2, PPIX-Lipo, and PPIX-Lipo-M were applied to wells at different concentrations. MnO_2 was used in the concentration range of 45 µM to 570 µM, while the concentrations of the PPIX in both PPIX-Lipo and PPIX-Lipo-M varied from 0 µM to 60 µM. The plates were protected from light with aluminum foil to prevent the unwanted excitation of PPIX by light and incubated for 24 hours to allow the uptake of the particles by cells. Following the incubation, 5 mg/mL of MTT solution in PBS was diluted to 0.5 mg/mL in the corresponding cell and then applied to each well and incubated for 3 hours at 37 °C. DMSO (100 µL) was added to each well to dissolve the formazan crystals. The optical density (OD) was recorded at 540 nm in a microplate reader (Multiskan). Cell viability was determined by comparing OD of treatment group with OD of the control group as depicted below:

$$\text{Cell viability} = \frac{\text{The OD of the treatment group}}{\text{The OD of the control group}} * 100\ \% \quad \text{.....(1)}$$

Each experiment was performed at least three times. Cell viabilities were expressed as mean ± standard deviation.

2.2.10. Hypoxia Induction and Detection

10,000 cells were seeded into 96-well plates and incubated for 24 hours for cell attachment. After the incubation, old media was replaced with new media having 100 µM of cobalt chloride hexahydrate and incubated for 16 hours.[106] Hypoxia induction was confirmed using a ROS-ID® Hypoxia/Oxidative stress detection kit (Enzo Life Sciences) and fluorescence microscopy detection according to the manufacturer's instructions.

2.2.11. PDT Effect Study

PDT effect studies were performed under the following groups: control, PPIX-Lipo, and PPIX-Lipo-M, under normoxia and hypoxia conditions. 10,000 cells/well were seeded in each experiment. Five equal concentrations of PPIX-Lipo and PPIX-Lipo-M were added to the 96-well plates and incubated for another 24 hours. Then, UV light (wavelength 365 nm) was applied to excite PPIX for 5 minutes to all the groups. After the treatment, cells were incubated for at least 6 hours to allow completion of apoptosis. Following the completion of apoptosis, 0.5 mg/mL MTT reagent was added and incubated for 3 hours. Formazan crystal formed was solubilized by using 100 µL DMSO to each well. Then, the OD of solubilized formazan crystal was recorded at 540 nm in the microplate reader. PDT effect was determined by using equation (1). At least three independent experiments were performed, and cell viabilities were expressed as mean ± standard deviation. One-way ANOVA was performed to determine the significance difference with $p<0.05$.

2.3. RESULTS

2.3.1 Synthesis of PPIX-Lipo, BSA-MnO_2, and PPIX-Lipo-M

PPIX is poorly water soluble, which adversely affects its efficacy in vitro and in vivo. Naked PPIX might cause unwanted toxicity to the cells or surrounding tissues.[107] To improve water solubility of the PPIX, we encapsulated the PPIX inside the liposome by using a well-known thin-film hydration method[108] as illustrated in the **Figure 1.** Liposomes are an accepted vehicle for drug delivery;[100,101] it can encapsulate both hydrophobic and hydrophilic drugs in between the phospholipid bilayer and in the core respectively.[99,101]

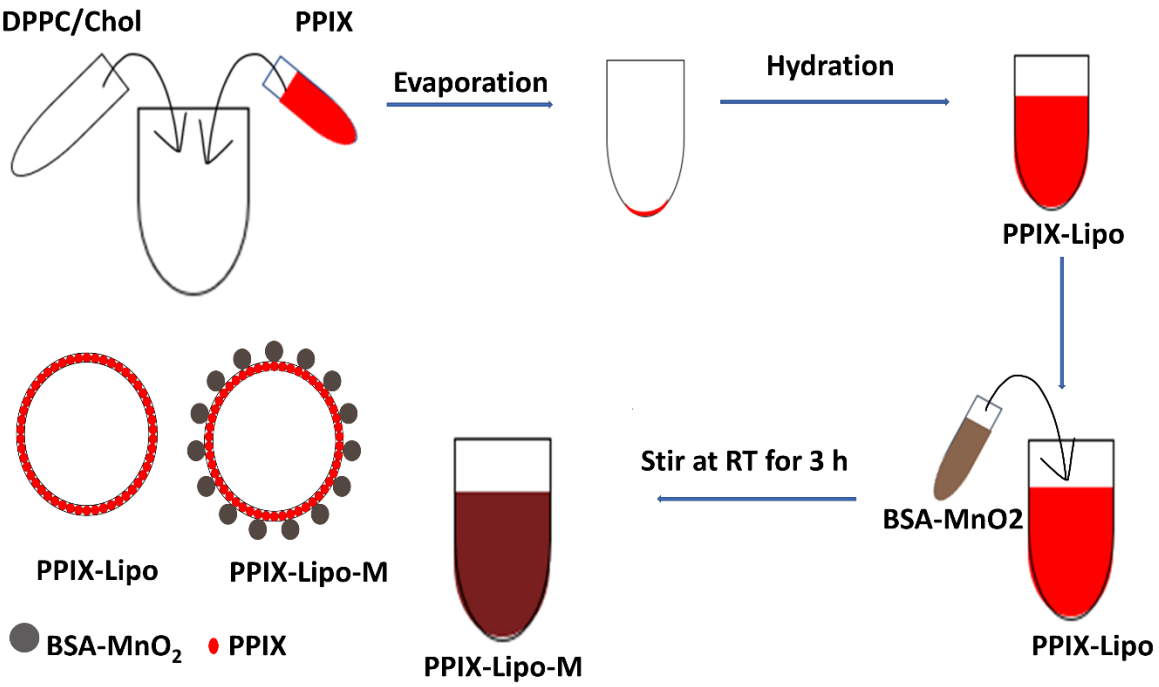

Figure 1: Schematic of synthesis of PPIX-Lipo and PPIX-Lipo.

PPIX, being a hydrophobic drug, was encapsulated between the lipid bilayer of the liposomes. PPIX-Lipo had a reddish color and is soluble in water **(Figure 2a(ii))**, while naked PPIX was black and precipitated in DI water as displayed in **Figure 2a(i).** Luminescence of naked PPIX and PPIX-

Lipo under UV light are depicted in **Figure 2b(i and ii)** respectively**;** PPIX-Lipo showed a bright red luminescence, but bare PPIX did not have luminescence under UV light. The dramatic improvement in solubility and the luminescence of PPIX infers its successful encapsulation into the liposomes.

MnO_2 nanoparticles were synthesized as described in the literature. [105] As-synthesized MnO_2 nanoparticles were highly soluble and stable in aqueous solution for several weeeks. MnO_2

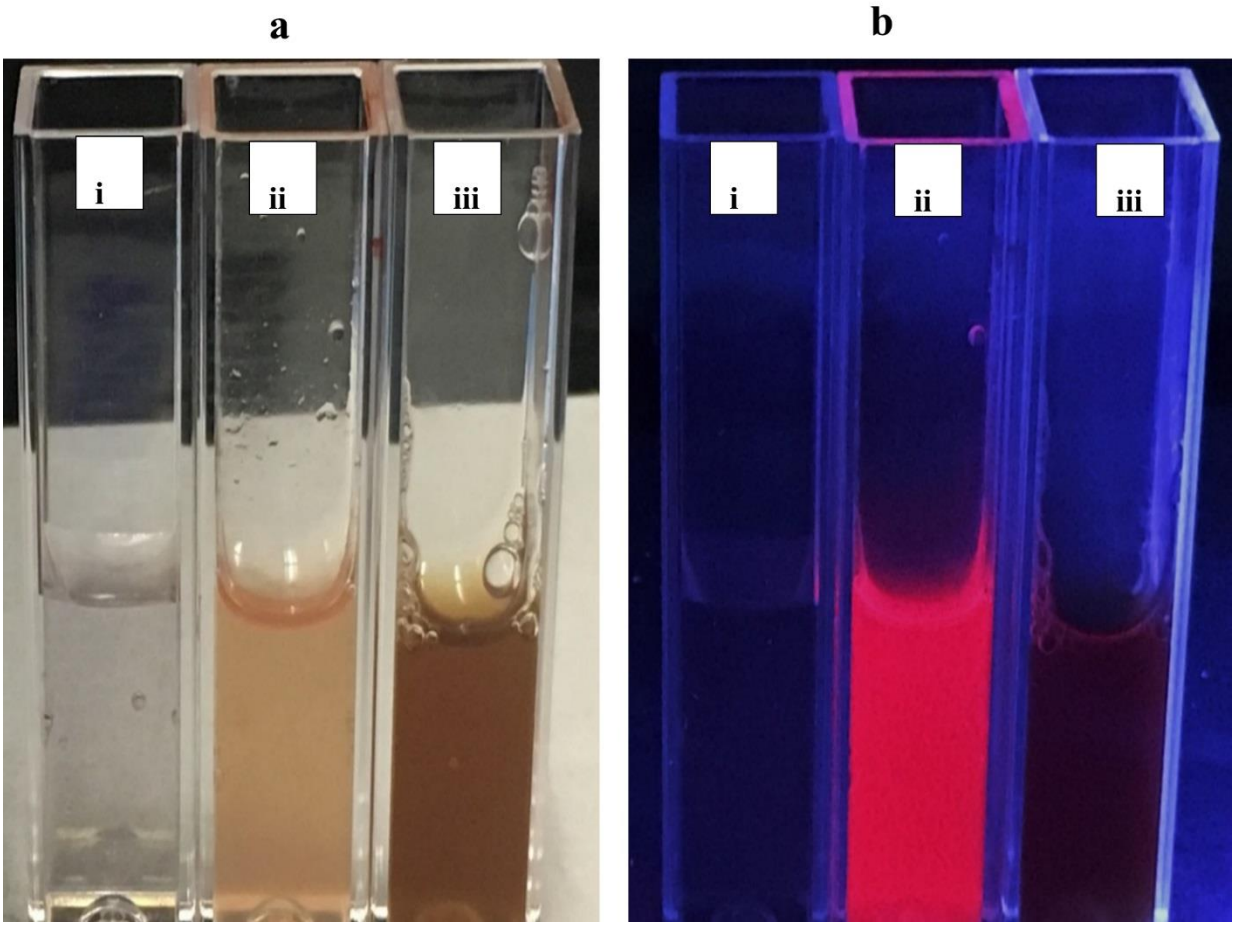

Figure 2: Images of bare PPIX(i), PPIX-Lipo(ii), and PPIX-Lipo-M(iii) under (a) room-light and (b) UV-light respectively.

nanoparticles were then coated to liposomal surface via physical interactions. We believe that MnO_2 was then adsorbed onto the liposome surface via hydrophobic effect as BSA has a strong tendency to interact with cholesterol and DPPC of the liposome.[33,34] As shown in **Figure 2a(iii) and 2b(iii)**, the luminescence of PPIX-Lipo-M was quenched compared to that of PPIX-Lipo. MnO_2 has a wide range of absorption from 200 nm to 700 nm, which coincides with PPIX emission spectra. Consequently, MnO_2 adsorbed onto the liposomal surface could effectively quench the luminescence of PPIX via FRET energy transfer[91] and/or an inner filter effect.[109]

2.3.2. UV-Vis Absorption and Photoluminescence Spectra Measurement

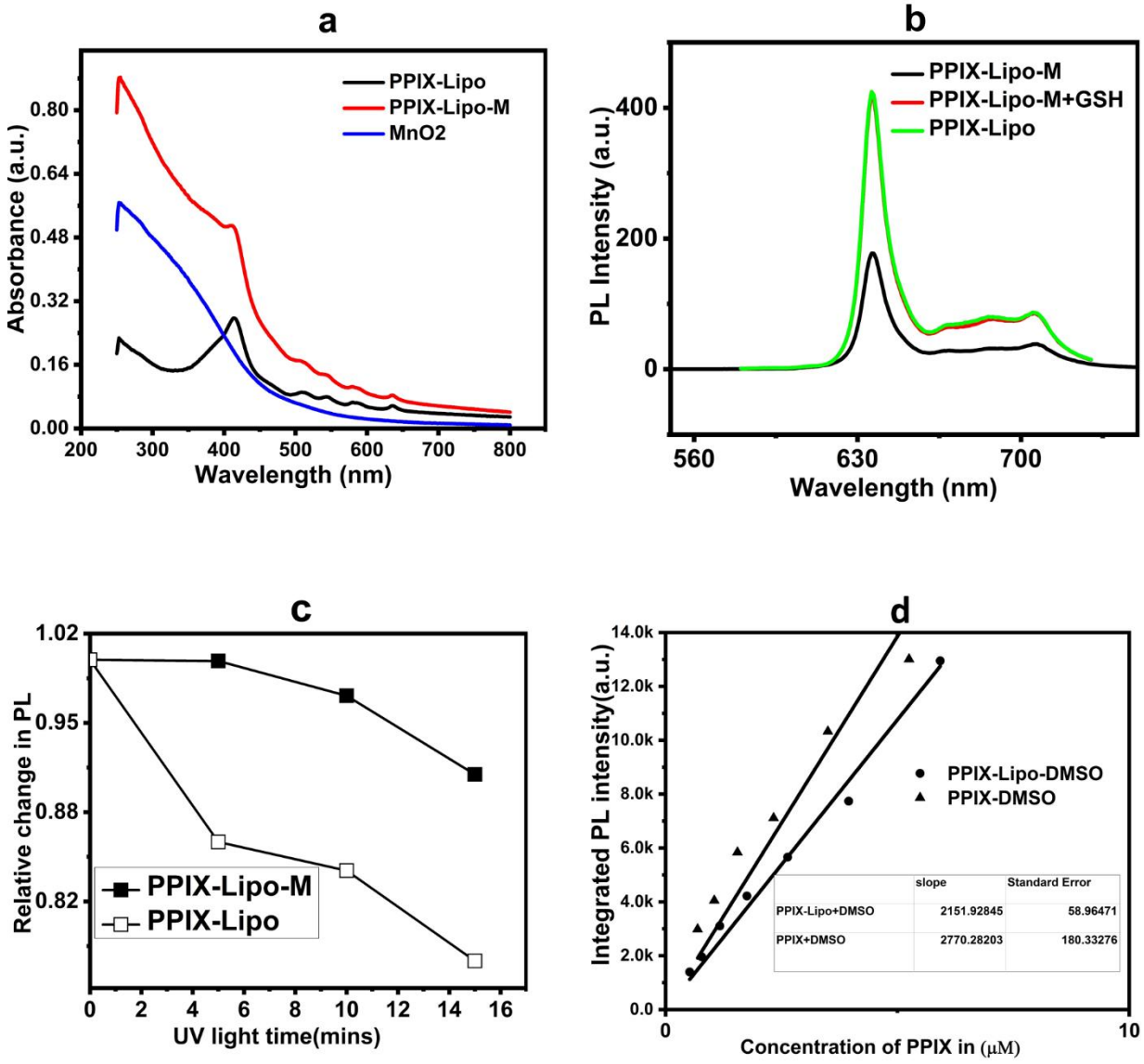

Figure 3: (a) UV-Vis absorption spectra of PPIX-Lipo, PPIX-Lipo-M, and MnO_2. PPIX-Lipo is more symmetric about 420 nm, whereas PPIX-Lipo-M has raised absorption in the range of 200 nm-350 nm. (b) PL spectra of PPIX-Lipo with or without 3 mM GSH. PPIX-Lipo-M regained its luminescence in the presence of GSH. (c) PL quenching of PPIX-Lipo and PPIX-Lipo-M under UV light excitation. (d) determination of encapsulation efficiency.

UV-Vis absorption spectra of PPIX-Lipo, PPIX-Lipo-M, and MnO_2 are shown in **Figure 3a**. PPIX-Lipo-M has increased absorptions in the 200– 400 nm region in UV region which indicates the conjugation of PPIX and MnO_2. Adsorption of MnO_2 on PPIX-Lipo surface was further confirmed by measuring the quenching of the luminescence of PPIX by MnO_2 (**Figure 3b)**. For

the same concentration of PPIX, PPIX-Lipo-M had less than 50 % PL intensity as compared to PPIX-Lipo. The quenching in PL intensity may be due to the energy transfer between PPIX and MnO_2. To further strengthen our claim that MnO_2 is responsible for the PL quenching, we added 3 mM GSH to PPIX-Lipo-M solution to disintegrate MnO_2 adsorbed onto PPIX-Lipo and measured the PL change **(Figure 3b)** to see if disintegrating MnO_2 helps to regain the lost PL intensity. As expected, the luminescent intensity of PPIX-Lipo-M increased and was almost equal to PPIX-Lipo in the presence of GSH at the given concentration. As shown in **Figure S1**, dark brown MnO_2 was completely disintegrated into a clear solution of Mn^{2+} after the addition of 3 mM GSH. We also measured the luminescence of PPIX-Lipo with and without GSH and observed that GSH itself did not alter the luminescence of PPIX **(Figure S2).**

MnO_2 adsorbed onto the liposome surface is expected to improve its resistance against photobleaching. We measured the change in luminescence after 5 minutes of UV light exposure to both PPIX-Lipo and PPIX-Lipo-M **(Figure 3c)**. As anticipated, it was observed that PPIX-Lipo lost its luminescence by 25 % within 15 minutes of cumulative UV light application, while PPIX-Lipo-M lost only 9 % of its luminescence. The improved resistance against photobleaching could be attributed to the MnO_2 adsorbed onto the liposome surface.

The encapsulation efficiency of PPIX into the liposome was determined by comparing the PL intensity of PPIX-Lipo and bare PPIX. Both PPIX-Lipo and PPIX were dissolved in DMSO. To start with, various known concentrations of PPIX-Lipo were prepared in DMSO and their PL intensities were monitored and integrated PL intensities were calculated. The integrated PL intensities were plotted against different concentrations. To determine the encapsulation

efficiency, the integrated PL intensities per unit molar concentration of PPIX-DMSO and PPIX-Lipo-DMSO were compared. As shown in **Figure 3d**, the slope (integrated PL intensity per unit micromolar concentration) of PPIX-Lipo was found to be $2151.9 \pm 58.9\ \mathrm{arb.unit/\mu M}$, whereas that of PPIX was $2770 \pm 180.3\ \mathrm{arb.unit/\mu M}$. Comparing these two slopes, it was calculated that $78\ \% \pm 7\ \%$ of PPIX was encapsulated in the liposome.

2.3.3. Size Distribution

The size distribution measurement suggests that the average sizes of MnO_2, PPIX-Lipo, and PPIX-Lipo-M were 144.9 nm ± 19.6 nm, 362.3 nm ± 12.1 nm, and 752.9 nm ± 50.7 nm, respectively. The increased size of PPIX-Lipo-M compared to PPIX-Lipo could be because of adsorption of MnO_2 onto the liposome surface due to the hydrophobic interaction between BSA and cholesterol and/or DPPC. [110,111] BSA can be effectively adsorbed onto the liposome surface (even negatively charged) via hydrophobic interaction. Accordingly, when MnO_2 and PPIX-Lipo were mixed, MnO_2 adsorbed onto the surface of liposome effectively. The size distribution of PPIX-Lipo and PPIX-Lipo-M was also measured using TEM **(Figure 4b and 4c)**. TEM images show that the PPIX was encapsulated in the phospholipid bilayer of the liposome. The denser (black layers) are the PPIX, while less dense centers are the empty core of the liposomes. **Figure 4c** shows the TEM image of PPIX-Lipo-M; MnO_2 can be seen adsorbed onto the surface of the liposome.

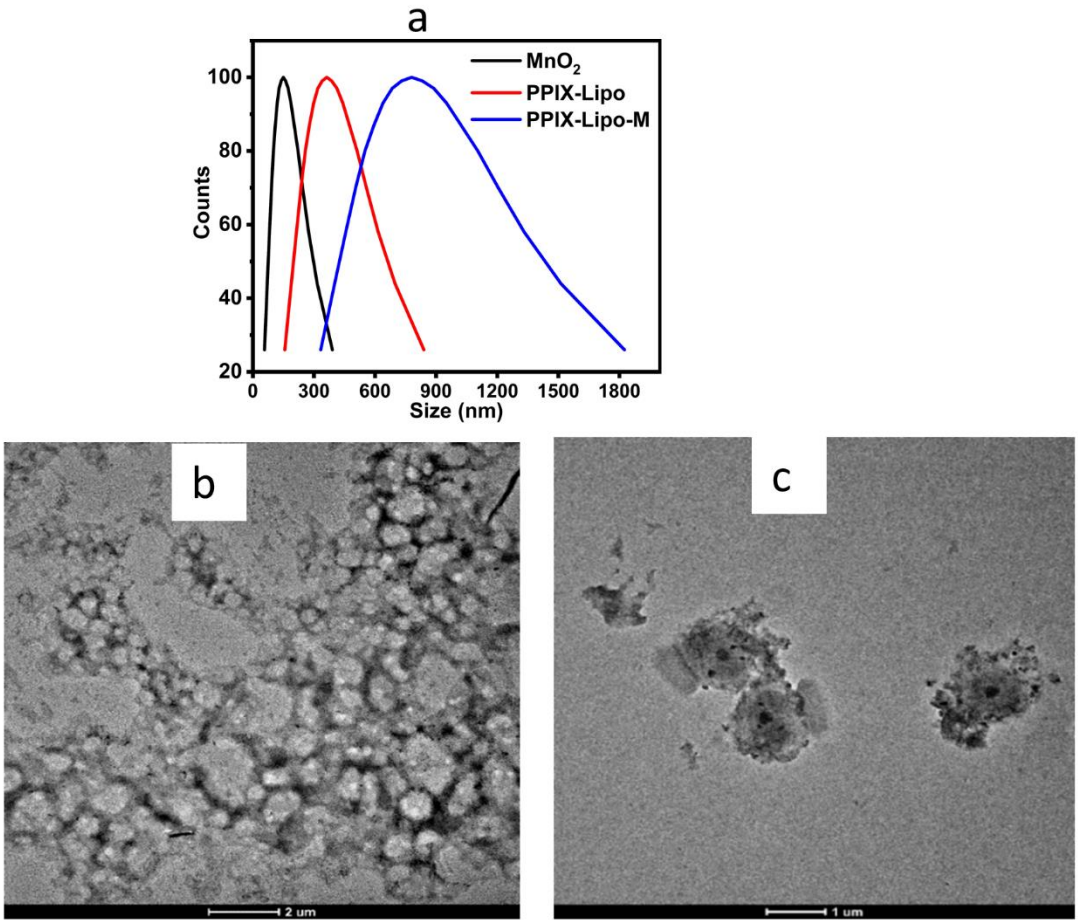

Figure 4: Size distribution measurement of PPIX-Lipo and PPIX-Lipo-M. (a) DLS Size distribution of MnO_2, PPIX-Lipo, and PPIX-Lipo-M. The proportional increase in size distribution shows that MnO_2 is adsorbed onto the surface of liposome due to hydrophobic interaction. (b) TEM image of PPIX-Lipo, and (c) TEM image of PPIX-Lipo-M. It is seen that MnO2 is adsorbed on the liposome surface.

2.3.4. Singlet Oxygen Measurement

We used SOSG to determine singlet oxygen generation by PPIX-Lipo and PPIX-Lipo-M with and without H_2O_2 under UV light excitation **(Figure 5a)**. Most cancer cells have an enhanced level of H_2O_2. MnO_2 reacts with H_2O_2 under acidic conditions and produces oxygen. Therefore,

our nanosystem can be beneficial by acting as the source of oxygen in the tumor microenvironment. We measured singlet oxygen generation from PPIX-Lipo and PPIX-Lipo-M with and without H_2O_2. To simulate an endogenous H_2O_2 environment, 100 µM H_2O_2 was added to the testing solution along with the sample and SOSG probe. The relative change in luminescence was plotted with respect to UV light time. It was found that in the absence of H_2O_2, PPIX-Lipo produced more singlet oxygen than PPIX-Lipo-M. It could be because PPIX in PPIX-Lipo has direct access to the light than PPIX in PPIX-Lipo-M in which most light is absorbed by MnO_2 adsorbed onto its surface. On the other hand, in the presence of H_2O_2, PPIX-Lipo-M produced more singlet oxygen than PPIX-Lipo because of extra oxygen produced by MnO_2 reacting with H_2O_2.

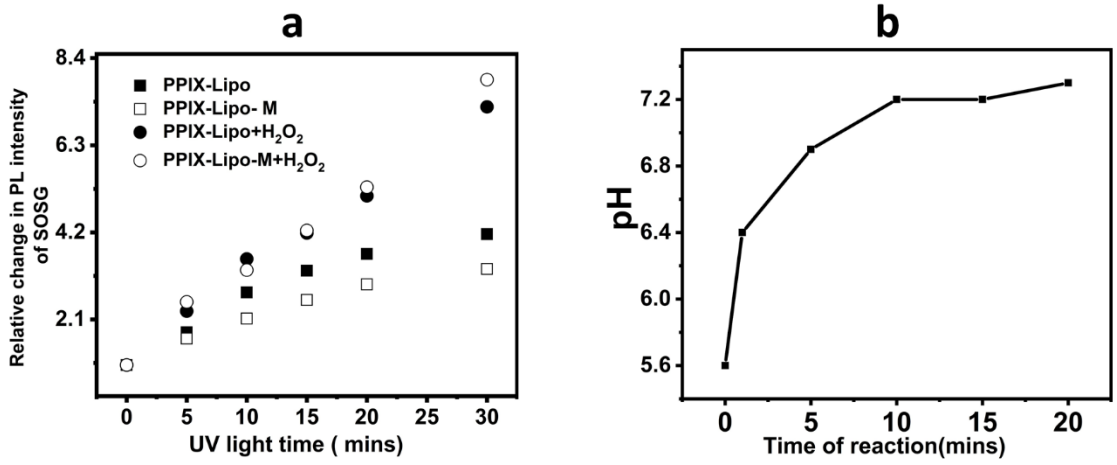

Figure 5: (a) Singlet oxygen measurement of PPIX-Lipo and PPIX-Lipo-M with and without H_2O_2. (b) Measurement of pH change of MnO2 treated acidic solution in the presence of 100 µM H_2O_2.

2.3.5. pH Change Induced by MnO_2

MnO_2 reacts with H_2O_2 under acidic conditions. In other words, MnO_2 nanoparticles, while reacting with H_2O_2, uses H^+ ions and disintegrates itself into Mn^{2+} ions. So, in order to measure

the reactivity of MnO_2 towards H_2O_2 under acidic conditions in an indirect way, we measured the change in the pH of acidic solution containing H_2O_2 with the addition of MnO_2 **(Figure 5b)**. The data shows that with the addition of 150 µM of MnO_2 to an acidic solution containing 100 µM H_2O_2, pH increased from 5.6 to 7.2 within 20 minutes. This result suggests that MnO_2 reacts with H_2O_2 under acidic condition efficiently and it may help to increase pH of tumor microenvironment.

2.3.6. Cellular Uptake

Cellular uptake study of PPIX-Lipo and PPIX-Lipo-M to MCF-7 cell lines are presented in **Figure 6**. The blue channel represents the HOECHST stained nucleus. The red channel represents the luminescence from PPIX. HOECHST and PPIX channels were merged to confirm the cellular uptake. It should be noted that both PPIX-Lipo and PPIX-Lipo-M have good cellular uptake. We also studied the cellular uptake of naked PPIX dissolved in DI water. As shown in **Figure S4,** naked PPIX aggregates into large crystals in cell media and there was almost no uptake by cells. Confocal images (**Figure S5)** reveals that PPIX-Lipo gets into the cell; bright red luminescent PPIX-Lipo can be seen localized in the same plane as nucleus.

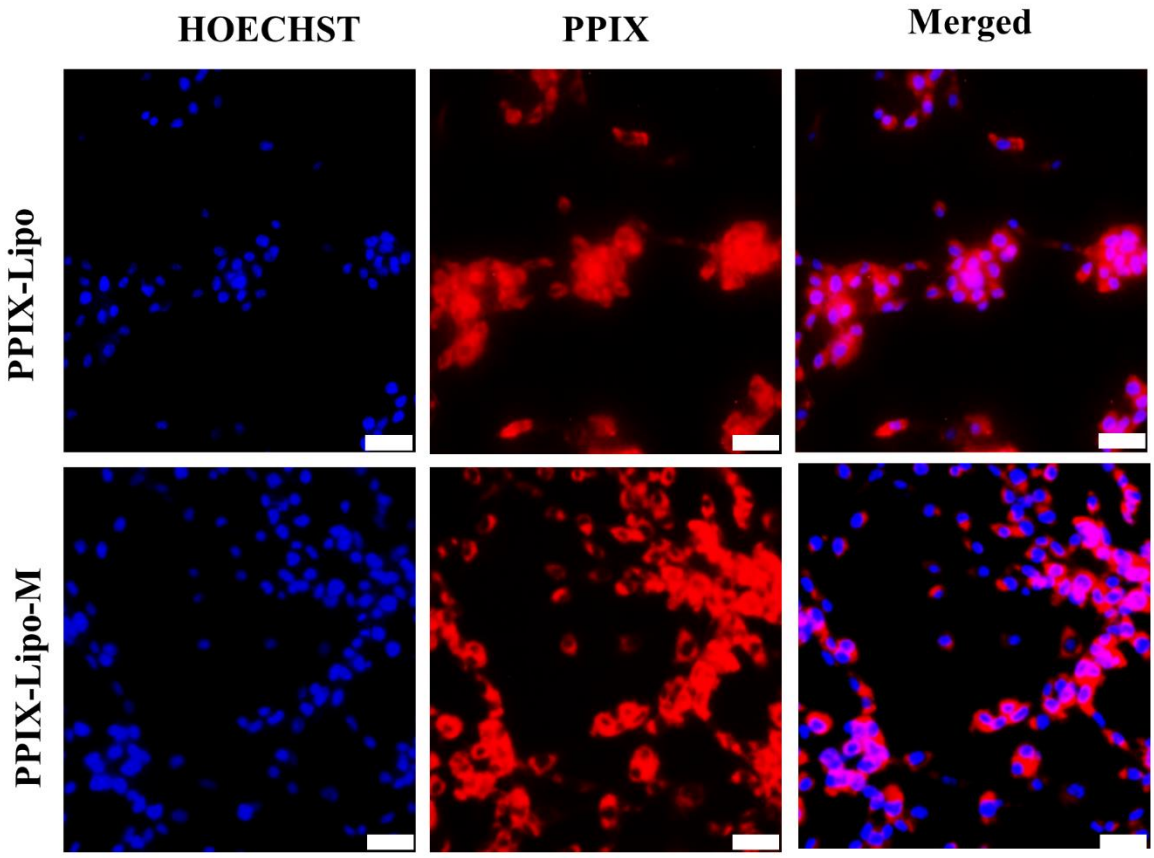

Figure 6: Cellular uptake study of PPIX-Lipo and PPIX-Lipo-M into MCF-7 cancer cells by using fluorescence microscopy. PPIX-Lipo and PPIX-Lipo-M were applied to MCF-7 following 24 hours incubation. HOECHST dye was applied 5 minutes before imaging to stain nuclei. (Scale bar: 50 µm)

2.3.7. Cellular Viability Study

Cell viability of PPIX-Lipo, PPIX-Lipo-M, and MnO_2 was determined by using an MTT assay. MnO_2 was applied with the concentration range 45 to 570 µM to MCF-7 and incubated for 18 hours. Even at 570 µM, 90 % of cells survived, indicating low cytotoxicity of MnO_2. The concentration of the PPIX varied from 0 to 60 µM for both PPIX-Lipo and PPIX-Lipo-M. All the plates were protected from light by covering with aluminum foil. We found that concentrations

below 3 µM had minimal dark toxicity. Consequently, 3 µM or less PPIX concentration (in PPIX-Lipo and PPIX-Lipo-M) was chosen for PDT effect evaluation.

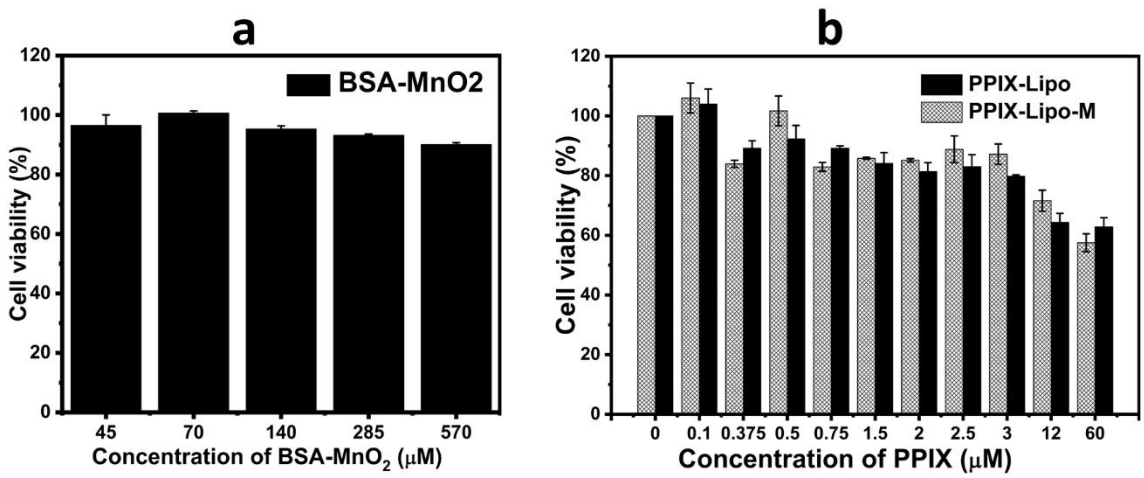

Figure 7: Cell viability study of MnO2, PPIX-Lipo, and PPIX-Lipo-M treated MCF-7 cell lines. Cells were incubated with the particles for 24 hours and were protected from light with aluminum foil. MnO2 does not show substantial toxicity to MCF-7 cell lines up to 570 µM concentration. PPIX-Lipo and PPIX-Lipo-M both have more than 80 % cell viability at and below 3 µM. No significant difference was observed between the toxicity of PPIX-Lipo and PPIX-Lipo-M.

2.3.8. Hypoxia Induction and Detection

Cobalt chloride is known as a hypoxia inducing agent in vitro and in vivo.[106,112–114] A 50 to 100 µM concentration has been reported as non-toxic and efficient at inducing hypoxia.[106,112–114] The use of cobalt chloride allows us to open the plate and to apply UV light outside the incubator without interrupting hypoxia. It induces hypoxia by occupying of the HIF-α binding domain of a von Hippel-Lindau protein, thereby preventing the degradation of HIF-α. [112] An alternative way of inducing hypoxia is incubating cell plates in a hypoxia chamber, which is supplied with gas mixtures 1 % O_2 + 94 % N_2 + 5 % CO_2. This method does not guarantee hypoxia if cell plates are taken outside the incubator. Furthermore, this method is expensive, time-

consuming, and not suitable for our purpose, as we need to excite cell plates with the UV light. The PPIX-Lipo-M killed a significantly higher percentage of cells than the PPIX-Lipo did.

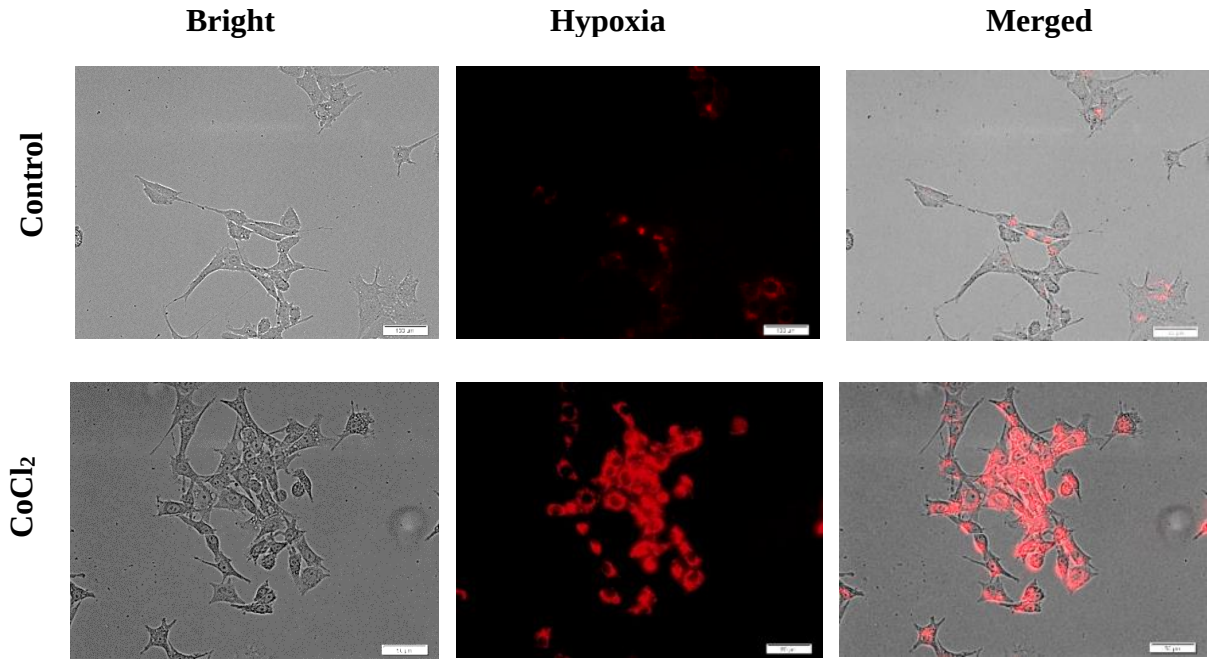

Figure 8: Confirmation of hypoxia induction by using ROS-hypoxia assay (Enzo Life Sciences) on MCF-7 cell lines. The red luminescence confirms cellular hypoxia. The increase in red luminescence of the assay in cobalt chloride treated cell indicates successful induction of hypoxia. (Scale bar: 50 µm).

The hypoxia induction was confirmed by using an ROS-ID® Hypoxia/Oxidative stress detection kit (Enzo Life Sciences) and fluorescence microscopy detection according to the manufacturer's instructions. The control group was incubated with regular media, while the hypoxia group was incubated with media containing 100 µM cobalt chloride for 16 hours. The non-luminescent probe becomes red fluorescent under hypoxic conditions. It takes advantage of the nitroreductase activity present in hypoxic cells which converts nitro-group to hydroxylamine and amino group and releases the red-luminescent probe. As can be seen in **Figure 8**, the cobalt chloride treated cells

shows the bright red luminescence from hypoxia red, whereas the cells incubated without cobalt chloride does not show red luminescence from hypoxia red. The result implies the successful induction of hypoxic conditions in the MCF-7 cell lines.

2.3.9. PDT Effect Study

2.3.9.1. Normoxic Conditions

Normoxia is regarded as a condition where the cellular oxygen level is at its normal value of 38 mmHg to160 mm Hg.[115] Cell culture media, which are incubated in an incubator with 95 % O_2 and 5 % CO_2, is expected to have normoxic conditions. **Figure 9a** depicts the PDT effect of PPIX-Lipo and PPIX-Lipo-M to the MCF-7 cell lines under normoxic conditions. Under normoxia, it was observed that the PPIX-Lipo killed more cells than the PPIX-Lipo-M **(Figure 9a)**. Although significant difference was observed only for 0.75µM group, PPIX-Lipo killed more cells than PPIX-Lipo-M for all the concentration groups. Under normoxic conditions, IC-50 values for PPIX-Lipo (0.982 µM ± 0.008 µM) were found to be significantly lower than the IC-50 values (1.19 µM ± 0.03 µM) of PPIX-Lipo-M. Furthermore, this implies that under normoxic conditions, the PPIX-Lipo may produce larger amounts of singlet oxygen than PPIX-Lipo-M, which is consistent with what was observed during the singlet oxygen measurement. Higher singlet oxygen production by PPIX-Lipo can be attributed to the fact that PPIX-Lipo-M does not have direct access to the light due to MnO_2 being adsorbed onto the liposome surface. Additionally, PPIX-Lipo has smaller size than PPIX-Lipo-M, which might result in higher cellular uptake of PPIX-Lipo and hence better efficacy of PPIX-Lipo.

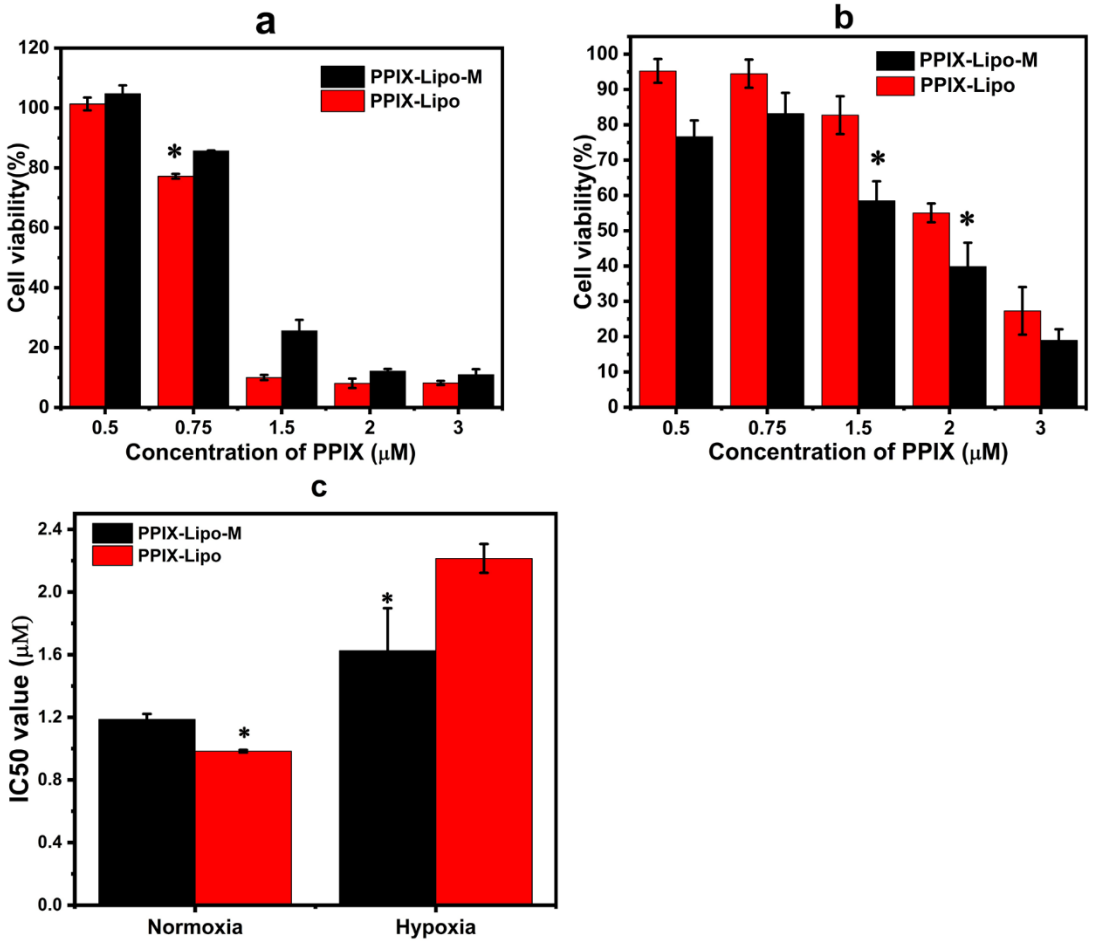

Figure 9: Study of PDT effect of PPIX-Lipo and PPIX-Lipo-M under (a) normoxia, (b) hypoxia, and (c)IC-50 values of PPIX-Lipo and PPIX-Lipo-M to MCF-7 cell lines and incubated for 24 hours. Commercial UV-light was used for 5 minutes as an excitation source. * indicates $p < 0.05$ significant difference from the corresponding group.

2.3.9.2. Hypoxic Conditions

The PDT efficacy was then evaluated under hypoxia conditions. As displayed in Figure 9b, for 1.5 and 2 μM concentration groups, PPIX-Lipo-M killed significantly more cells than PPIX-Lipo did. Although the difference was not statistically significant, PPIX-Lipo-M was more effective than PPIX-Lipo for all other concentrations we used. The IC-50 value of PPIX-Lipo-M (1.625 μM ± 0.27 μM) was significantly lower than that of PPIX-Lipo (2.21 μM ± 0.09 μM) **(Figure 9c)** which indicates that during hypoxic conditions, PPIX-Lipo-M performs better than PPIX-Lipo. During

hypoxic conditions, cells suffer from a lack of oxygen such that the photosensitizer performs suboptimally. [28] In this case, the addition of MnO_2 to PPIX-Lipo for the production of PPIX-Lipo-M can aid in overcoming the hypoxic conditions of the cancer cells by generating oxygen from reacting with endogenous H_2O_2. In turn, this results in a higher production of singlet oxygen species as compared to the PPIX-Lipo. Therefore, the PPIX-Lipo-M kills more cells as compared to PPIX-Lipo in the cancer cells.

2.4. DISCUSSIONS

Tumors have a unique environment called the tumor microenvironment (TME), which helps for the sustained growth, invasion, and metastasis of cancer cells.[116,117] Some of the characteristics of the most TME are hypoxia, lower pH, and elevated levels of both glutathione and H_2O_2. It has been reported that tumor hypoxia might be responsible for poor radiotherapy efficacy.[28,29,115,118,119]

In recent years, MnO_2 involved smart strategies, which took advantage of its reactivity towards H_2O_2 and GSH were investigated.[38,42,89,91] In this work, we investigated whether PPIX-Lipo-M can reduce hypoxia in the TME by reacting with endogenous H_2O_2. MnO_2 possesses several characteristics to enhance the PDT effect of photosensitizers; it has high specificity and reactivity toward H_2O_2 producing O_2 and H_2O while consuming protons in the reaction.[38]

As shown in **Figure 5b**, MnO_2 can react with GSH and H_2O_2 under acidic conditions producing oxygen as well as increasing pH value. The reaction scheme of MnO_2 with H_2O_2 is presented below[90]:

$MnO_2+2H_2O_2 \rightarrow Mn^{2+}+O_2+2H_2O$

$MnO_2+2H_2O_2 \xrightarrow{H^+} Mn^{2+}+O_2+2H_2O$

Following the reaction, the MnO_2 nanoparticles disintegrate into Mn^{2+} ions which can easily be cleared via renal clearance.

The proposed treatment method incorporates unique combination of generally understood strategies for drug delivery and PDT. Liposomes were utilized for drug delivery because of their known capacity to encapsulate both hydrophilic and hydrophobic drugs.[99] PPIX is an FDA approved photosensitizer. The amphiphilic nature of PPIX causes it to aggregate in the aqueous environment either via π-π stacking or intermolecular interactions between the hydrophilic -COOH group and the hydrophobic porphyrin core.[93] In this work, we successfully encapsulated water insoluble PPIX into liposomes (PPIX-Lipo) and then conjugated them with BSA coated MnO_2 to fabricate the PPIX-Lipo-M nanosystem. Liposomal encapsulation drastically improved the solubility of PPIX. PPIX-Lipo had good aqueous solubility, improving its luminescence. As compared to naked PPIX, PPIX-Lipo had much better cellular uptake that enhanced its photodynamic effect. It is generally accepted that liposome encapsulation reduces drug toxicity. Moreover, the conjugation of PPIX-Lipo and MnO_2 by simple physical mixing has several advantages over other chemical methods of conjugation, as it avoids the retention of unwanted chemicals and the consequential purification steps to remove them.

PPIX-Lipo-M can improve the efficacy of photodynamic therapy by supplying oxygen to the cancer cells. We observed that under normoxic conditions, PPIX-Lipo is more efficient than PPIX-Lipo-M. The higher efficiency of PPIX-Lipo in the normoxic environment may have originated due to one or a combination of the following reasons: (1) The normoxic media has

sufficient oxygen levels and therefore having MnO_2 may not offer an additional advantage, (2) PPIX-Lipo has more direct access to the excitation light than PPIX-Lipo-M, and (3) due to its smaller size, PPIX-lipo may have higher cellular uptake than PPIX-Lipo-M. Due to these reasons, PPIX-Lipo-M is less effective than PPIX-Lipo under normoxia conditions.

However, when hypoxia was created, PPIX-Lipo was not effective due to the lack of oxygen, whereas PPIX-Lipo-M could produce oxygen due to the reactions between MnO_2 and H_2O_2. Accordingly, PPIX-Lipo-M produces significantly more singlet oxygen than PPIX-Lipo.

We used cobalt chloride to induce cellular hypoxia, a reliable and economical alternative to the hypoxia chamber. The use of cobalt chloride allowed us to handle the cell plates and apply UV-light outside the incubator without disturbing hypoxia.

2.5. CONCLUSIONS

In this work, PPIX was encapsulated into liposomes to improve its aqueous solubility. Then, PPIX-Lipo was coated with MnO_2 nanoparticles. The coating of MnO_2 on the PPIX-Lipo surface was confirmed by measuring the PL quenching effect of MnO_2 on PPIX-Lipo. We then tested its PDT effect to the MCF-7 cell lines under normoxic and hypoxic conditions. Hypoxia was successfully induced to MCF-7 cell lines by incubating it with cobalt chloride for 16 hours. Although PPIX-Lipo killed more cancer cells than PPIX-Lipo-M under normoxic conditions, the PPIX-Lipo-M was much more effective than the PPIX-Lipo under hypoxic conditions. In summary, PPIX-Lipo-M could solve hypoxia issues in the tumor microenvironments by converting the ever-present H_2O_2 into oxygen, which improves the PDT efficacy of the photosensitizer and deserves for further investigation on PDT.

Acknowlegments:

We would like to acknowledge the support from the U.S. Army Medical Research Acquisition Activity (USAMRAA) under Contracts of W81XWH-10-1-0279 and W81XWH-10-1-023. We would like to acknowledge Dr. Nguyen Kytai for allowing us to use zeta potential analyzer.

Conflicts of Interest:

There are no conflicts of interest to declare.

SUPPORTING INFORMATION

Investigation of PPIX-Lipo-MnO_2 to Enhance Photodynamic Therapy by Improving Tumor Hypoxia

Lalit Chudal[1], Nil Kanatha Pandey[1], Jonathan Phan[1],Omar Johnson[1],Xiuying Li[2], Wei Chen[1]*

1 Nano-Biophysics Lab, Department of Physics, The University of Texas at Arlington, TX 76019, USA

2 Department of Mechanical Engineering, University of Texas at Dallas, TX, 75080, USA

**Corresponding author:* weichen@uta.edu

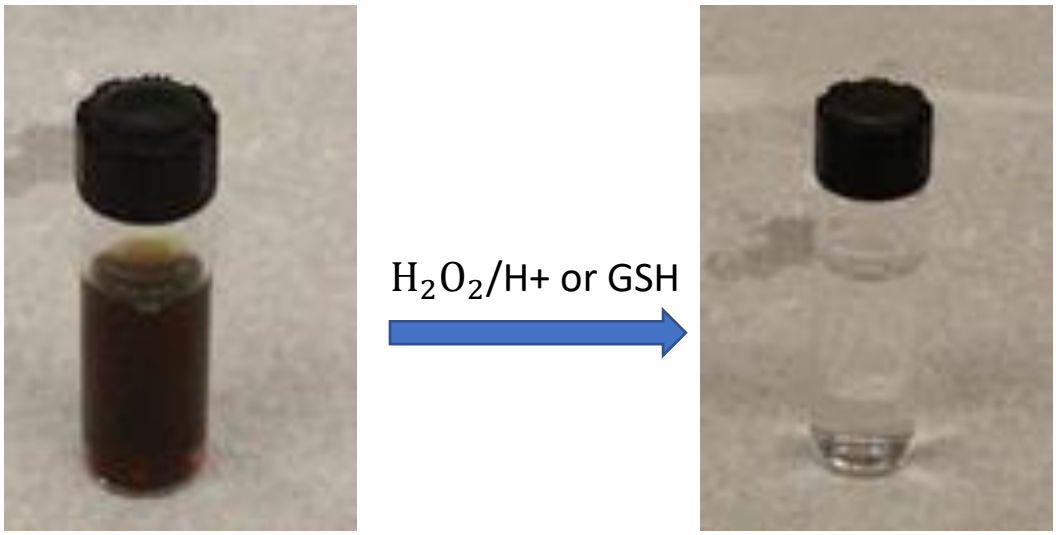

Figure S1: MnO_2 nanoparticles disintegrates in presence of GSH or H_2O_2.

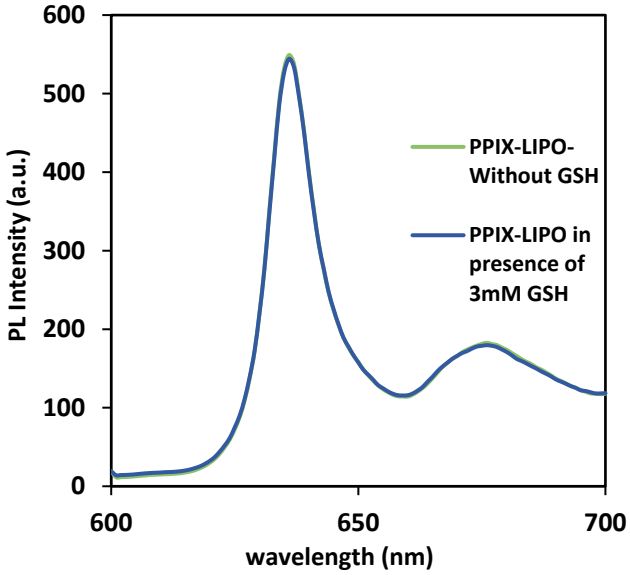

Figure S2: Photoluminescence of PPIX-Lipo with or without 3mM GSH. There is no change in intensity showing that GSH does not react with PPIX-Lipo.

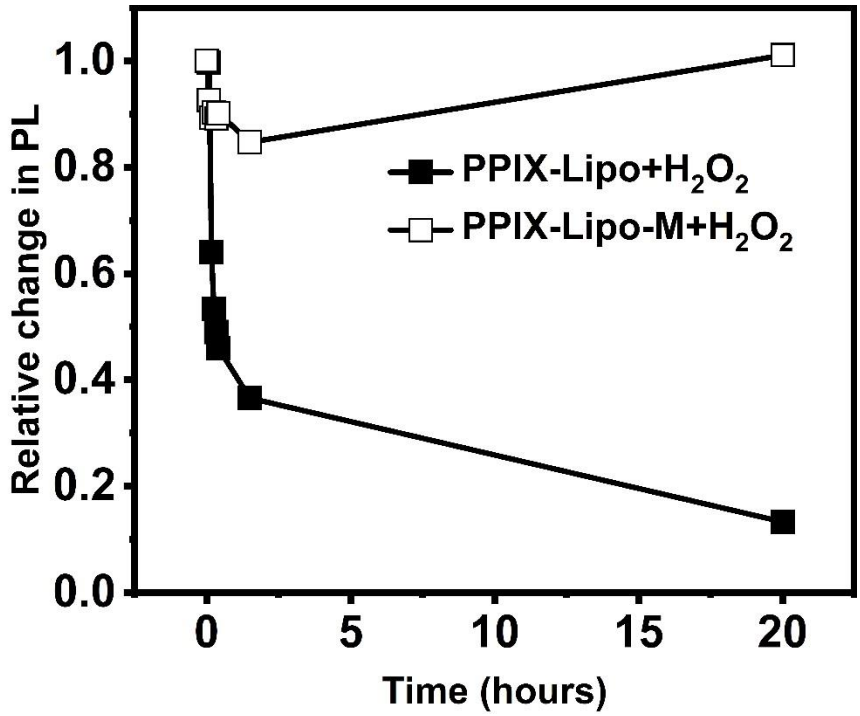

Figure S3: Change in PL intensity of PPIX-Lipo and PPIX-Lipo-M in presence of 100 µM H_2O_2. The change in PL intensity was expressed as ratio with corresponding initial PL intensity. PL intensity of PPIX-Lipo decreases over the time while PPIX-Lipo-M decreases initially and then start to increase. The increase in PL intensity could be due to disintegration of MnO_2 by H_2O_2 and hence regain in initially quenched luminescence.

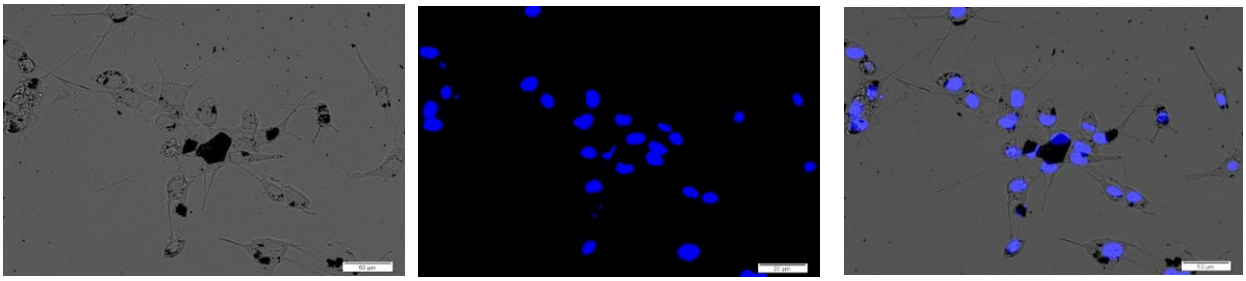

Figure S4: Cellular uptake of bare PPIX mixed in DI water. Large PPIX aggregates can be seen on the top of cells indicating that naked PPIX has poor cellular uptake. Scale bar: 50µM

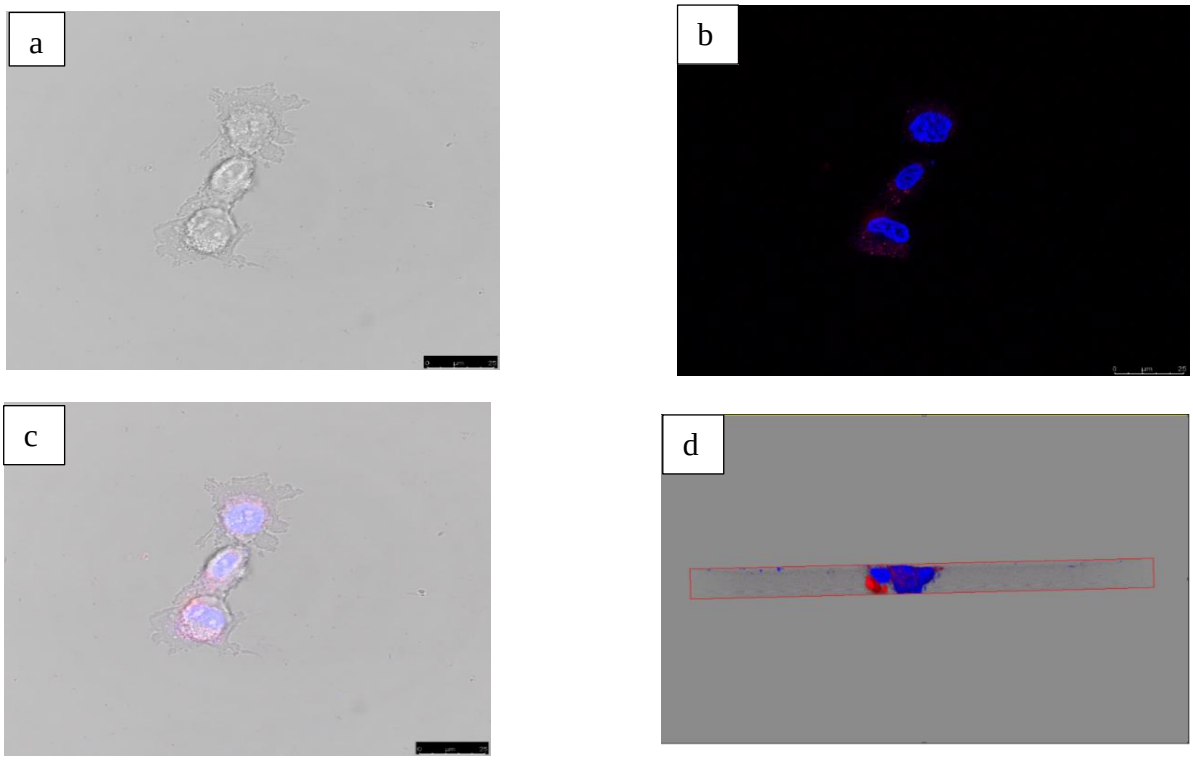

Figure S5: Confocal imaging to confirm cellular uptake of PPIX-Lipo into MCF7 cell lines. A. bright field image B. merged image of HOECHT and PPIX Channel. C. Merged image of HOECHT (blue), PPIX(red) and brightfield image. D. 3D image showing PPIX inside the MCF7 cell lines. Scale bar: 25µm

Chapter 3:

(In preparation for publication)

COPPER-CYSTEAMINE NANOPARTICLES AS NEW RADIO-PHOTOSENSITIZER WITH LOW SUNLIGHT TOXICITY

ABSTRACT

Photodynamic therapy carries great potential as a safer and effective cancer treatment method. However, photodynamic therapy suffers from some severe disadvantages, such as poor penetration depth and unwanted photosensitivity. The issue of photosensitivity arises from the fact that most photosensitizers readily be activated by visible light and the photosensitizing drugs can stay in the upper dermal layer for a prolonged period. In this work, we propose copper-cysteamine nanoparticle (Cu-Cy NP) that has alternative excitation sources such as X-ray, microwave, UV light (but not visible light), and as a result, can keep the issue of photosensitivity to a minimal level. A systematic study was conducted to compare the sunlight-induced toxicity between copper cysteamine nanoparticles and protoporphyrin IX (PPIX), an FDA approved photosensitizing drug. The result demonstrated that Cu-Cy NPs are significantly less phototoxic when compared to that of PPIX.

3.1 INTRODUCTION:

Photodynamic therapy (PDT) refers to a promising cancer treatment method in which light of a suitable wavelength in combination with photosensitizers and molecular oxygen is used to generate reactive oxygen species.[4,120–122] The effectiveness of the PDT process heavily depends on photosensitizer, light, and oxygen.[4,120–122] PDT has some notable advantages over other cancer treatment techniques such as low side effects, non-invasiveness, and high

targetability.[4,120–122] Despite these advantages, the practical applications of the PDT method are severely limited owing to three major issues: (1) hypoxia issue in the tumor microenvironment, (2) poor penetration depth, and (3) occurrence of phototoxic effect following the PDT treatment. The scarcity of oxygen (hypoxia) in tumor and tumor microenvironment is a serious problem that adversely affects the efficiency of PDT. To combat the hypoxia issue, numerous innovative strategies that can supply oxygen during PDT have been developed.[42,43,90] Furthermore, the issue of low penetration depth of light limits the application of conventional PDT to treat only some of the non-melanoma skin cancers. To address these issues, researchers are developing sensitizers with alternative excitation sources such as X-ray [56,57,123], microwave [59,60,124], and ultrasound[61] that have much more penetration depth than that of light.

Another major issue of current photodynamic therapy is the occurrence of phototoxic effects following the treatment, particularly if exposed to bright light.[14,44–46] The phototoxic effect originated from the fact that most existing photosensitizers can readily be stimulated by visible light to produce highly toxic reactive oxygen species. Furthermore, the photosensitizers take up to several weeks to get cleared from the body and can accumulate underneath dermal skin layers and eyes for a long time. The common symptoms of phototoxicity include pain, burns, erythema, edema, blistering, pustular formation, desquamation.[125] The primary mechanism responsible for photosensitivity is the ROS generation mediated damage of vital cell organelles, including lipid, DNA, and protein. Alternatively, the formation of a stable photo-adduct between DNA and photosensitizer could also be responsible for observed phototoxicity.[53]

Accordingly, several reports have shown that light exposure can be problematic following the PDT treatment.[14,46,47,126] Therefore, patients are advised to avoid daylight for up to several weeks

after the treatment. Despite the compliance with the guidance by the hospital, a large number of patients report the phototoxic effects.[14,47] Photofrin (Porfimer sodium), an approved sensitizer in many countries, including the United States, induces cutaneous photosensitivity that can last up to 3 months. [48–50] The issue of prolonged phototoxicity was also seen in a Foscan, a second-generation photosensitizer.[45,50] Some improvements have been reported in more recent sensitizers. However, the occurrence of phototoxicity and the requirement to avoid direct sunlight has not been eliminated yet.[44] Moreover, phototoxicity is the problem of many other drugs as well, and therefore comprehensive phototoxicity evaluations of new drugs are often warranted.[51,52]

5-Aminolevulinic acid (ALA) is a second-generation photosensitizer that gets converted into PPIX endogenously. The ALA induced PPIX has been approved by the US-FDA for non-oncological treatment of actinic keratosis in 1999.[24] It has also shown potential for PDT treatment to some other diseases, including Bowen's disease and basal cell carcinoma.[25,26]

In this contribution, we propose that using sensitizer with alternative excitation sources such as X-ray, MW, or US could effectively eliminate the issue of phototoxicity. In 2014, our lab invented copper-cysteamine nanoparticles that are activatable with various excitation sources such as X-ray,[54–58] MW,[59,60], ultrasound[61], UV light[62,63], and acidic pH/H_2O_2 (cancer-specific condition).[64] We will systematically compare the sunlight-induced photosensitivity by Cu-Cy NPs with PPIX, a current clinical photosensitizer.

3.2. MATERIAL AND METHODS

3.2.1. Materials

Copper chloride dihydrate and Protoporphyrin IX were purchased from Sigma Aldrich. Calcein-AM, Ethidium homodimer-1, and (3- (4,5-dimethylthiazol-2-yl)-2,5-diphenyltetrazolium bromide (MTT assay) were purchased from ThermoFisher Scientific.

3.2.2. Synthesis of copper-cysteamine nanoparticles

Copper cysteamine nanoparticles were synthesized using our previously reported method.[59] In brief, $CuCl_2.2H_2O$ (273 mg) was dissolved in DI water (50 mL) at room temperature. Afterward, cysteamine hydrochloride (381 mg) and PEG-4000 (40 mg) were added into the above mixture under an inert atmosphere. The pH of the solution was then adjusted to 7 using NaOH and stirred for 5 min under atmospheric condition. When the solution turned to deep violet, it was boiled for 5 min under the inert environment with rapid magnetic stirring. The solution was then allowed to cool naturally. Cu-Cy NPs were collected by centrifuging and washing by DI water/ethanol 3 times. The obtained Cu-Cy NPs were vacuum dried at 40 ^{0}C overnight.

3.2.3. Preparation of Protoporphyrin IX (PPIX) solution

The working solution of PPIX was prepared by dissolving a desired amount of PPIX into DMSO. The as-prepared PPIX solution was diluted in the culture medium to obtain desired concentrations for cellular treatment. The final concentration of DMSO in the PPIX solution applied to the cell was always kept less than 1%. The Cu-Cy solution was prepared

3.2.4. Instrumentation

The absorption and photoluminescence (PL) spectra of PPIX and Cu-Cy were measured employing a UV-vis spectrophotometer (Shimadzu UV-2450) and a photoluminescence spectrophotometer (Shimadzu RF-5301PC, Tokyo, Japan).

3.2.5. MTT assay

The cytotoxicity of Cu-Cy and PPIX was evaluated using the MTT assay. 1 $\times 10^4$ cells/well were harvested in 96 well plates and incubated for 24 h. The cells were then treated with various doses of Cu-Cy and PPIX (0-30 μg/mL) and incubated for another 24h. The MTT plates were either exposed to sunlight or kept in the dark for 10 min. The cells were then treated with 0.05 mg/mL of MTT solution for 3 h. The formazan crystals were then dissolved with DMSO, and the optical density of the purple-colored formazan solution was then monitored using multiskan microplate reader. The cell viability was calculated using the following equation:

$$\text{Cell viability} = \frac{\text{The O. D. of the treatment group}}{\text{The O. D. of the control group}} * 100\%$$

3.2.6. Live/Dead Assay

The toxicity of Cu-Cy and PPIX against healthy cell lines was further evaluated by using Live/dead assay. The 2 $\times 10^5$ cells were seeded in a 35 mm imaging plate and incubated for 24 h. Afterward, the cells were treated with the desired amount of PPIX or Cu-Cy and incubated for 24 h. Then, the plates were exposed to sunlight or kept in the dark for 10 min. After incubating for another 6 h, the cells were applied with 0.125 μg/mL calcein-AM and ethidium homodimer (Ethd-1) for 40 min. Afterward, the calcein and Ethd-1 homodimer positive cells were imaged using 495/515 nm and 528/617 nm filters of IX-71 Olympus microscope, respectively. The live and dead cells were quantified using imageJ, as described in our previous publication.

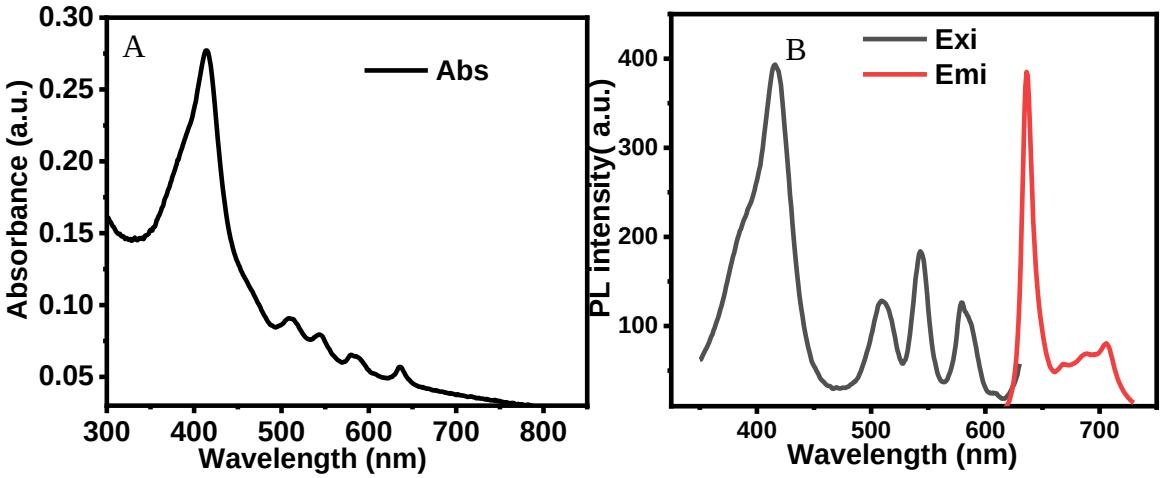

Figure 1. (A) Absorption and (B) photoluminescence (Excitation wavelength = 420 nm and Emission wavelength= 630 nm) spectra of PPIX.

3.3. RESULTS

3.3.1. Absorption and Photoluminescence spectra of PPIX and Cu-Cy

In this work, we have used PPIX as a representative traditional photosensitizer. PPIX is commonly used in the form of its prodrug aminolevulinic acid (ALA), which then converted into PPIX inside the body. [26] The ALA induced PPIX has US FDA approval for the non-oncological treatment of actinic keratosis. [24,127]

The absorption and PL spectra of PPIX are presented in **Figure 1**. PPIX exhibits a strong Soret peak at 405 nm and four relatively weaker Q bands between 500 -700 nm (**Figure 1A** and **1B**), suggesting that PPIX can easily be excited by UV radiation, visible light, and infrared radiation. Similar to PPIX, most of the existing porphyrin or chlorin based clinical and pre-clinical photosensitizers are excitable by wavelength in visible or NIR region, thereby generating ROSs and leading to various toxic side effects.[14,45,127–129] In terms of energy, sunlight spectrum possesses 3-5% ultraviolet radiation, 42-43% Visible light, 52-55% infrared light. As a result,

current porphyrin and chlorin based sensitizers treated patients tend to produce mild to severe photosensitivity following the sunlight exposures.

One way to combat the photosensitivity issue of current photosensitizers is to develop novel sensitizers that can be excited by alternative excitation sources such as X-ray, microwave, ultrasound, and UV light but not by visible light. In this direction, we invented a transition-metal based copper cysteamine nanoparticles that can be excited by X-ray, MW, US, and UV radiation but not by visible light. [55–57,59,61] As displayed in **Figure 2A**, the Cu-Cy nanoparticles have an absorption band in the UV region, with the absorption peak at 365 nm. Furthermore, Cu-Cy nanoparticles have an excitation peak at 365 nm (**Figure 2B**, black line) and emission peaks at 607 and 633 nm (**Figure 2B**, red). Consequently, it can be anticipated that Cu-Cy may not be excited by visible light and could be much safer than current clinical photosensitizers in terms of unwanted photosensitivity.

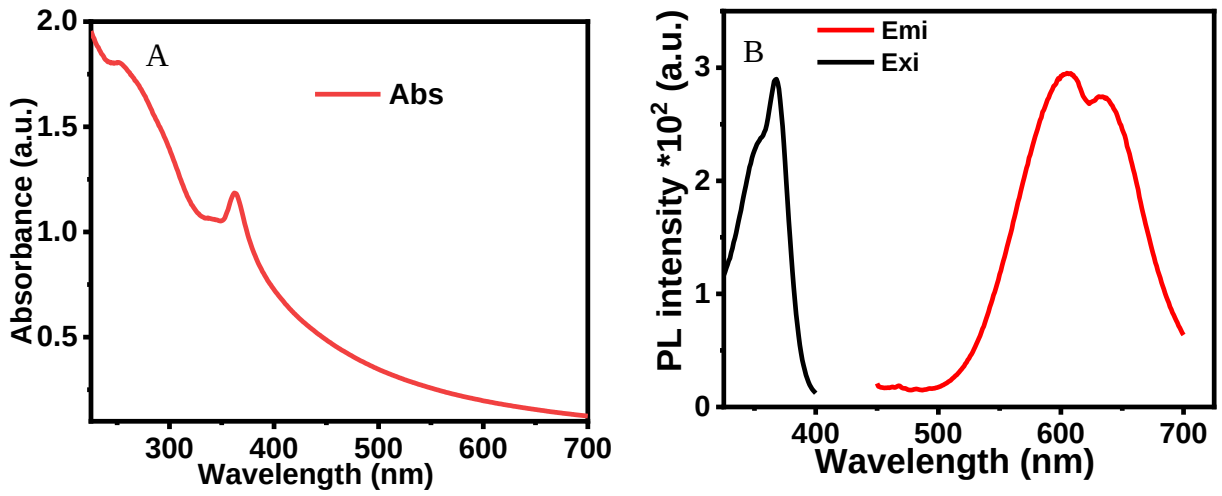

Figure 2. Absorption and photoluminescence spectra (excitation wavelength = 365 nm, emission wavelength = 607 nm) of copper cysteamine nanoparticles.

3.3.2. In Vitro Studies

3.3.2.1 MTT assay

MTT assay was conducted to evaluate the sunlight-induced phototoxicity in vitro. Two healthy cell lines (HDF and HET1A) were chosen. The PPIX and Cu-Cy treated cells were either protected from light or exposed sunlight for 10 min. Clear sunny days were chosen during Summer and Fall in the University of Texas at Arlington, Arlington, Texas, for sunlight irradiation. As presented in **Figure 3A**, the Cu-Cy induced minimal dark toxicity towards both cell lines when 1.88 - 15 μg/mL of Cu-Cy nanoparticles was applied. However, the cell viability drops to around 70% for both the cell lines when 30 μg/mL of Cu-Cy was used. Likewise, PPIX treated cells exhibited good but slightly lower cell viability as compared to the Cu-Cy treated cell lines.

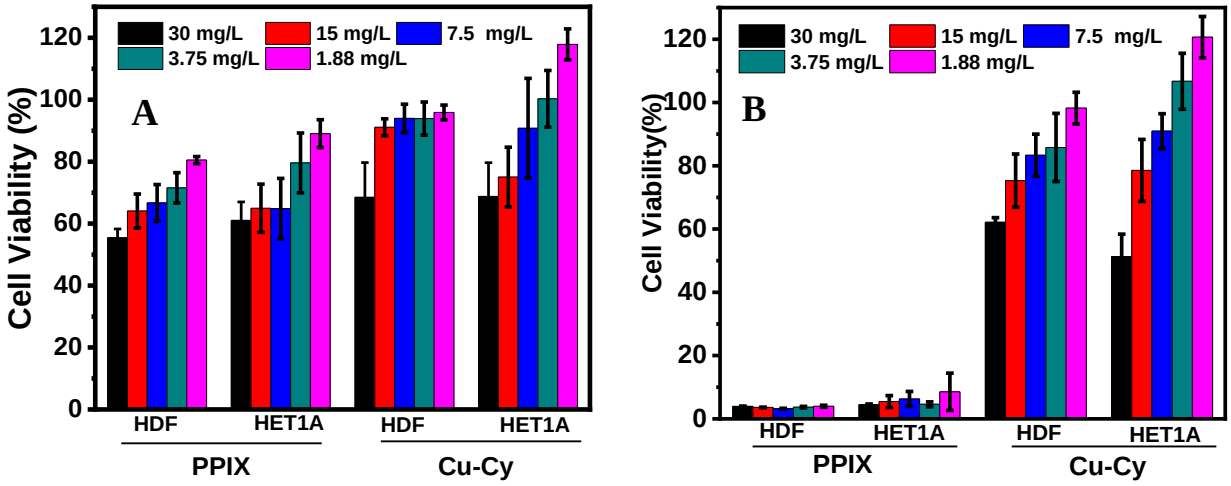

Figure 3. (A) Evaluation of dark toxicity and (B) sunlight toxicity of Cu-Cy and PPIX towards healthy cell lines (HDF and HET1A) using MTT assay.

Sunlight toxicities induced by PPIX and Cu-Cy to HET1A and HDF cell lines are presented in **Figure 3**B. The result shows that PPIX treated cells were completed destructed when exposed to sunlight for 10 mins. On the other hand, Cu-Cy treated cells exhibit good viability in the concentration range of 1.88 –15 μg/mL. The cell viability reduced to around 60% for HDF cell

lines and 50% for HET1A when 30 μg/mL of Cu-Cy was used. The result suggests that PPIX is much more toxic under sunlight irradiation, while Cu-Cy did not induce obvious sunlight toxicity.

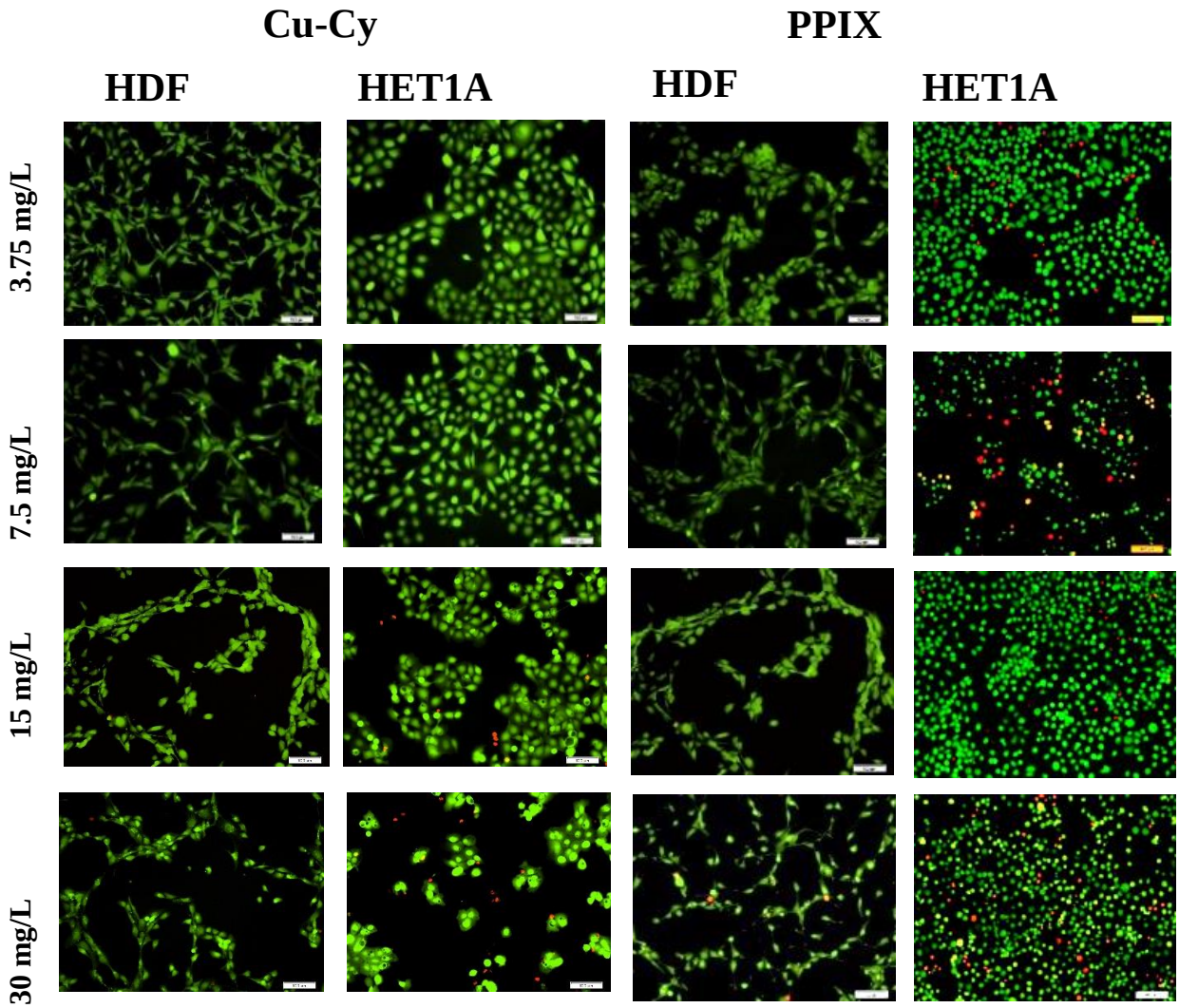

Figure 4: Evaluation of dark toxicity of Cu-Cy and PPIX towards HET1A and HDF using Live/Dead assay. Green color represents calcein-positive (live cells), and red color represents Ethidium homodimer-1 (dead cells). (scale bar= 100 μM).

3.3.2.2. Live/dead assay

To further compare the viability of PPIX and Cu-Cy treated healthy cell lines under dark and sunlight exposure, Live/dead assay was carried out. As can be seen in **Figure 4**, Cu-Cy

nanoparticles caused minimal toxicity towards both HDF and HET1A under dark conditions. PPIX treated cells also showed good viability, except there was a significant amount of round shaped cell bodies, indicating that PPIX induces apoptosis under dark conditions. The result is consistent with the previous report, where PPIX was found to induce apoptosis to HeLa cells under dark conditions.[130]

Figure 5 presents the live/dead assay results of Cu-Cy and PPIX applied cells following the sunlight treatment. Most of the PPIX treated cells were dead (Ethd-1 positive) when irradiated with sunlight. On the other hand, Cu-Cy treated cells were mostly viable with sunlight exposure. The result suggests that Cu-Cy can not be activated by sunlight exposure, which is in contrast to what was observed with PPIX treated cell lines.

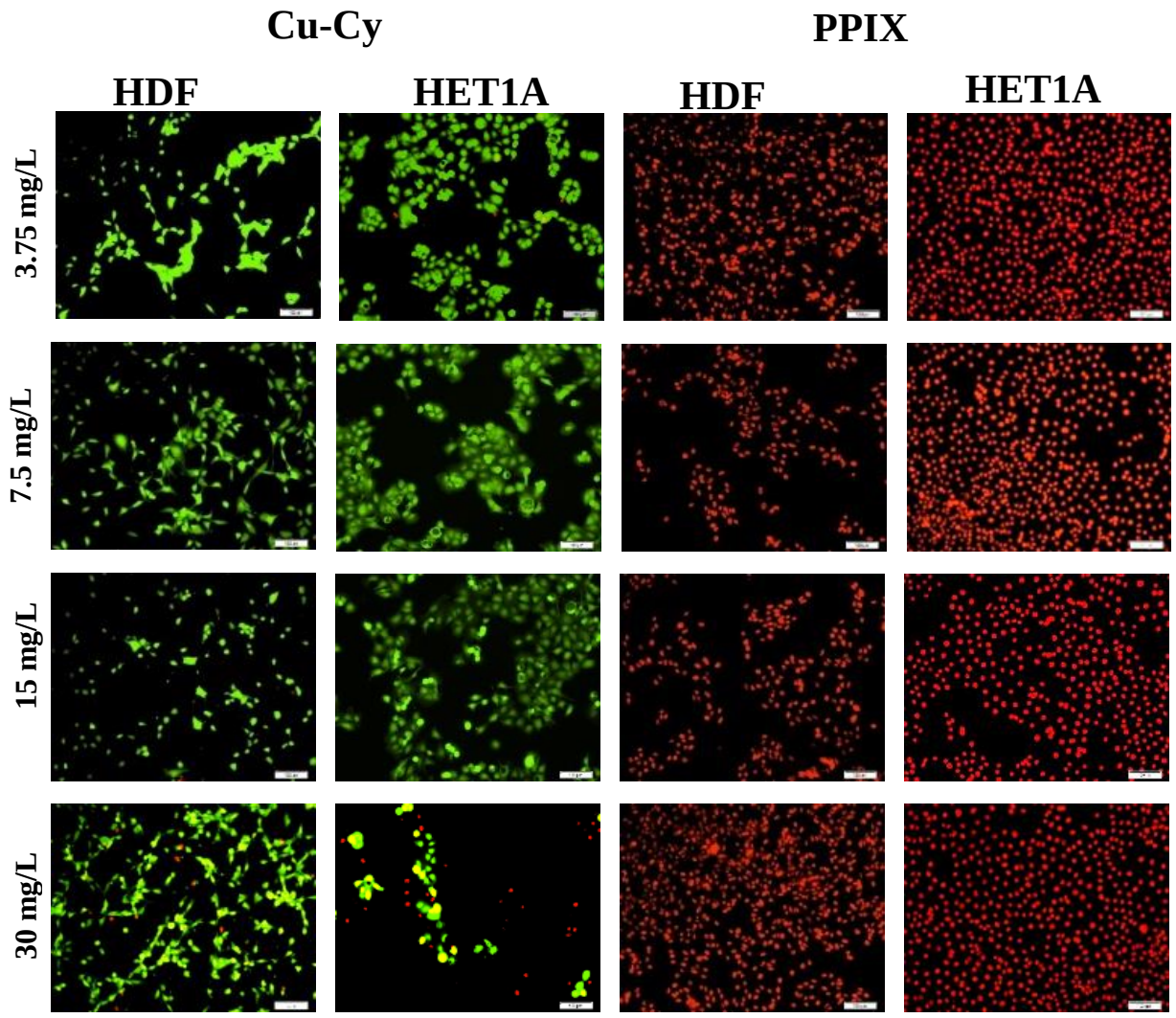

Figure 5: Evaluation of sunlight toxicity of Cu-Cy and PPIX using Live/Dead assay. Green and red colors represent live and dead cells, respectively. (Scale bar =100 μM)

3.4. DISCUSSION

Unwanted photosensitivity is one of the major limitations of current photosensitizers. Most of the clinical and pre-clinical photosensitizer are porphyrin or chlorin based, which have excitation wavelength in the UV-NIR region. Since the sunlight spectrum consists of 44% of visible light, photosensitizers with excitation wavelength in the visible range are prone to produce a phototoxic

effect when the PDT treated patients are exposed to sunlight. Photofrin, first FDA approved photosensitizer, was found to induce mild to severe photosensitivity even when hospital recommendations were strictly followed.[14] A significant level of photosensitivity issue has also been reported in Foscan, a second-generation photosensitizer, for a prolonged period. [45,50] Although some improvements have been reported in recent sensitizers, photosensitivity remains as one of the major limitations of photodynamic therapy.[44] The photosensitivity issue, however, is somehow anticipated owing to their intrinsic nature. Daylight is even being used in some countries as painless photodynamic therapy.[131] In this regard, photosensitivity is somewhat anticipated and may not be completely avoidable in photodynamic therapy. The only practical way to solve the issue is to devise a new type of sensitizers having alternative excitation sources, such as X-ray, microwave, or ultrasound.

Copper-cysteamine nanoparticles are recently invented sensitizers with excitation sources UV, MW, X-ray, and US. These nanoparticles have additional advantages, such as it can also be activated by internal cancer-specific stimuli such as H_2O_2/pH. Considering these multiway excitabilities of Cu-Cy NP, it is already advantageous than other photosensitizing and chemosensitizing drugs.

The present study was carried out with the aim of providing new avenue on designing sunlight toxicity free sensitizer. The result clearly demonstrates that copper-cysteamine nanoparticles do not induce obvious toxicity under sunlight exposure, which is in sharp contrast with what was observed with PPIX, a traditional photosensitizer. Furthermore, Cu-Cy NPs being activatable with multiple excitation sources, such as X-ray [54,56–58], microwave [59,60], ultrasound [61], and cancer-specific stimuli (pH/H_2O_2) [64] is already a superior sensitizer with the potential for deep

cancer treatment. Besides, the occurrence of minimal sunlight toxicity, as demonstrated in the present study, greatly enhances its translation potential. This work may provide some insight into improving the photosensitivity issue of the traditional photosensitizers.

3.5. CONCLUSION

In this contribution, we proposed copper-cysteamine nanoparticles as sunlight toxicity free sensitizer. The comparison of sunlight-induced toxicity of Cu-Cy NPs and a conventional photosensitizer (PPIX) was carried out in vitro, and the result suggests that Cu-Cy NPs produce significantly lower sunlight toxicity when compared to PPIX. This study not only makes Cu-Cy NPs a strong candidate of next-generation nanomedicine but also provide an approach to devise novel sensitizer with translation potential.

Chapter 4:

COPPER-CYSTEAMINE NANOPARTICLES AS A HETEROGENEOUS FENTON-LIKE CATALYST FOR HIGHLY SELECTIVE CANCER TREATMENT

Lalit Chudal[a], Nil Kanatha Pandey[a], Jonathan Phan[a], Omar Johnson[a], Liangwu Lin[b], Hongmei Yu[c]*, Yang Shu[d], Zhenzhen Huang[e], Meiying Xing[a], J. Ping Liu[a], Minli Chen[d]*, and Wei Chen*[a]

[a]Department of Physics, The University of Texas at Arlington, Arlington, Texas 76019, USA

[b] Laboratory on High-Strength Structural Materials, Central South University, Changsha 410083, P. R. China

[c] School of Chemical Engineering, University of Science and Technology Liaoning, Anshan 114051, China

[d] Department of Chemistry, College of Sciences, Northeastern University, Shengyang 110819, China

[e] Jilin University, Changchun, Jilin, China

*Corresponding authors: weichen@uta.edu (W. Chen); chenml@mail.neu.edu.cn (M. L. Chen); seesea0304@163.com (H. M. Yu)

Permission obtained from ACS Applied Bio Materials

Chudal L, Pandey NK, Phan J, Johnson O, Lin L, Yu H, Shu Y, Huang Z, Xing M, Liu JP, Chen ML. Copper-cysteamine Nanoparticles as a Heterogeneous Fenton-like Catalyst for Highly Selective Cancer Treatment. ACS Applied Bio Materials. 2020 Feb 10.

ABSTRACT

Herein, for the first time, we report copper-cysteamine (Cu-Cy) nanoparticles having Cu^{1+} instead of Cu^{2+} as an efficient heterogeneous Fenton-like catalyst for highly selective cancer treatment. Initial measurements of Cu-Cy's hydroxyl radical generation ability show that it behaves as a Fenton-like reagent in the presence of H_2O_2 (100 µM) at pH = 7.4 and that its Fenton-like activity is dramatically enhanced under acidic conditions (pH = 6.5 and 5.5). Notably, Cu-Cy exhibits high stability and minimal copper release during the Fenton-like reaction, demonstrating its potency as a heterogeneous Fenton-like catalyst with a low cytotoxic effect. Through extensive in vitro studies, Cu-Cy NPs are found to generate a significantly higher level of ROS, thereby causing significantly more destruction to cancerous cells than to normal cells without the need for exogenous additives, such as H_2O_2. To the best of our knowledge, the average IC-50 value of Cu-Cy to cancer cells (11 µg/mL) is the lowest among reported heterogeneous Fenton-like nano-catalyst so far. Additionally, compared to cancer cells, Cu-Cy NPs display substantially higher IC-50 value towards normal cells (50 µg/mL), suggesting high selectivity. Overall, Cu-Cy NPs can participate in heterogenous Fenton-like activity with elevated H_2O_2 under acidic conditions to produce significantly higher levels of hydroxyl radicals in cancer cells when compared to normal cells, resulting in selective cytotoxicity to cancer cells.

Keywords: Copper-cysteamine, Heterogenous, Fenton reaction, hydrogen peroxide, cancer treatment, Fenton therapy, low pH, highly selective, Nanoparticles, hydroxyl radical

4.1 INTRODUCTION

The vast majority of conventional cancer drugs lack selectivity, leading to the manifestation of toxic effects on healthy cells resulting in numerous side effects. One of the most effective ways to

enhance the selectivity of cancer drugs is to fabricate a drug that can be activated by cancer-specific stimuli.[65,66] The tumor microenvironment (TME) is characterized by mild acidity,[67] elevated H_2O_2 levels,[30] hypoxia,[29,119] low catalase activity,[31] and elevated levels of GSH.[68] Although the unique TME aids in cell proliferation and metastasis, it can also be exploited to design effective and highly selective cancer treatment modalities. In fact, in the past few decades, we have witnessed numerous cancer treatment modalities which exploit the unique tumor microenvironment.[43,65,66,69]

Fenton reactions refer to the process in which Fe and its salts catalyze the conversion of H_2O_2 to $^{\bullet}OH$.[78,132] If other cations, such as Cu, Ag, Mn, and Au, participate in the catalytic conversion, then such reactions are referred to as Fenton-like reaction.[132] Considering elevated levels of H_2O_2 and slightly acidic pH in TME, Fenton and Fenton-like reactions can be exploited to achieve highly selective cancer treatment. In recent years, several redox-active nanoformulations, mainly iron-based, were designed and investigated for their potential in Fenton reactions mediated cancer treatment modalities.[80,81,133–140] However, Fe-based Fenton reagents are optimally effective only in low pH conditions ($pH < 4$) that are beyond what would be encountered in their applied biological context, thereby limiting their practicality in future clinical settings.[79,132,141,142] Consequently, most Fe-based Fenton reagents require exogenous additives, including ascorbic acid and H_2O_2 to achieve a desired therapeutic outcome.[134,136,137,143] Additionally, the nanocatalysts that were used without external additives needed to be administered at high doses in order to achieve desired therapeutic outcomes.[133,135,144]

Cu-based materials are regarded as an efficient Fenton catalyst at circumneutral pH[141] and have thus been considered excellent candidates to be the basis for developing new cancer treatments. Furthermore, it is noteworthy mentioning that the highest reaction rate of Cu^{1+} with H_2O_2 (10^4

$M^{-1}s^{-1}$) is considerably higher than that of Fe^{2+} (63 $M^{-1}s^{-1}$).[145] Despite their ability to undergo Fenton-like catalysis at circumneutral pH, only a handful of studies using Cu based Fenton catalysts have been reported as cancer-killing agents.[85,87,146–148] Among reported catalysts, heterogeneous Fenton-like catalysts show great promise as they can generate •OH in the targeted region without leaching free metal ions, thereby avoiding unwanted toxicity. In particular, Ma et al. developed a promising Cu^{2+} based heterogenous nano-catalyst that can be activated by GSH and H_2O_2 following a logic "AND" gate, however, this catalyst requires a high dose of 200 μg/mL for optimum efficacy.[85] Higher levels of copper could cause damage to vital organs, including the brain and liver. Therefore, if Cu-based catalysts are to be used for cancer therapy, then we must find a way to lower their effective dose such that they may be physiologically tolerable. One way to improve the efficiency of a heterogenous Cu-based catalyst is developing the catalyst that has copper in its reduced state (Cu^{1+}) rather than in its oxidized state (Cu^{2+}) as the reaction rate of Cu^{1+} is approximately 22 times faster than that of Cu^{2+} (eqn.1-2).[82]

$$Cu^{1+} + H_2O_2 \rightarrow Cu^{2+} + \bullet OH + OH^- \quad (k = 1\times10^4\ M^{-1}S^{-1}) \quad (1)$$

$$Cu^{2+} + H_2O_2 \rightarrow Cu^{1+} + \bullet HO_2^- + H^+ \quad (k = 460\ M^{-1}S^{-1}) \quad (2)$$

Copper-cysteamine nanoparticle (Cu-Cy NP)[88] is a novel sensitizer having Cu^{1+} instead of Cu^{2+}, which can be stimulated by X-ray,[57,88,149] UV-light,[88] microwave,[59,60] and ultrasound[61] to produce various types of ROS for cancer treatment. Furthermore, Cu-Cy can be used to inactivate bacteria upon UV light activation.[150] The Cu-Cy NP being activatable by multiple excitation sources, is already a promising candidate for a new nanomedicine to combat cancer. However, activation of Cu-Cy by some cancer-specific stimuli has never been investigated before. Due to the existence of Cu^{1+}, Cu-Cy NPs can be anticipated to act as an efficient Fenton like reagent for highly selective cancer treatment, as discussed above.

In this work, Cu-Cy NPs are explored for their heterogeneous Fenton-like activity and their potential use in highly selective cancer therapy. To the best of our knowledge, this is the first work that uses Cu^{1+} based nanoparticles for Fenton-like reaction mediated cancer therapy without the involvement of external excitation sources. The $^{\bullet}OH$ produced by Cu-Cy NPs and H_2O_2 (100 µM) in aqueous solutions were systematically explored at different pHs and doses using coumarin as an $^{\bullet}OH$ detecting probe. Through extensive in-vitro studies, the selective cancer-killing ability of Cu-Cy NPs was assessed.

4.2. EXPERIMENTAL SECTION

4.2.1. Materials

Copper(II) chloride dihydrate (99.99%), polyethylene glycol 4000 (PEG-4000), 2-mercaptoethylamine hydrochloride (cysteamine hydrochloride or Cys, 98%), and sodium hydroxide (98%) were obtained from Sigma (USA). MTT assay (3-(4,5-dimethylthiazol-2-yl)-2,5-diphenyltetrazolium bromide) and live/dead cell viability assays were purchased from Thermo Fisher Scientific. All chemicals were used as obtained without further purification.

4.2.2. Instrumentations

A UV-vis spectrophotometer (Shimadzu UV-2450) and a photoluminescence spectrophotometer (Shimadzu RF-5301PC, Tokyo, Japan) were used to measure absorption and photoluminescence spectra of samples, respectively. The size and crystallinity of the samples were studied by using a TEM-2100 HR transmission electron microscope (TEM, JEOL Ltd., Japan). X-ray powder diffraction (XRD) with a 2θ angle ranging from $5\text{-}80^0$ was carried out employing a Rigaku Ultima IV diffractometer with Cu K_α radiation (λ = 0.15406 nm) operated at 40 kV and 40 mA with step-size 0.02 ^{0}/sec. To prepare XRD sample, the sample solution was deposited on a glass substrate and allowed to dry out overnight. The oxygen consumption rate (OCR) spectra were collected

using an XFp analyzer (demo version) (Seahorse Bioscience, North Billerica, MA, USA). Fourier transform infrared (FTIR) spectra of the samples were collected using a Shimadzu IRPrestige/PIKE MIRacle FTIR spectrometer.

4.2.3. Synthesis and characterization of Cu-Cy

Cu-Cy NPs were synthesized using a facile synthesis method as reported in our recent publication.[59] Briefly, 273 mg of $CuCl_2.2H_2O$ was dissolved in 50 mL of DI water at room temperature. Then, 381 mg of cysteamine hydrochloride and 40 mg of PEG-4000 was introduced into the solution under an inert atmosphere. Afterward, the pH was adjusted to 7. Following the pH adjustment, the inert atmosphere was removed and the solution was stirred for 5 min until the solution turned to deep violet color. The solution was subsequently heated at 100 ^{0}C for 5 min under the inert environment with vigorous magnetic stirring. The solution was cooled to ambient temperature, centrifuged, and washed with DI water and ethanol 3 times to obtain the Cu-Cy particles. The obtained product was then dried in a vacuum oven at 40 ^{0}C overnight.

4.2.4. Study of Fenton-like reaction in aqueous solution

4.2.4.1. Hydroxyl radical (•OH) measurement

Cu-Cy NPs were examined for their ability to participate in Fenton-like reactions using coumarin as the •OH detection probe.[151,152] A typical testing solution contained an appropriate amount of Cu-Cy, H_2O_2, and 0.1 mM coumarin at different pH values (7.4, 6.5, and 5.5). The PL spectrum of coumarin with excitation 332 nm was monitored at various time intervals for up to 6 h. The PL intensity of coumarin at 452 nm was plotted against various time intervals to serve as a semi-quantitative •OH detection.

3.2.4.2. Stability study

To determine whether free coppers were leached from the Cu-Cy during Fenton-like reactions, a spectrophotometric technique was employed.[153] Briefly, we prepared a standard calibration curve between Cu^{+2} concentration and absorbance by using $CuCl_2.2H_2O$ as a source of free Cu^{+2} **(Figure S2)**. 1 mg/mL of Cu-Cy and 100 µM of H_2O_2 were mixed and incubated for 24 h at room temperature. Then, the mixture was centrifuged at 12000 rpm for 30 min and the supernatant was used to detect any free copper leached from Cu-Cy. A 3 mL testing solution was prepared by mixing 1200 µL of the supernatant of the sample, 300 µL of PEI, 300 µL of Bronstate-Robinson buffer, and 1200 µL of DI water. Absorption of the testing solution was collected, and the calibration equation $A= 4093.964C \pm 0.03327$ was used to determine the concentration of Cu^{2+}. $CuCl_2$ (0.2 mM), a source of free Cu^{2+}, was used as a positive control.

The stability of Cu-Cy during the Fenton-like reaction was also assessed by monitoring PL intensity of Cu-Cy incubated with or without H_2O_2 under different pHs at various time points up to 24 h. The XRD patterns and FTIR spectra of Cu-Cy incubated with or without H_2O_2 (pH 7.4 and 5.5) for 24 h were also collected in order to determine the stability of Cu-Cy NPs during the Fenton-like reaction.

3.2.5. In-Vitro ROS measurement

2',7'-dichlorofluorescein diacetate (DCFH-DA) was employed to detect intracellular ROS levels after Cu-Cy treatment. 2×10^5 cells per imaging plate were cultured and incubated for 24 h. Then, the old media was replaced with new media with or without Cu-Cy (30 µg/mL) and incubated overnight. On the next day, the cells were treated with serum-free media containing 20 µM of DCFH-DA and incubated for 1 h. Afterward, the cells were replaced with regular media and

imaged using an Olympus IX-71 fluorescence microscope (495/515 nm filter), keeping the same exposure time and sensitivity throughout the experiment.

The DCF intensities were quantified using ImageJ software as follows: first, the background luminescence of each image was subtracted. Next, the "Threshold" function was applied to select only DCF luminescence in the cellular body. Finally, "Measure" function was used to obtain the average gray value of the DCF luminescence.

3.2.6. In vitro selective toxicity study

3.2.6.1 Oxygen consumption rate assay

The effect of Cu-Cy on the mitochondrial function of the cancer cell lines (KYSE-30 and DM6) and normal (HET1A) cells were evaluated by measuring the oxygen consumption rates (OCR) via the Seahorse XFp analyzer. The cells were seeded in XFp culture microplates (Seahorse Bioscience, North Billerica, MA, USA). Each plate was seeded with 3×10^4 cells/well in 80 µL of culture medium. Following 2 h of incubation, various concentrations of 120 µL of Cu-Cy was added so that a final concentration of 45, 30, 22.5, and 11.25 mg/L in a 200 µL culture medium were achieved. The plates were then incubated overnight in a humidified incubator (37 ^{0}C, 5% CO_2). The control group was supplemented with 120 µL of the respective medium. On the next day, the culture media was replaced with freshly prepared Seahorse Assay Media (Seahorse Bioscience, Billerica, MA) and incubated in a non-CO_2, 37 ^{0}C incubator for 1 h.

After measuring the basal OCR, a number of mitochondrial modulators were sequentially injected. First, 2 µM oligomycin (an ATP synthase inhibiter) was added to determine the respiration contributed by proton leakage. After that, a mitochondrial uncoupler (FCCP(0.5 µM)) was used to

force the cells to operate at their maximal respiration rates. Finally, Rotenone/antimycin (0.5 μM), a mitochondrial oxidative phosphorylation inhibitor, was used. Various respiration parameters were obtained by using the manufacturer's built software (Wave). To compare the effect of Cu-Cy on OCR values of different cell lines, they were expressed as the percentage of the respective control group (without Cu-Cy).

3.2.6.2. Live/dead cell assay

We also performed live/dead assay to evaluate cell viability. 2×10^5 cells were seeded in a 35 mm petri-dish and then incubated at 37 ^{0}C in a humidified atmosphere of 5 % v/v CO_2 for 24 h. Then, 1 mL of new media containing desired concentrations of Cu-Cy NPs were added to the Petri-dishes. The cell samples were stained with 0.25 μmol/L of calcein-AM and 5 μmol/L of ethidium homodimer-1 (Invitrogen, USA) for 45 min at 37 °C. Fluorescent images were then taken with an Olympus IX-71 fluorescence microscope. The results of the live/dead assay were quantified using the "Particle analyzer" feature of imageJ.[31–33] The detailed quantification method can be found in supporting information.

3.2.6.3. Bright-field imaging

To observe the changes in the morphology of the cell lines following the Cu-Cy treatment, bright field imaging of the cells were collected with the help of an Olympus IX-71 fluorescence microscope.

3.2.6.4. MTT assay

The cytotoxicity of Cu-Cy to cancer and normal cell lines were further evaluated using MTT assay.[30] 1×10^4 cells/well were seeded in 96 well plates and incubated for 24 h. A stock solution of a desired concentration of Cu-Cy was prepared in DI water. 100 μL of various doses of Cu-Cy

NPs were applied and incubated for 24 h. Afterward, the old media was replaced with 100 µL of MTT assay and incubated for 3 h. Then, 150 µL DMSO was used to solubilize formazan crystals, and the absorption of the purple-colored formazan crystals was measured using a microplate reader (Multiskan). Cell viability was then calculated as presented in the following equation:

$$\text{Cell viability} = \frac{\text{The absorbance of the treatment group}}{\text{The absorbance of the control group}} * 100\%$$

Selectivity was quantified by calculating selectivity index[135] as follows:

$$\text{Selectivity index} = \frac{\text{IC} - 50 \text{ of normal cells}}{\text{IC} - 50 \text{ of cancer cells}}$$

All the data were collected at least three times and expressed as mean ± standard error of mean unless otherwise stated. To determine the statistical significance of difference, one-way of analysis of variance (ANOVA) was performed. $P < 0.05$ was considered as a significant differenc

4.3. RESULTS AND DISCUSSION

4.3.1. Characterization of as-synthesized Cu-Cy

The excess amount of cysteamine can reduce Cu^{2+} of $CuCl_2$ to Cu^{1+} resulting in a highly crystalline copper(I)-cysteamine nanoparticles (Cu-Cy NPs).[88] It has been reported that Cu-Cy NPs are highly sensitive to different external stimulating agents such as UV-light, X-rays, ultrasound, and microwave to produce reactive oxygen species and therefore explored as a potential drug for cancer treatment.[57,59–61,88,149] The optical properties of as-synthesized Cu-Cy NPs were studied by measuring UV-vis absorption and PL spectrum. **Figure 1A** shows that Cu-Cy has an absorption in the UV region with a strong peak at 365 nm. As displayed in **Figure 1B**, the PL spectrum of Cu-Cy has two emission peaks at 607 nm and 633 nm with an excitation peak at 365 nm. The two

emission peaks can be attributed to two different types of Cu atoms (Cu(1) and Cu(2)) in Cu-Cy structure as reported in our previous work.[88] **Figure 1C** presents images of Cu-Cy dispersed in DI water under ambient light (left) and UV light (right). The XRD pattern of as-synthesized Cu-Cy was also carried out **(Figure 1D)** and found to match with our previous reports.[59,88] The HRTEM (**Figure 1E**) depicts high crystallinity of as-synthesized Cu-Cy NPs. A representative TEM image of Cu-Cy NPs used in this work is presented in **Figure 1F.**

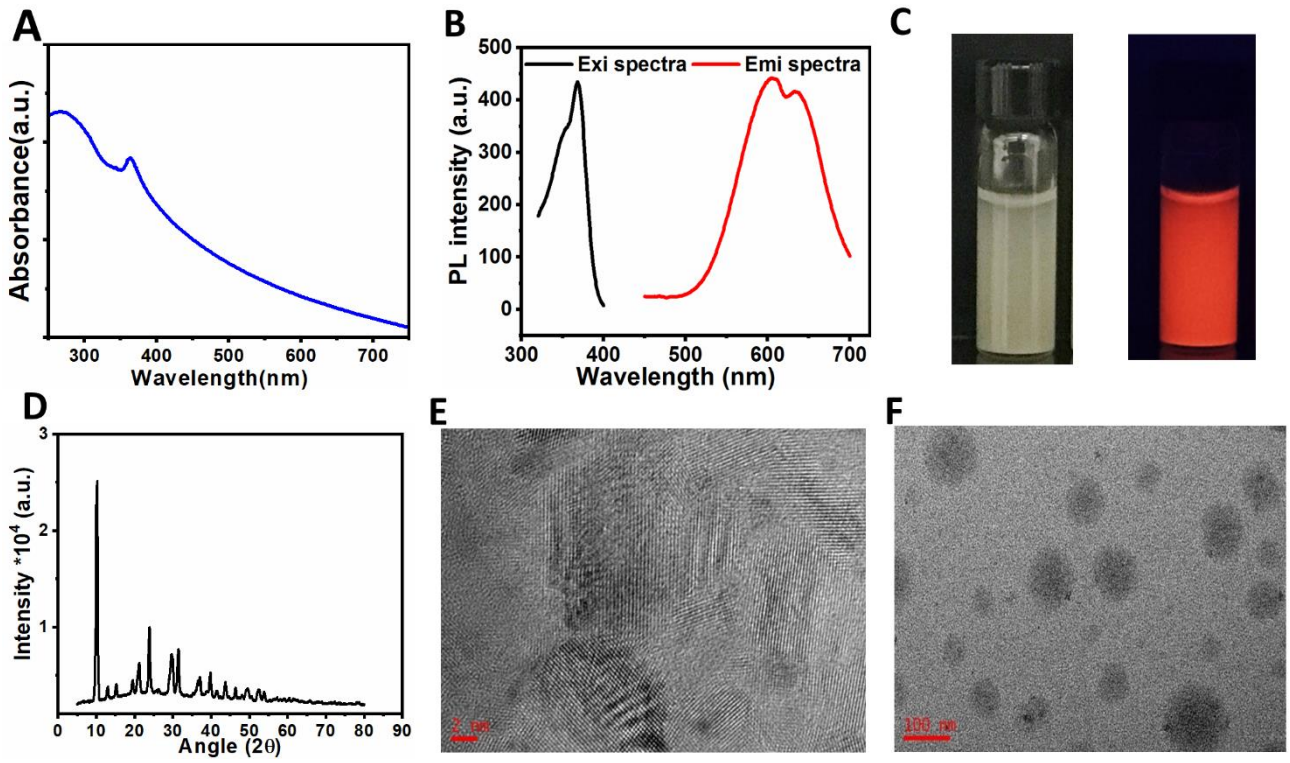

Figure 1. (A) Absorption spectrum of Cu-Cy NPs dispersed in DI water. (B) Photoluminescence spectra of Cu-Cy with excitation and emission peaks taken at 365 nm and 607 nm, respectively. (C) Image of Cu-Cy dispersed in DI water under ambient light (Left) and UV light (Right). (D) XRD pattern of Cu-Cy powders. (E) HRTEM image of Cu-Cy NPs. (F) A representative TEM image of Cu-Cy NPs used in this study.

4.3.2. Study of Fenton-like reaction mediated by Cu-Cy

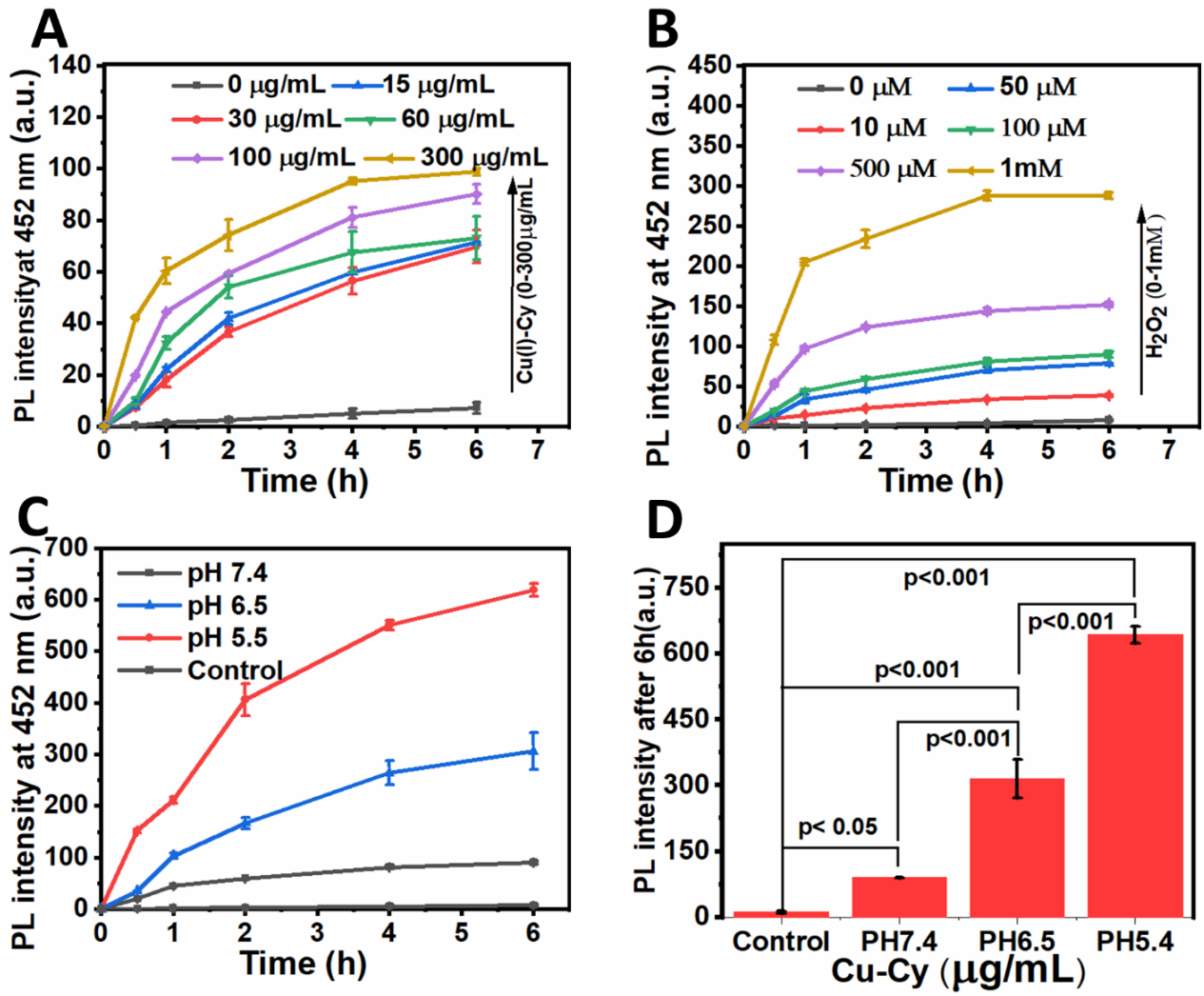

Figure 2. Measurement of hydroxyl radical generated by Cu-Cy/H_2O_2 using coumarin as a probe. The ˙OH produced by (A) Cu-Cy (0-300 μg/mL) and H_2O_2 (100 μM) and (B) Cu-Cy (100 μg/mL) and (0-1mM H_2O_2) at various time intervals. (C) The ˙OH generated by Cu-Cy (100 μg/mL)+ H_2O_2 (100 μM) at different pH conditions and (D) statistical analysis of ˙OH production after 6h of (C).

It is no secret that Cu^{1+}/Cu^{2+} can actively catalyze H_2O_2 to produce ˙OH via a Fenton-like reaction.[83,84] Consequently, Cu-Cy NPs are expected to act as a heterogeneous Fenton-like catalyst for the conversion of H_2O_2 to ˙OH. The catalytic effect of Cu-Cy was studied using coumarin as an ˙OH detecting probe. The non-fluorescent coumarin becomes a fluorescent 7-hydroxycoumarin with excitation and emission peaks at 332 nm and 452 nm,[152] respectively.

The PL spectra of coumarin, with an excitation wavelength at 332 nm, were collected at various time intervals, and the PL intensity at 452 nm was plotted against corresponding time points to serve as the semi-quantitative representation of the ˙OH generated.

The ˙OH generated by various concentrations of Cu-Cy (0-300 µg/mL) and H_2O_2 (100 µM) is presented in **Figure 2A** and **S1A**. The PL intensity of 7-hydroxycoumarin increased with the increase in the Cu-Cy dosages, suggesting a higher level of ˙OH formation with increases in the Cu-Cy dose. Likewise, the ˙OH generated by various concentrations of H_2O_2 (0-1 mM) and Cu-Cy (100 µg/mL) demonstrated a clear correlation between ˙OH generation and H_2O_2 concentration **(Figures 2B** and **S1B)**. The results suggest that ˙OH generation depends upon the dose of the catalyst (Cu-Cy) and H_2O_2, ensuring the increasing levels of ˙OH production in cancer cells due to the elevated levels of H_2O_2 (100 µM-1mM). Subsequently, we measured the ˙OH produced by Cu-Cy (100 µg/mL) in the presence of 100 µM H_2O_2 at different pH values (pH= 7.4, 6.5, and 5.5), and the result is presented in **Figures 2C** and **S1C**. The result suggests that even at pH 7.4, Cu-Cy + H_2O_2 can produce significantly more ($p < 0.05$) ˙OH than that of the control (Cu-Cy without H_2O_2).

Furthermore, when compared to pH =7.4, the ˙OH generation enhanced by 4 and 8 folds at pH=6.5 and pH =5.5, respectively. A detailed statistical analysis of ˙OH production at different pH after 6h of reaction is displayed in **Figure 2D**. The analysis showed that Cu-Cy + H_2O_2 produced significantly more ($p < 0.001$) ˙OH at pH = 6.5 and 5.5 as compared to pH = 7.4. These results collectively indicated that Cu-Cy NPs can exploit low pH and higher levels of H_2O_2 in cancer cells to yield substantial amounts of ˙OH, leading to the subsequent destruction of cancer cells.

4.3.3. Stability study during Fenton-like reaction

A spectrophotometric method[153] was employed to measure the free Cu^{2+} leached from Cu-Cy dispersion (1 mg/mL). This method is capable of measuring only free Cu^{2+} by making a PEI-Cu^{2+} complex that has a strong absorption at 275 nm and 630 nm **(Figure S2)**. **Figure 2B** displays free Cu^{2+} detected in the supernatant of Cu-Cy (1 mg/mL) incubated with or without H_2O_2 (100 µM). The control group showed 22 µM of free Cu^{2+}, which is equal to around 0.25% of the total available Cu (7936 µM, calculated from the molecular weight of Cu-Cy: $Cu_3Cl(SR)_2$ ($R=CH_2CH_2NH_2$), 378 g/moL) in 1 mg/ mL. Incubating Cu-Cy with H_2O_2 (100 µM) and pH = 5.5 did not leach significantly different amounts of free Cu^{2+} than the control group. The result eliminates any potential concerns regarding toxicity caused by copper leaching and signifies the stability of Cu-Cy during the Fenton-like reaction.

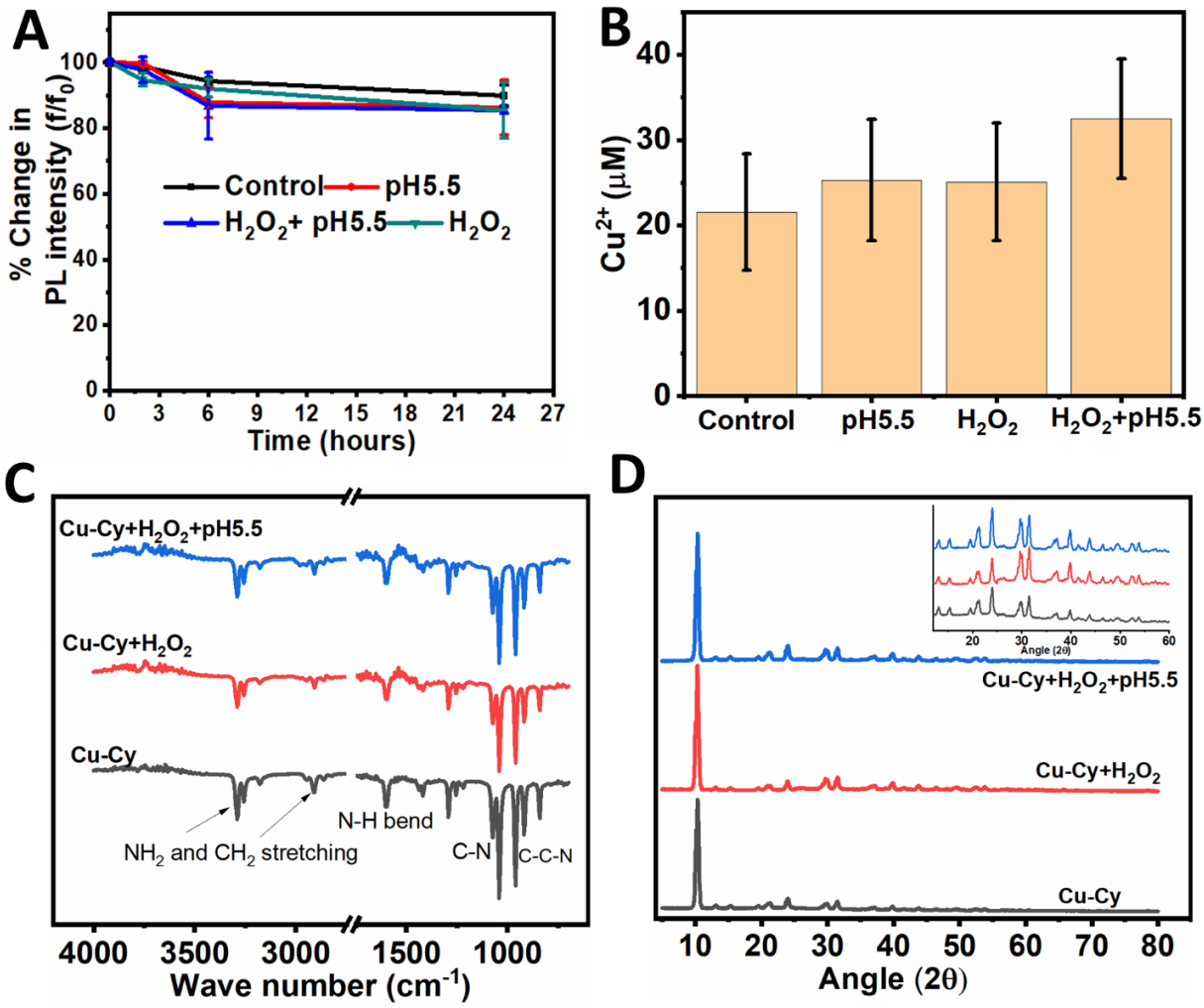

Figure 3. Stability test of Cu-Cy following the Fenton-like reaction. (A) The PL intensity change of Cu-Cy following the incubation with H_2O_2 up to 24 h. (B) Free Cu^{2+} detected in the supernatant of the Cu-Cy (1 mg/ mL) following the incubation with H_2O_2 (100 μM) up to 24 h. (C) FTIR spectra and (D) XRD patterns of Cu-Cy before and after Fenton-like reaction for 24 h.

The stability of Cu-Cy during the Fenton-like reaction was further assessed by monitoring the PL intensity of Cu-Cy incubated with or without H_2O_2 up to 24 h. As depicted in **Figure 3A**, there was no apparent difference in PL intensity between the control group, Cu-Cy + H_2O_2 and Cu-Cy + H_2O_2 + pH = 5.5 after 24 h incubation. From this result, we can infer the high stability of Cu-Cy during the reaction with endogenous levels of H_2O_2 (100 μM). The excellent stability of Cu-Cy

also suggests that it can continuously convert endogenous H_2O_2 to $^{\bullet}OH$ for many cycles, acting as a replenishable source of $^{\bullet}OH$ in cancer cells.

We further measured the FTIR spectra and XRD patterns of Cu-Cy before and after the Fenton-like reaction (**Figures 3C and D)**. As shown in **Figure 3C**, the FTIR spectra of Cu-Cy matched with previously reported results.[154] The peaks at 3300 cm^{-1}, 2800 cm^{-1}, and 1600 cm^{-1} correspond to NH_2 stretching, CH_2 stretching, and N-H bending, respectively. Additionally, the peaks that are in the range of 700-1300 cm^{-1} correspond to C-N and C-C-N vibrations. As can be seen in **Figure 3C**, the FTIR spectra of Cu-Cy after the incubation with H_2O_2 at pH 7.4 and H_2O_2 (100 μM) at pH 5.5 for 24 h did not noticeably change, indicating its high stability during Fenton-like reactions. Likewise, no change was noticed in the XRD pattern of Cu-Cy following the incubation with H_2O_2 (100 μM) at pH 7.4 and H_2O_2 (100 μM) at pH 5.5 during 24 h, further confirming the high stability of Cu-Cy (**Figure 3D)**. Overall, Cu-Cy exhibits high stability during the Fenton-like reaction, making it a potential candidate for Fenton-reaction mediated cancer therapy.

4.3.5. Intracellular ROS measurement:

In order to evaluate whether Cu-Cy can produce a higher level of ROS in cancer cells than in normal cells, we used DCFH-DA as a ROS detection probe. As shown in **Figure 4A**, the luminescence of DCF in HDF was not noticeably different for cells with or without Cu-Cy treatment, suggesting that Cu-Cy did not induce noticeable ROS generation in HDF (normal cells). On the contrary, Cu-Cy treated DM6 (cancer cells) showed noticeably higher luminescence than DM6 cells without Cu-Cy (control). **Figure 4B** represents the quantification of the DCF luminescence. The fluorescence (FL) intensity of DCF in Cu-Cy treated DM6 cells is significantly higher ($p < 0.01$) than that of the control. On the other hand, no such difference was noticed for

HDF cells treated with or without Cu-Cy. A similar outcome was observed for a breast cancer cell line (MCF-7); the FL intensity of DCF was substantially higher in Cu-Cy treated cells than in the control group, implying higher levels of ROS in Cu-Cy treated cell lines **(Figure S3)**. These results suggest that Cu-Cy can selectively produce higher amounts of ROS in cancer cells than in normal cells, most likely due to elevated levels of H_2O_2 and low pH in cancerous cells. The results further corroborate our hypothesis that Cu-Cy NPs can be exploited for highly selective cancer treatment.

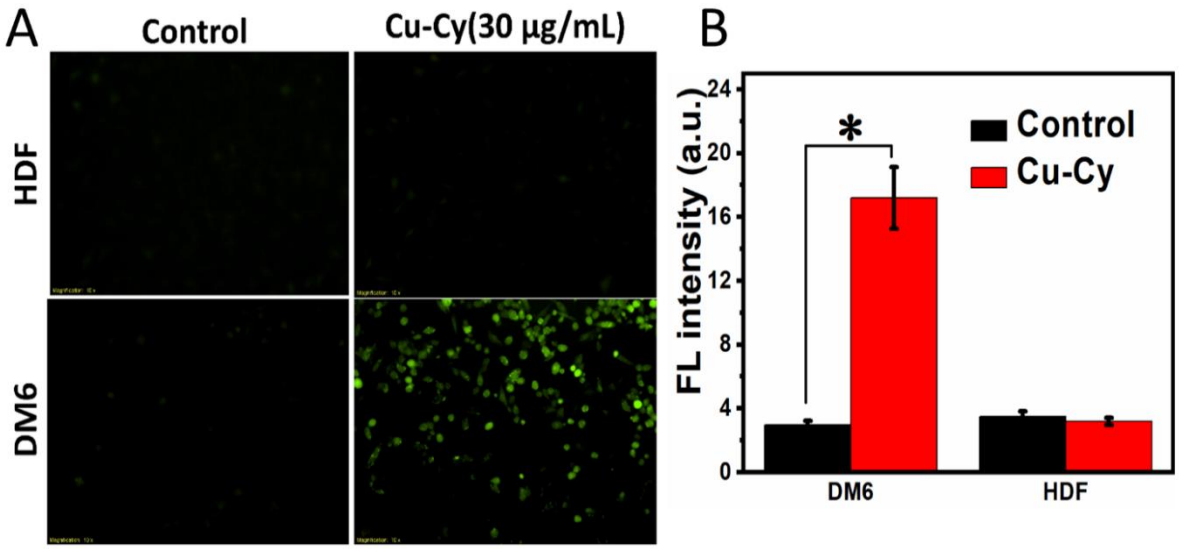

Figure 4. Intracellular •OH detection using DCFH-DA. (A) Representative images (B) Quantification of ROS level. The cells pre-incubated with or without Cu-Cy for 12h were treated with 20 µM DCFH-DA for 1 h. The green luminescence of DCF was imaged using 495/515 nm filter of Olympus IX-71 and quantified using imageJ. (* $p < 0.01$)

4.3.6. In-vitro selective toxicity

4.3.6.1. Oxygen consumption rate assay

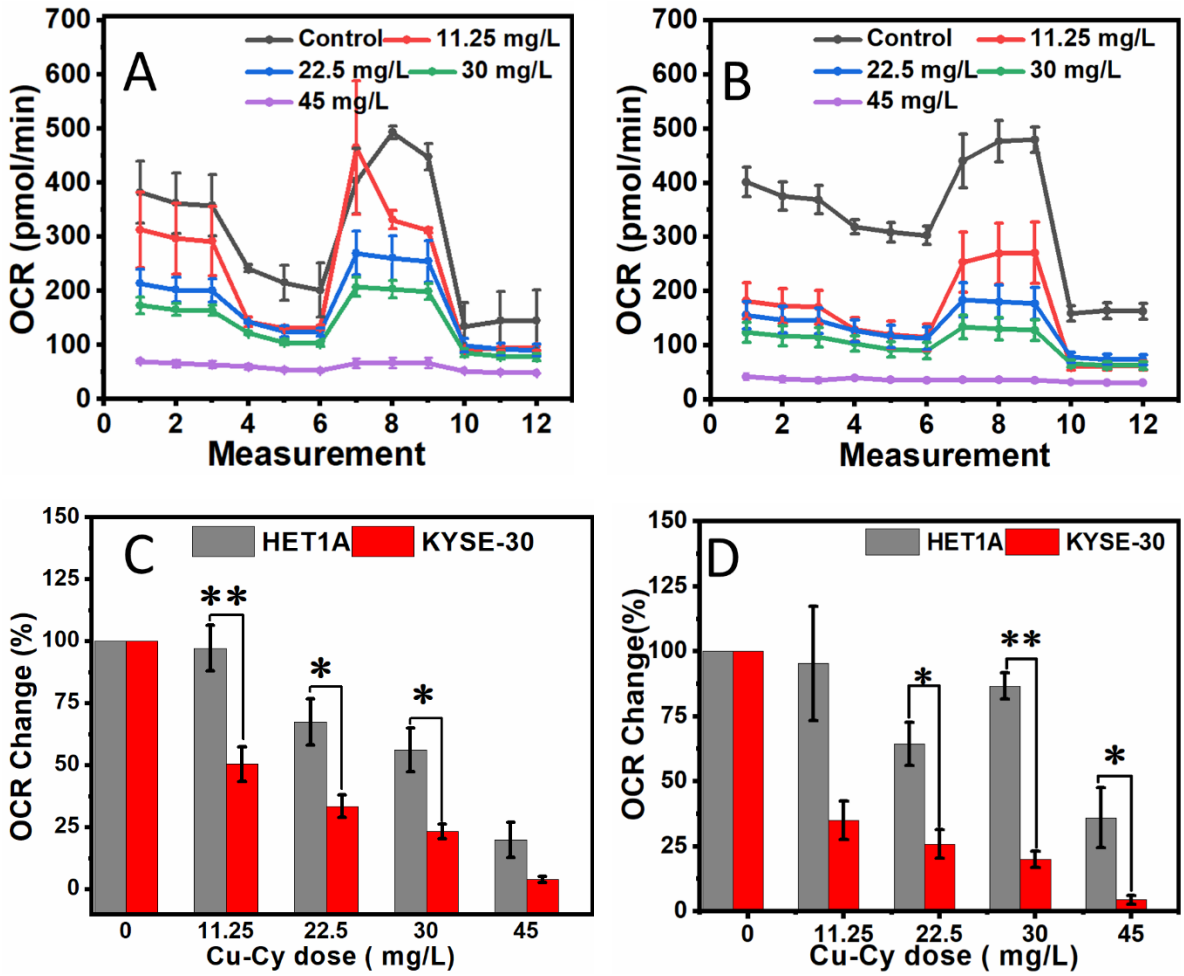

Figure 5. Oxygen consumption rate assay of **(A)** HET1A **(B)** KYSE-30 at various concentrations of Cu-Cy (0-45 mg/L). **(C-D)** Normalized **(C)** ATP and **(D)** Basal respiration at various concentrations of Cu-Cy. Normalization was done with respect to control (without Cu-Cy). * $p< 0.05$ ** $p<0.01$.

We carried out OCR assay to evaluate the effect of Cu-Cy on the mitochondrial function of both cancerous and normal cells. The assay was carried out after 24 h incubation of the cells with Cu-Cy. **Figures 5A and B** represent the OCR spectra of HET1A and KYSE-30 cell lines treated with various doses of Cu-Cy, respectively. It was observed that Cu-Cy induced more mitochondrial dysfunction in the cancer cell type (KYSE-30) than in its corresponding normal type (HET1A). For the purpose of comparison, the changes in basal, ATP, and proton leak rates are presented as a percentage of the corresponding control (without Cu-Cy treatment). The reduction in the basal

respiration **(Figure 5C)** was more pronounced for the KYSE-30 cells than that of HET1A cells; with the differences being significant at 11.25, 22.5, and 30 mg/L. Furthermore, Cu-Cy caused a significant decrease in ATP turnover (**Figure 5D**) in KYSE-30 than in HET1A cell lines, particularly at 22.5 and 30 mg/L. As shown in **Figure S5D,** the changes in proton leaks of various cell lines after the Cu-Cy treatment followed a similar pattern as that of basal and ATP rates. Additionally, DM6, another cancer cell line, had a comparable effect with that of KYSE-30 on their basal, ATP, and proton leak as demonstrated in **Figure S5 (A-C).** These results further support the claim that Cu-Cy can induce selective cytotoxicity to cancer cells while inducing minimal toxicity to normal cells.

4.6.3. Live/dead cell assay

A live-dead cell assay was performed to further evaluate the cytotoxicity of Cu-Cy NPs in cancer and normal cells. The live/dead assay consists of calcein-AM and ethidium homodimer-1 to stain live and dead cells, respectively.[155] The calcein-AM stains nucleus and cytoplasm in the ratio of 3:1, indicating that it is a suitable dye for staining the whole cell body.[156] Calcein-AM can also be used as a reliable probe for staining early apoptotic cells.[156,157] Apoptotic cells undergo slow and systemic changes in cell morphology; in its early stage, the nucleus and cytoplasm condense to become round in shape while keeping the plasma membrane intact.[158–160] Therefore, the apoptotic cells retain the calcein with stronger luminescence than that in viable cells.

For each Cu-Cy treated cells, the green (live) and red channels (dead) were merged, and representative images are presented in **Figure 6A**. The results reveal that most of the Cu-Cy treated cancer cell lines (DM6 and KYSE-30) were EthD-1 positive (dead). Besides, among the calcein positive cells, a large number of cells turned into a round-shaped structure, a characteristic feature

of early apoptotic cells.[158–160] On the other hand, the Cu-Cy treated HET1A and HDF cells were mostly calcein positive and retained their structure, suggesting low toxicity of Cu-Cy towards healthy cells.

We also attempted to quantify live, dead, and apoptotic cells by using the particle analyzer feature of imageJ.[161] A detailed method, along with a flow chart of image quantification, is presented in supporting information (**Figure S6)**. The quantified live/dead assay result is presented in **Figure 6B**. The result reveals that Cu-Cy NPs induced significant cytotoxicity to cancerous cells (DM6 and KYSE-30); most of the cells are either dead or apoptotic after 24 h of incubation. On the other hand, under similar experimental conditions, most of the normal cells were viable with intact cell bodies.

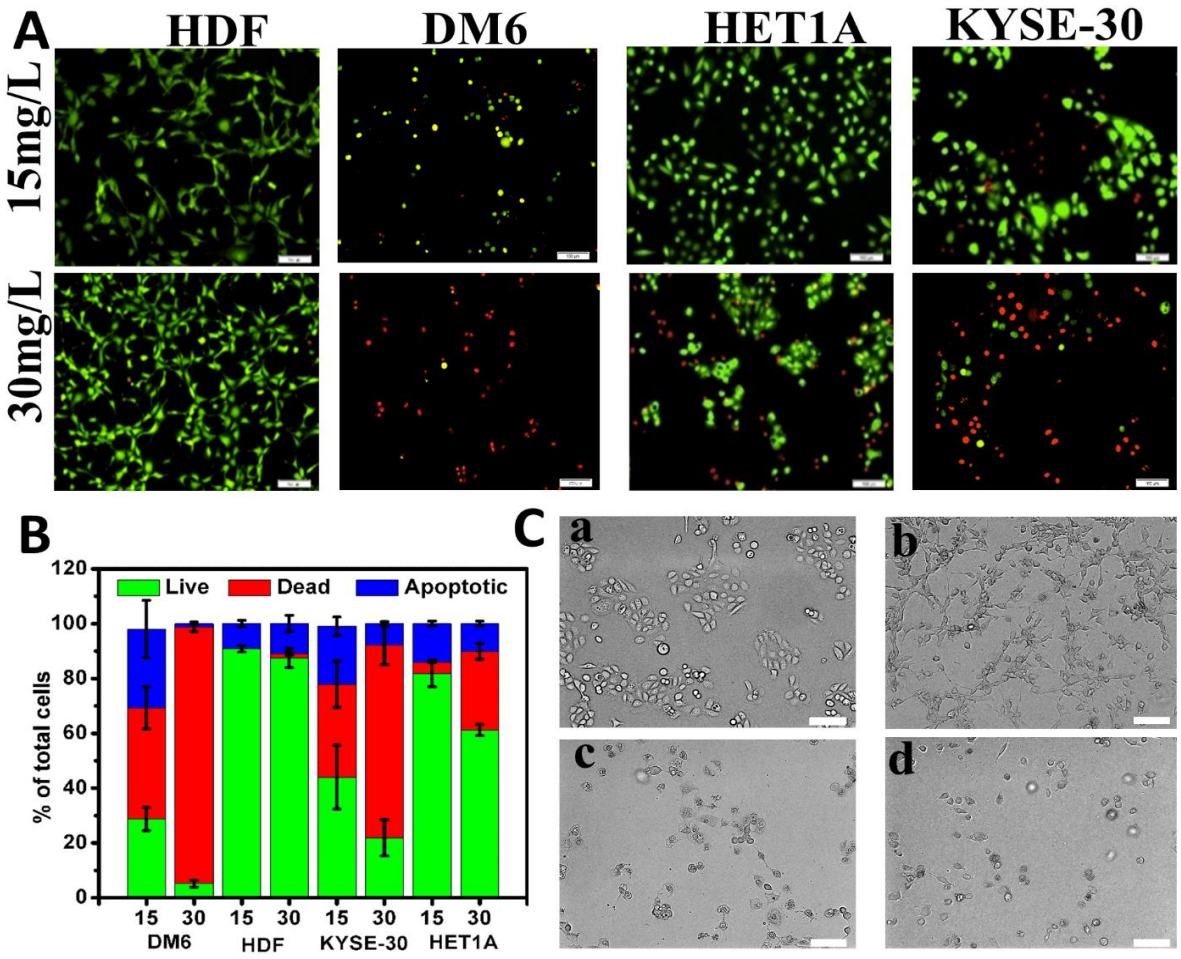

Figure 6. (A) Live/dead assay to assess the toxicity of Cu-Cy to cancer (DM6 and KYSE-30) and normal (HDF and HET1A) cell lines: Green and red channels are from calcein-AM (Live) and Ethidium homodimer (Dead), respectively. **(B)** Quantification for the cell viability and early apoptosis using imageJ. **(C)** Bright-field imaging to observe morphological changes of the Cu-Cy (15 µg/mL) treated normal and cancer cell lines: **(a)** HET1A, **(b)** HDF, **(c)** KYSE-30, and **(d)** DM6. Scale bar: 100 µm.

4.6.4. Bright-field imaging of Cu-Cy treated cells

We also carried out bright field imaging to monitor morphological differences among both normal and cancer cells, following the Cu-Cy (15 mg/L) treatment **(Figure 6C)**. It can be seen that normal cell lines (HET1A and HDF) retained their structure after incubation with Cu-Cy for 24 h. The intact structure indicates low cytotoxicity of Cu-Cy towards normal cell lines. On the contrary, Cu-Cy treated cancer cell lines (DM6 and KYSE-30) showed a significant loss in their structure and were generally more roundly shaped. This result further confirms that Cu-Cy is highly toxic to cancer cell lines, but it has minimal toxicity to normal cell lines.

4.6.5. MTT assay

The selective toxicity of Cu-Cy was also explored by conducting MTT assays on two cancer cell lines (DM6 and KYSE-30) and corresponding normal cell lines (HDF and HET1A). As depicted in **Figure 7A,** normal cells treated with Cu-Cy had higher cell viabilities than those of cancer cell lines. DM6 cell lines have 15 % and 39 % viability at 30 and 15 µg/mL of Cu-Cy, respectively, which is significantly lower ($p < 0.01$) than that of HDF (77 % and 90 % at 30 and 15 µg/mL, respectively). Similarly, cell viabilities of KYSE-30 (22 and 50% at 30 and 15 µg/mL, respectively) are significantly lower ($p < 0.05$) than that of HET1A (58 and 80 % at 30 and 15 µg /mL, respectively). Likewise, low cell viabilities were observed for Cu-Cy (8 % and 27 % for 30

and 15 µg /mL Cu-Cy, respectively) treated breast cancer cells (MCF-7) **(Figure S4B)**. A complete MTT assay data at various concentrations is presented in **Figure S4A**.

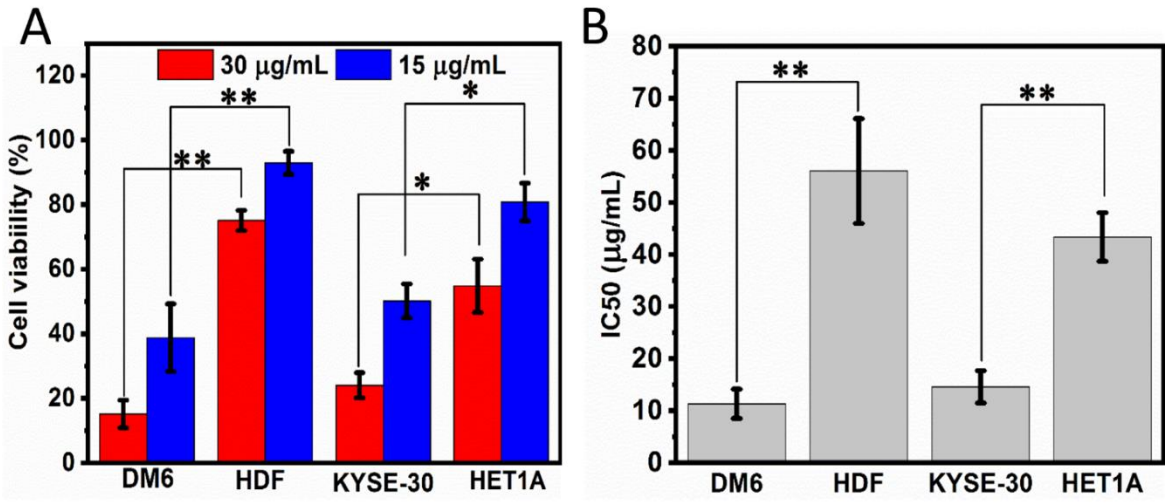

Figure 7. Evaluation of cytotoxicity of Cu-Cy to different cell lines using MTT assay. (A) Cell viability of different cell lines with Cu-Cy treatment. (B) IC-50 value of Cu-Cy towards normal and cancerous cells. (* $p < 0.05$, ** $p < 0.01$)

The IC-50 value of Cu-Cy against DM6 and KYSE-30 (11 and 14 µg/mL, respectively) are significantly lower ($p < 0.01$) than HDF and HET-1A (56 and 44 µg/mL, respectively) (**Figure 7B)**. The IC-50 value of Cu-Cy against the MCF-7 cell was found to be 8 µg/mL (**Figure S4B**). To the best of the authors' knowledge, an average IC-50 value of 11 µg/mL to cancerous cells is the lowest reported among heterogeneous Fenton and Fenton-like nanocatalyst for cancer therapy thus far. In addition, the average selectivity index was calculated to be 4.5, which is comparable to most Fenton based chemo-dynamic cancer drugs.[80,162]

Table 1. Comparison of Cu-Cy with other reported homogeneous and heterogeneous Fenton-like catalyst for cancer treatment.

System Name	Cytotoxicity	Dose Needed	Exogenous Additive	Type	Ref.
$SnFe_2O_4$	60 %	~1 mM	-	heterogeneous	[133]
P@rMOF-FA	50 %	60 µg/mL	-	homogeneous	[144]
GSF@AuNps	60 %	45 µg/mL	Ascorbic acid /H_2O_2	heterogeneous	[143]
Fe_3O_4@C-FA NPs	60 %	20 µg/mL	Ascorbic acid /H_2O_2	heterogeneous	[134]
r-MOF-FA	60 %	43 µg/mL	-	homogeneous	[135]
Cu-Cys NPs	~70 %	200 µg/ mL [a]	-	heterogeneous	[85]
Amorphous Fe NPs	~40 %	100 µg/mL	H_2O_2 (100µM)/pH6.5	heterogeneous	[136]
FeOx-MSNs	~ 60 %	100 µg/mL	Exogenous H_2O_2	heterogeneous	[137]
CuO NPs	~ 60 %	0.5 mg/mL[a]	-	heterogeneous	[146]
Cu-Cy	50 %	11 µg/mL	-	heterogeneous	This work

a. Cytotoxicity after 24 h treatment

Overall, Cu-Cy NPs' performance is markedly better at a much lower dose than most Fenton-like nano-catalysts reported so far, which require high doses and/or exogenous additives in order to achieve desired cytotoxicity (**Table 1**).[85,133–137,143,144,146] Besides, Cu-Cy NPs being a heterogenous catalyst would leach a much lower amount of free copper ions compared to homogenous catalysts, thereby ensuring lower toxicity to healthy cells. The excellent performance of Cu-Cy can be attributed to the existence of copper in its reduced state (Cu^{1+}) rather than in the oxidized state Cu^{2+}. It should be noted that the Cu^{1+} can react with H_2O_2 much faster (22 times) than that of Cu^{2+} as illustrated in equations (1-2).[82] Furthermore, the reaction rate of Cu is 160 times faster than Fe, making Cu-based nano-catalysts more efficient than Fe-based nano-catalysts.

$$Cu^{1+} + H_2O_2 \rightarrow Cu^{2+} + \bullet OH + OH^- \quad (k=1\times10^4\ M^{-1}S^{-1}) \quad (1)$$

$$Cu^{2+} + H_2O_2 \rightarrow Cu^{1+} + \bullet HO_2^- + H^+ \quad (k=460\ M^{-1}S^{-1}) \quad (2)$$

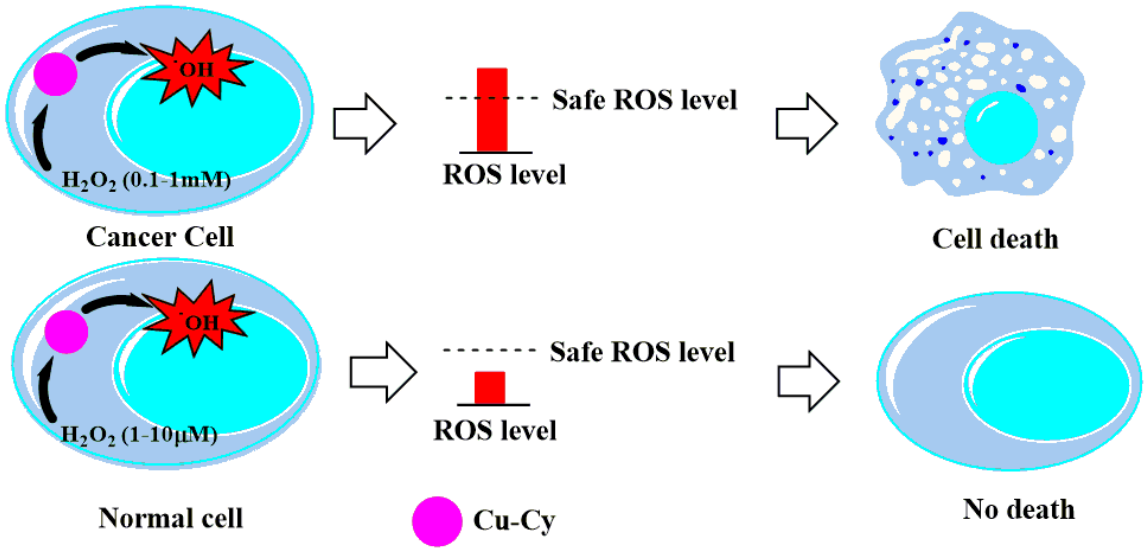

Figure 8. Schematic of Cu-Cy mediated Fenton-like reaction for selective cancer treatment. Cu-Cy NPs can undergo Fenton-like reaction with overproduced H_2O_2 in cancer cells resulting in ROS levels that is above the safe ROS level, causing cell death. On the other hand, owing to lower level of H_2O_2, Cu-Cy is harmless to normal cells.

Taken together, our findings suggest that the redox reactions between Cu-Cy and over present H_2O_2 in cancer cells can continue for many cycles, resulting in a ROS level that is beyond what the cell can withstand and thereby inducing cancer cell death. However, due to the lower production of H_2O_2 in normal cells, the Cu-Cy NPs can not generate a high level of ROS to reach the cell-death threshold (**Figure 8**).

Our future work on Cu-Cy NPs will focus on surface coating, functionalization, and further evaluation in vitro and in vivo. We believe that surface coating and functionalization will help to further reduce the toxicity towards healthy cells by enhancing its stability and targeted accumulations in the tumor.

4.4. CONCLUSIONS

We investigated the Cu-Cy NPs for heterogeneous Fenton-like reactions facilitated cancer therapy with high selective toxicity. Our results suggest that Cu-Cy NPs, which have copper in its reduced state(Cu^{1+}), can catalyze over-produced H_2O_2 in cancerous cells to produce significantly higher levels of ROS, thereby inducing significantly more cancer cell destruction than healthy cells. The catalytic effect of Cu-Cy dramatically increased in slightly acidic conditions, which further contributes towards high selectivity owing to the acidic nature of tumor cells. The excellent stability of Cu-Cy and its low average IC-50 value (11 μg/mL) towards cancer cells helps to pave the way for the development of translational nano-medicines in the context of cancer treatment with low systemic toxicity.

Supporting information

Calibration curve for Cu^{2+} measurement, PL spectra of coumarin for hydroxyl radical, ROS measurement in MCF-7 cell, full MTT assay data, Cell viability and IC-50 of MCF-7 cell, OCR data of DM6 cell line, and live/dead assay quantification method.

Conflicts of interest

There are no conflicts of interest to declare.

Acknowledgments

We would like to acknowledge the support from the U.S. Army Medical Research Acquisition Activity (USAMRAA) under Contracts of W81XWH-10-1-0279 and W81XWH-10-1-0234 as well as the partial support from NIH/NCI 1R15CA199020-01A1. We are thankful to Seahorse Bioscience (North Billerica, MA, USA) and Craig Smith for allowing us to use the demo version

of XFp analyzer. We would like to thank Dr. Zui Pan and Dr. Nguyen Kytai for arranging cell lines and Dr. Roy McDougald for helping with FTIR measurement.

SUPPORTING INFORMATION

COPPER-CYSTEAMINE NANOPARTICLES AS A HETEROGENEOUS FENTON-LIKE CATALYST FOR HIGHLY SELECTIVE CANCER TREATMENT

Lalit Chudal[a], Nil Kanatha Pandey[a], Jonathan Phan[a], Omar Johnson[a], Liangwu Lin[b], Hongmei Yu[c]*, Yang Shu[d], Zhenzhen Huang[e], Meiying Xing[a], J. Ping Liu[a], Minli Chen[d]*, and Wei Chen*[a]

[a]Department of Physics, The University of Texas at Arlington, Arlington, Texas 76019, USA

[b] Laboratory on High-Strength Structural Materials, Central South University, Changsha 410083, P. R. China

[c] School of Chemical Engineering, University of Science and Technology Liaoning, Anshan 114051, China

[d] Department of Chemistry, College of Sciences, Northeastern University, Shengyang 110819, China

[e] Jilin University, Changchun, Jilin, China

*Corresponding authors: weichen@uta.edu (W. Chen); chenml@mail.neu.edu.cn (M. L. Chen); seesea0304@163.com (H. M. Yu)

*Corresponding authors: weichen@uta.edu ; chenml@mail.neu.edu.cn

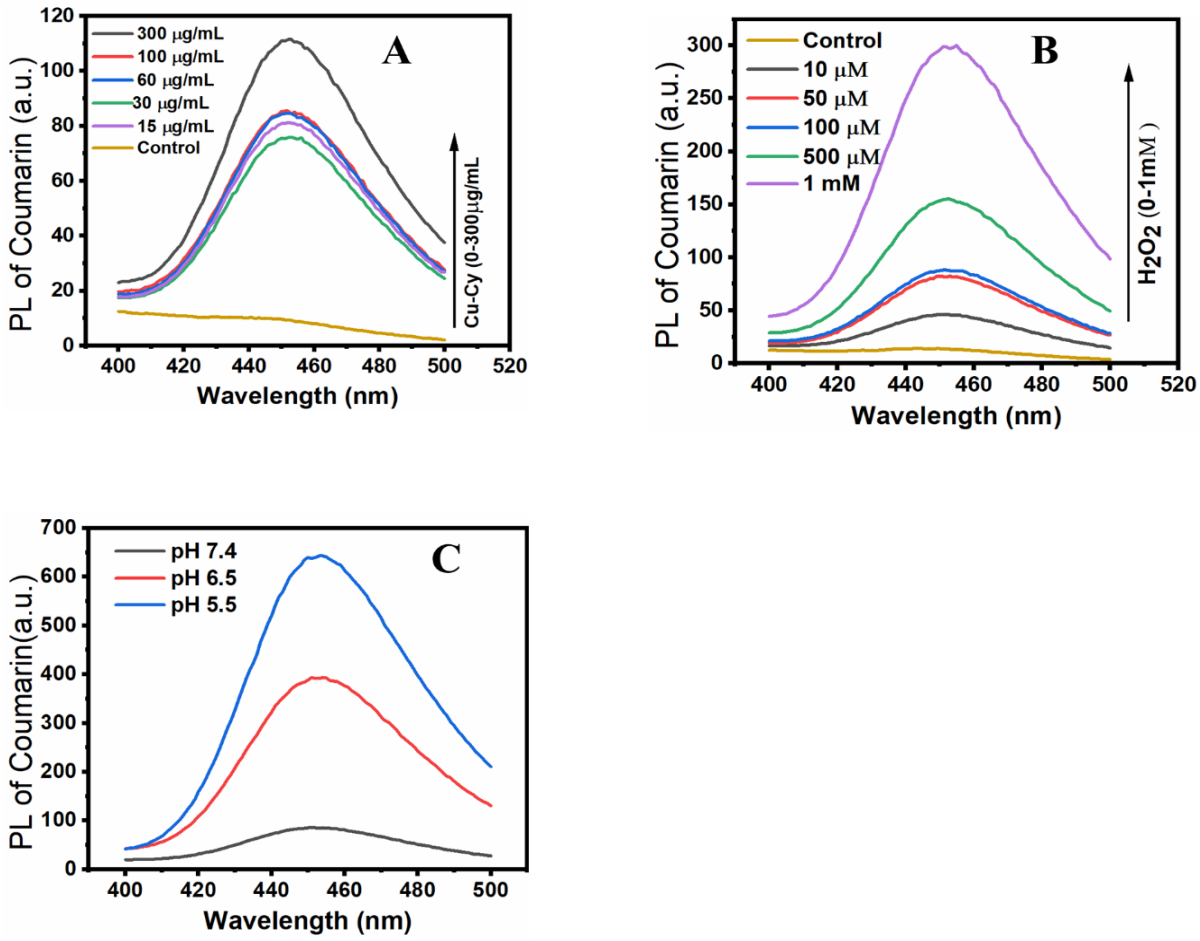

Figure S1. Hydroxyl radical(·OH)measurement using coumarin as a probe. The PLspectraof coumarin monitored after 6h of the reaction with the mixture of **(A)** various doses(0-300μg/mL) of Cu-Cywith100 μMH_2O_2. **(B)**Various doses of H_2O_2 (10μM-1mM)with Cu-Cy(100 μg/mL),and **(C)**Cu-Cy(100 μg/mL) andH_2O_2(100 μM).The excitation wavelength was 332 nm.

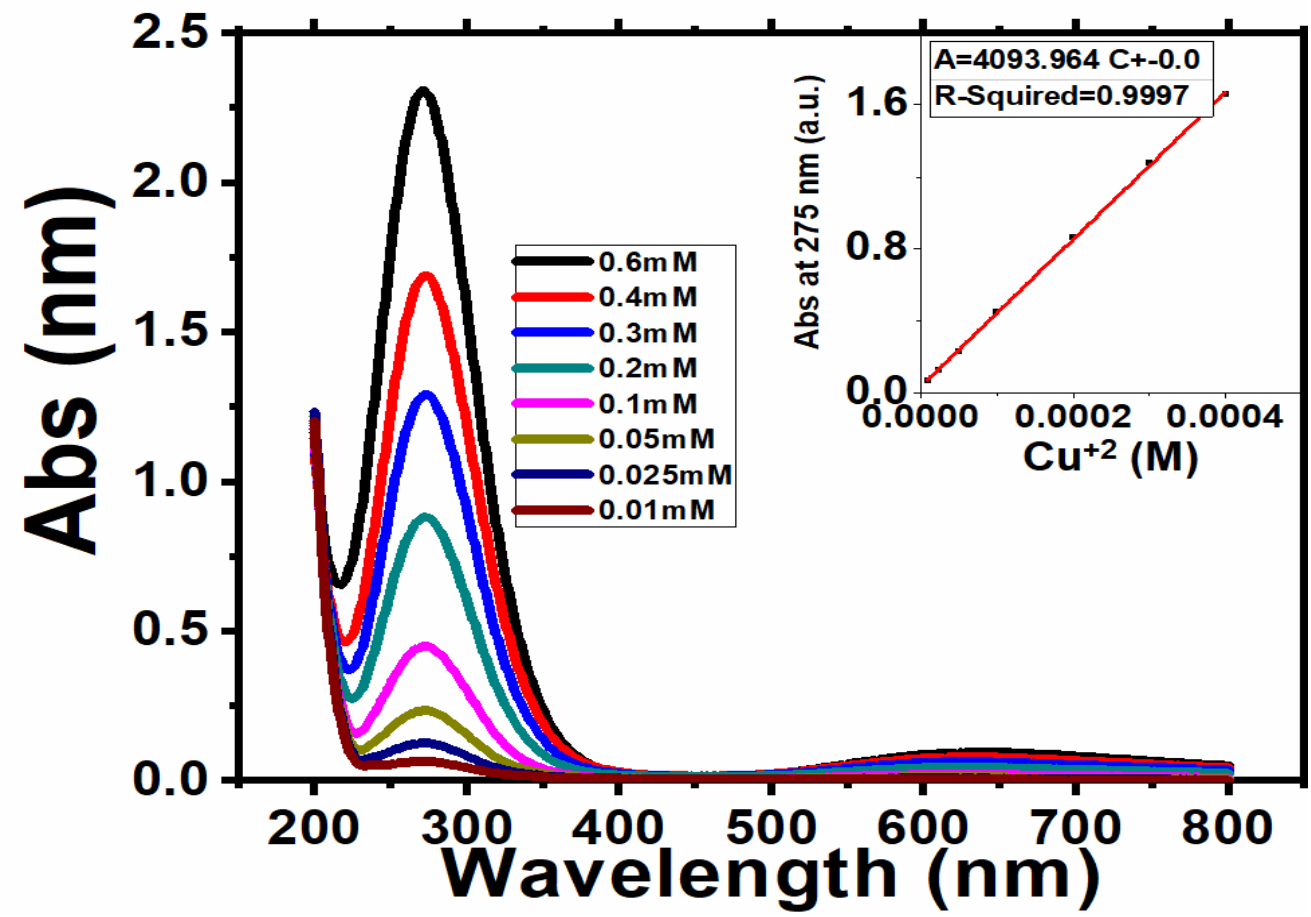

Figure S2. A spectrophotometric method to detect free Cu^{2+} in aqueous solution. A calibration curve was obtained using $CuCl_2.2H_2O$ as a source of free Cu^{2+}. Inset shows the calibrated equation to determine the free Cu^{2+} concentration in an aqueous solution.

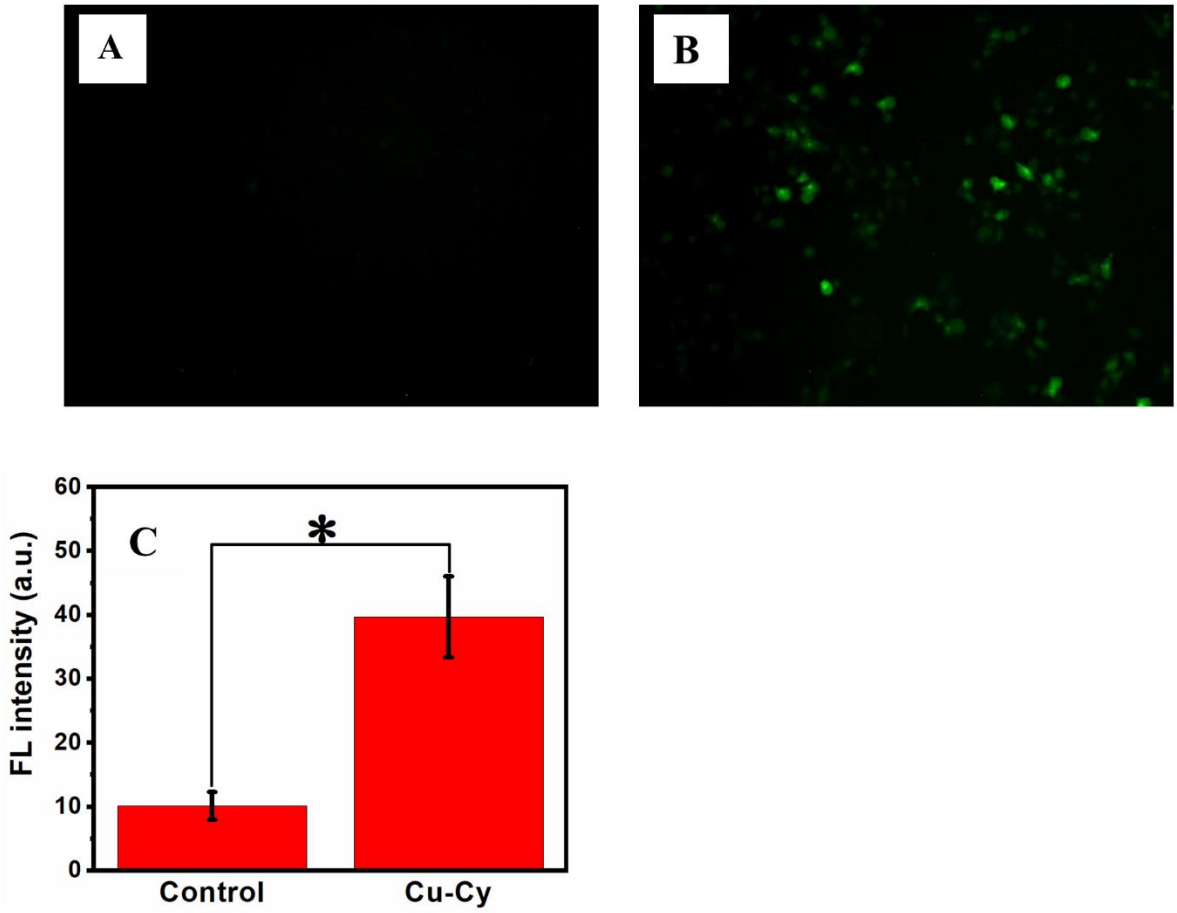

Figure S3. Intracellular ROS measurement in MCF-7 cell lines using DCFH-DA. FL-intensity of DCF on MCF-7 cell lines incubated (A) without Cu-Cy (control), (B) with Cu-Cy (30 µg/ mL) for 12 h, and (C) quantification of DCF intensity using imageJ. (*) indicates $p<0.01$.

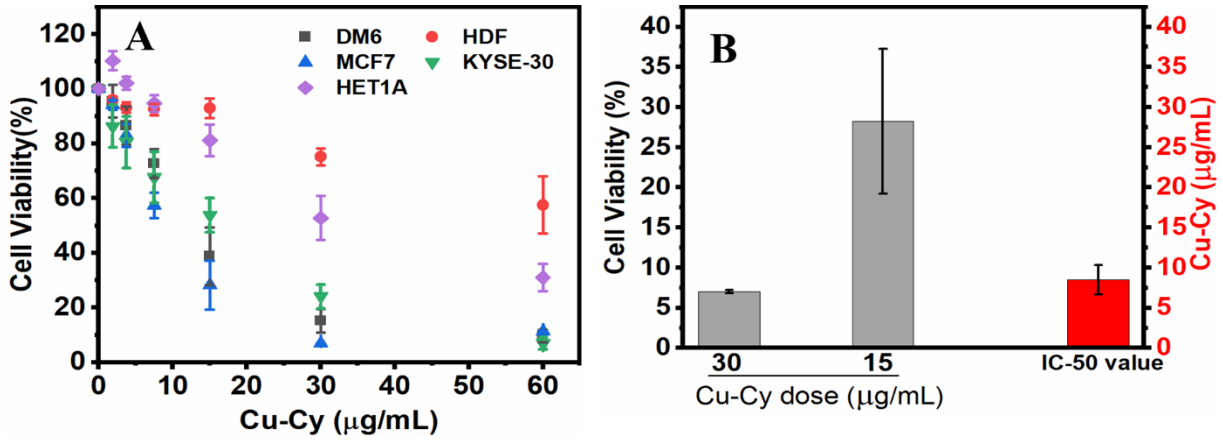

Figure S4. (A) Cell viability of different cell lines with Cu-Cy treatment. (B) Cell viability and IC-50 value of MCF-7 cell line.

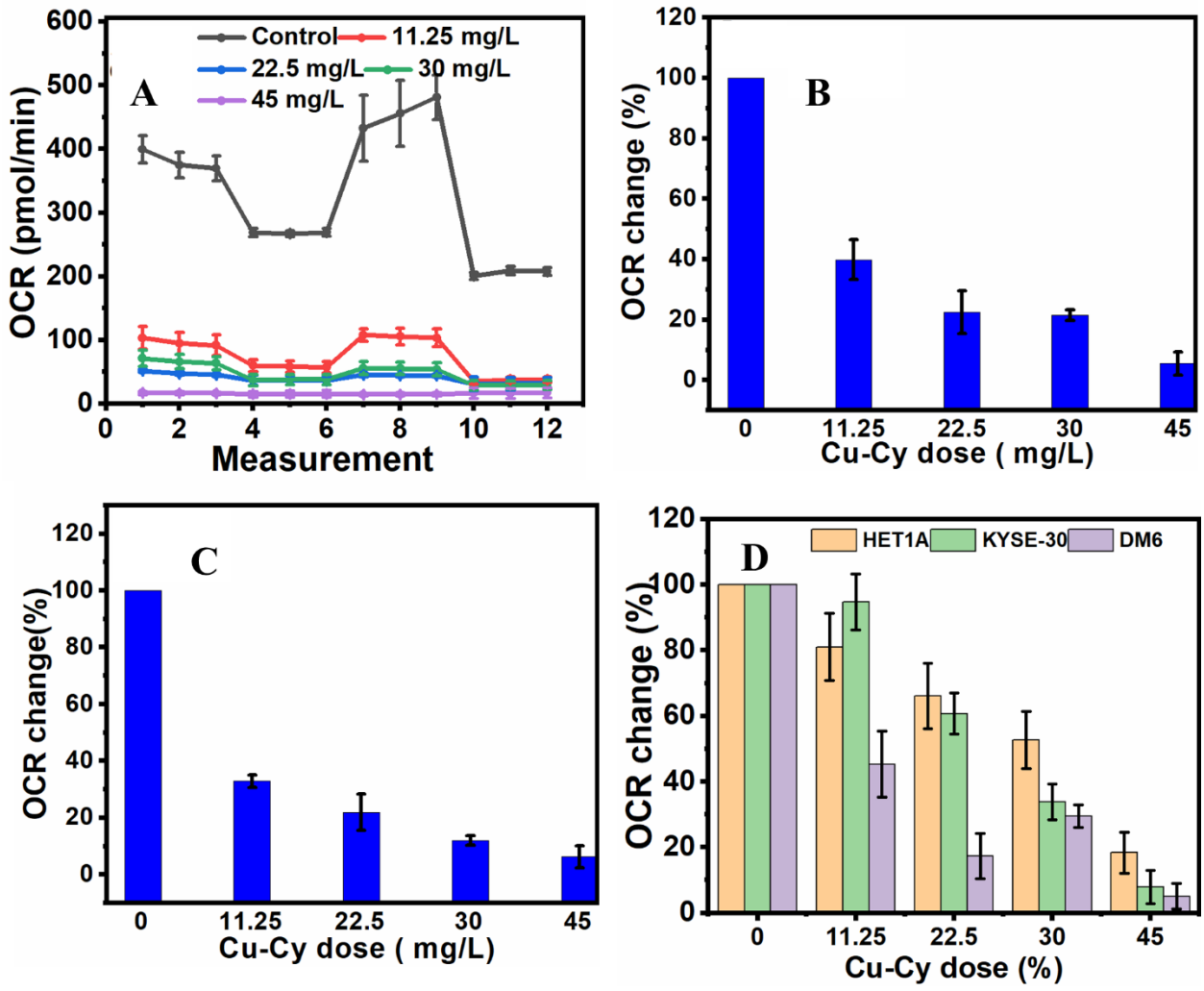

Figure S5. Oxygen consumption rate assay on Cu-Cy treated DM6 cell line. (A) OCR spectra, (B) basal respiration rate, and (C) ATP turnover rate with respect to the control (without Cu-Cy). (D) Comparison of proton-leak of HET1A, KYSE-30, and DM6 cell lines.

Quantification of Live/dead assay

To quantify the cell viability and apoptosis, we used the "Particle analyzer" feature of ImageJ software.[161,163,164] Firstly, the merged RGB images were split into red and green channels. Then, each channel (green and red) was processed in a number of steps, as illustrated in **Figure S6**. Following the processing, the number of cells in the image were counted using the particle analyzer feature. The particle analyzer allows applying filters based on the area (0- infinity) pixel^2 and circularity (0.00-1.00). Small debris and large bodies, such as scale bar and multiple unresolved cells, were filtered out by using area filter: the lower and upper value of area were set as 30 and 3000 pixel^2, respectively.

Cell viability was calculated as follows:

$$\text{Cell viability} = \frac{\text{No. of live cells}}{\text{No of live cells} + \text{No of dead cells}} * 100\%$$

Roundness filter >0.9 was applied to the calcein positive cells to quantify the number of early apoptotic cells.

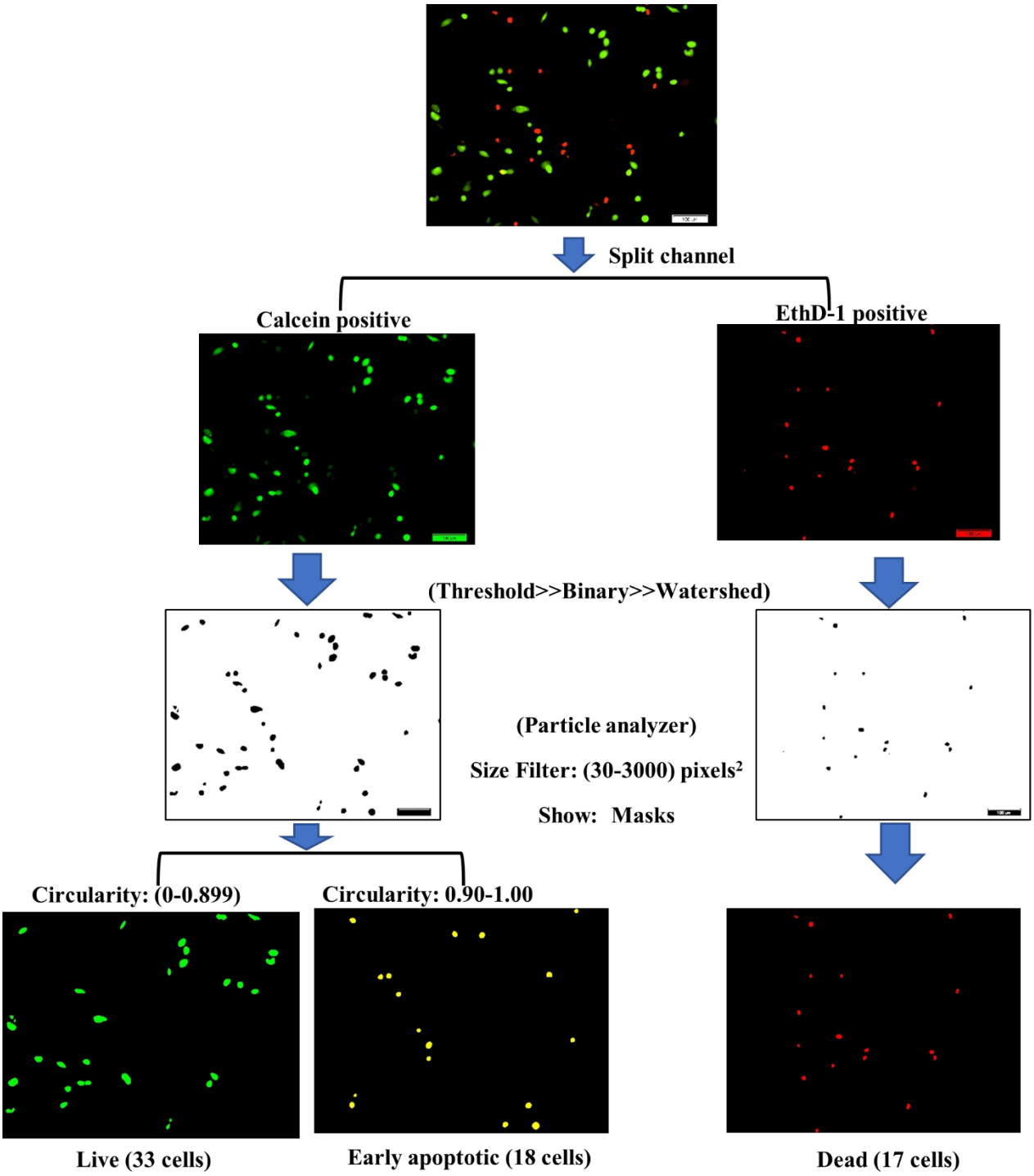

Figure S6: Flow-chart for Live/dead assay quantification using ImageJ.

Chapter 5:

GENERAL CONCLUSIONS

Tumor microenvironment responsive nanomaterials carry great potential as next-generation medicines to tackle various fatal diseases, including cancers. Cancer cells employ unique environments to proliferate and invade nearby tissues. However, a greater understanding of tumor microenvironment in the past decade enabled researchers to develop smart strategies that can exploit the tumor's own uniqueness to destroy themselves. Among the unique features of the tumor microenvironment, an elevated level of H_2O_2 and slightly acidic pH have widely been utilized to develop several smart therapeutic and/or diagnostic systems.

This dissertation attempted to develop tumor microenvironment responsive nanosystems to improve current photodynamic and chemotherapy. In the first work, a nanosystem was fabricated to alleviate the tumor hypoxia, and subsequently enhance photodynamic therapy performance under hypoxic conditions. For this purpose, a representative FDA approved photosensitizing drug, PPIX, was encapsulated into the liposomal bilayer. Then the liposomal surface was coated with MnO_2 nanoparticles, resulting in a final product PPIX-Lipo-M. The coating was confirmed by multiple methods; TEM and DLS were used as a direct method, whereas, absorption spectra and study of PL quenching effect were used as indirect evidence of MnO_2 coating on the liposomal surface. The MnO_2 nanoparticles can yield oxygen by reacting with endogenous H_2O_2 under the slightly acidic condition of the tumor microenvironment and tumor cells.

Under normoxia condition, the PDT induced cytotoxicity of PPIX-Lipo is higher than PPIX-Lipo-M. However, under simulated hypoxia conditions, PPIX-Lipo-M exhibited higher PDT efficacy than PPIX-Lipo under the same experimental condition. The enhanced PDT effect of PPIX-Lipo-

M under hypoxia conditions can be attributed to the local oxygen generated by the reaction between MnO_2 and endogenous H_2O_2. The result suggested that as-synthesized PPIX-Lipo-M is capable of improving PDT outcomes under hypoxia conditions. In conclusion, PPIX-Lipo-M successfully alleviated tumor hypoxia and improved the PDT effect. The future work will focus on synthesizing smaller sized liposomes and MnO_2 nanoparticles. Using smaller MnO_2 nanoparticles would help to increase the amount of the MnO_2 nanoparticles coated on the liposomal surface, thereby positively impacting the therapeutic effect of PPIX-Lipo-M.

In the second project, a smart approach is proposed to tackle the photosensitivity issue of current photosensitizers. The existing photosensitizer can readily be activated by sunlight to produce reactive oxygen species, leading to various toxic effects to skin and eye. The result demonstrated that using copper-cysteamine nanoparticles instead of existing photosensitizer offers reduced photosensitivity. Previous reports have demonstrated that copper-cysteamine nanoparticles could be excited by various excitation sources such as X-ray, MW, and ultrasound, making them much more advantageous than traditional photosensitizer. A systematic study was conducted to compare the photosensitivity of Cu-Cy NPs and PPIX. In vitro study revealed that Cu-Cy NP does not induce any obvious photosensitivity, while PPIX is capable of destroying cells even at low concentration. In vivo study on the skin of healthy mice is currently underway. Overall, Cu-Cy NP is an excellent candidate as next-generation nanomedicine for cancer treatment

Finally, copper-cysteamine nanoparticles were fabricated and explored as a Fenton catalyst for highly selective cancer treatment. The treatment method has some notable advantages over traditional chemotherapy. Chemotherapy lacks selectivity and kills both cancerous cells and some

types of healthy cells, leading to a multitude of side effects such as hair loss, vomiting, diarrhea. In other words, the lack of selectivity is one of the main challenges of chemotherapy. The copper-cysteamine NPs generate reactive oxygen species in response to cancer-specific conditions (slightly acidic pH and elevated level of H_2O_2). Due to this reason, Cu-Cy generates a substantial amount of ROS in cancer cells as compared to healthy cells, resulting in highly selective cancer-killing ability. Furthermore, Cu-Cy NPs were found to leach Cu at a minimal level during the Fenton-like reaction, ensuring acceptable systemic toxicity. To the best of our knowledge, the IC-50 value of 11 µg/mL is the lowest among reported heterogeneous systems and also has a high selectivity index of 4.5 against cancer cells.

Future research would direct towards the exploitation of active targeting to improve tumor accumulation in vivo. In fact, surface coating with hyaluronic acid, which is known to have an affinity towards cancer-specific antigen CD44) is currently being investigated. Besides, other targeting agents, such as peptides may be conjugated on the surface of Cu-Cy NPs and explore the tumor accumulation and pharmacokinetics in detail.

REFERENCES

[1] R.L. Siegel, K.D. Miller, A. Jemal, Cancer statistics, 2019., CA. Cancer J. Clin. 69 (2019) 7–34. https://doi.org/10.3322/caac.21551.

[2] E.M. Ward, R.L. Sherman, S.J. Henley, A. Jemal, D.A. Siegel, E.J. Feuer, A.U. Firth, B.A. Kohler, S. Scott, J. Ma, R.N. Anderson, V. Benard, K.A. Cronin, Annual Report to the Nation on the Status of Cancer, Featuring Cancer in Men and Women Age 20–49 Years, JNCI J. Natl. Cancer Inst. 111 (2019) 1279–1297. https://doi.org/10.1093/jnci/djz106.

[3] T.J. Dougherty, J.G. Levy, Photodynamic therapy (PDT) and clinical applications, Biomed Photonics Handb, 2003. https://doi.org/10.1201/9780203008997.ch38.

[4] P. Agostinis, K. Berg, K.A. Cengel, T.H. Foster, A.W. Girotti, S.O. Gollnick, S.M. Hahn, M.R. Hamblin, A. Juzeniene, D. Kessel, M. Korbelik, J. Moan, P. Mroz, D. Nowis, J. Piette, B.C. Wilson, J. Golab, Photodynamic therapy of cancer: An update, CA. Cancer J. Clin. 61 (2011) 250–281. https://doi.org/10.3322/caac.20114.

[5] F.S. De Rosa, M.V.L.B. Bentley, Photodynamic therapy of skin cancers: Sensitizers, clinical studies and future directives, Pharm. Res. 17 (2000) 1447–1455. https://doi.org/10.1023/A:1007612905378.

[6] H.I. Pass, Photodynamic therapy in oncology: mechanisms and clinical use., J. Natl. Cancer Inst. 85 (1993) 443–56. http://www.ncbi.nlm.nih.gov/pubmed/8445672 (accessed June 18, 2018).

[7] O. Raab, On the effect of fluorescent substances on infusoria (in German), Z Biol. (1900) 524.

[8] F. F, Fisher H; Meyer-Betz, Formation of porphyrins., Z. Physiol. Chem. 82 (1912) 96–

108.

[9] H. Schwartz, S., Absolon, K., Vermund, Some relationships of porphyrins, x rays and tumours, 1955.

[10] T.J. Dougherty, A brief history of clinical photodynamic therapy development at Roswell Park Cancer Institute., J. Clin. Laser Med. Surg. 14 (1996) 219–221. https://doi.org/10.1089/clm.1996.14.219.

[11] R.R. Allison, V.S. Bagnato, R. Cuenca, G.H. Downie, C.H. Sibata, The future of photodynamic therapy in oncology, Futur. Oncol. 2 (2006) 53–71. https://doi.org/10.2217/14796694.2.1.53.

[12] R. Baskaran, J. Lee, S.-G. Yang, Clinical development of photodynamic agents and therapeutic applications, Biomater. Res. 22 (2018). https://doi.org/10.1186/s40824-018-0140-z.

[13] V.G. Schweitzer, M.L. Somers, PHOTOFRIN-mediated photodynamic therapy for treatment of early stage laryngeal malignancies, Oncol. Rev. 4 (2010) 203–209. https://doi.org/10.1007/s12156-010-0059-7.

[14] T.J. Dougherty, M.T. Cooper, T.S. Mang, Cutaneous phototoxic occurrences in patients receiving Photofrin®, Lasers Surg. Med. 10 (1990) 485–488. https://doi.org/10.1002/lsm.1900100514.

[15] P.J. Lou, H.R. Jäger, L. Jones, T. Theodossy, S.G. Bown, C. Hopper, Interstitial photodynamic therapy as salvage treatment for recurrent head and neck cancer, Br. J. Cancer. 91 (2004) 441–446. https://doi.org/10.1038/sj.bjc.6601993.

[16] W. Story, A.A. Sultan, G. Bottini, F. Vaz, G. Lee, C. Hopper, Strategies of airway management for head and neck photo-dynamic therapy, Lasers Surg. Med. 45 (2013) 370–

376. https://doi.org/10.1002/lsm.22149.

[17] S.G. Bown, A.W.R. Hatfield, A.Z. Rogowska, D.E. Whitelaw, W.R. Lees, L.B. Lovat, P. Ripley, L. Jones, P. Wyld, A. Gillams, Photodynamic therapy for cancer of the pancreas, Gut. 50 (2002) 549–557. https://doi.org/10.1136/gut.50.4.549.

[18] P. Wyss, V. Schwarz, D. Dobler-Girdziunaite, R. Hornung, H. Walt, A. Degen, M. Fehr, Photodynamic therapy of locoregional breast cancer recurrences using a chlorin-type photosensitizer, Int. J. Cancer. 93 (2001) 720–724. https://doi.org/10.1002/ijc.1400.

[19] S.P. Pereira, L. Ayaru, A. Rogowska, A. Mosse, A.R.W. Hatfield, S.G. Bown, Photodynamic therapy of malignant biliary strictures using meso-tetrahydroxyphenylchlorin, Eur. J. Gastroenterol. Hepatol. 19 (2007) 479–485. https://doi.org/10.1097/MEG.0b013e328013c0bd.

[20] K.A. Bradley, T. Zhou, R.Y. McNall-Knapp, R.I. Jakacki, A.S. Levy, G. Vezina, I.F. Pollack, Motexafin-gadolinium and involved field radiation therapy for intrinsic pontine glioma of childhood: A children's oncology group phase 2 study, Int. J. Radiat. Oncol. Biol. Phys. 85 (2013) e55. https://doi.org/10.1016/j.ijrobp.2012.09.004.

[21] J. Trachtenberg, A. Bogaards, R.A. Weersink, M.A. Haider, A. Evans, S.A. McCluskey, A. Scherz, M.R. Gertner, C. Yue, S. Appu, A. Aprikian, J. Savard, B.C. Wilson, M. Elhilali, Vascular Targeted Photodynamic Therapy With Palladium-Bacteriopheophorbide Photosensitizer for Recurrent Prostate Cancer Following Definitive Radiation Therapy: Assessment of Safety and Treatment Response, J. Urol. 178 (2007) 1974–1979. https://doi.org/10.1016/j.juro.2007.07.036.

[22] S.S. Taneja, J. Bennett, J. Coleman, R. Grubb, G. Andriole, R.E. Reiter, L. Marks, A.-R. Azzouzi, M. Emberton, Final Results of a Phase I/II Multicenter Trial of WST11

(TOOKAD ® Soluble) Vascular-Targeted Photodynamic Therapy (VTP) for Hemiablation of the Prostate in Men with Unilateral Low Risk Prostate Cancer Conducted in the United States, (n.d.). https://doi.org/10.1016/j.juro.2016.05.113.

[23] R.A. Weersink, J. Forbes, S. Bisland, J. Trachtenberg, M. Elhilali, P.H. Brún, B.C. Wilson, Assessment of Cutaneous Photosensitivity of TOOKAD (WST09) in Preclinical Animal Models and in Patients¶, Photochem. Photobiol. 81 (2005) 106. https://doi.org/10.1562/2004-05-31-ra-182.1.

[24] T.J. Dougherty, An update on photodynamic therapy applications, J. Clin. Laser Med. Surg. 20 (2002) 3–7. https://doi.org/10.1089/104454702753474931.

[25] A.B. Ormond, H.S. Freeman, Dye sensitizers for photodynamic therapy, Materials (Basel). 6 (2013) 817–840. https://doi.org/10.3390/ma6030817.

[26] Q. Peng, K. Berg, J. Moan, M. Kongshaug, J.M. Nesland, 5-Aminolevulinic acid-based photodynamic therapy: Principles and experimental research, Photochem. Photobiol. 65 (1997) 235–251. https://doi.org/10.1111/j.1751-1097.1997.tb08549.x.

[27] I.A.N.J. Macdonald, T.J. Dougherty, Basic principles of photodynamic therapy, J. Porphyr. Phthalocyanines. (2008) 1–18. papers://c7e2c9f4-f55f-43ef-843e-da85e2e186c1/Paper/p116.

[28] L.H. GRAY, A.D. CONGER, M. EBERT, S. HORNSEY, O.C. SCOTT, The concentration of oxygen dissolved in tissues at the time of irradiation as a factor in radiotherapy, Br. J. Radiol. 26 (1953) 638–648. https://doi.org/10.1259/0007-1285-26-312-638.

[29] J.M. Brown, Tumor Hypoxia in Cancer Therapy, Methods Enzymol. 435 (2007) 295–321. https://doi.org/10.1016/S0076-6879(07)35015-5.

[30] T.P. Szatrowski, C.F. Nathan, Production of Large Amounts of Hydrogen Peroxide by Human Tumor Cells, 1991. http://cancerres.aacrjournals.org/content/canres/51/3/794.full.pdf (accessed May 20, 2019).

[31] T.D. Oberleyll, L.W. Oberlefl, Antioxidant enzyme levels in cancer, Histol. Histopathol. 12 (1997) 525–535. http://www.ncbi.nlm.nih.gov/pubmed/9151141 (accessed June 19, 2019).

[32] W. Tang, Z. Zhen, M. Wang, H. Wang, Y.J. Chuang, W. Zhang, G.D. Wang, T. Todd, T. Cowger, H. Chen, L. Liu, Z. Li, J. Xie, Red blood cell-facilitated photodynamic therapy for cancer treatment, Adv. Funct. Mater. 26 (2016) 1757–1768. https://doi.org/10.1002/adfm.201504803.

[33] W. Zhang, S. Li, X. Liu, C. Yang, N. Hu, L. Dou, B. Zhao, Q. Zhang, Y. Suo, J. Wang, Oxygen-Generating MnO2Nanodots-Anchored Versatile Nanoplatform for Combined Chemo-Photodynamic Therapy in Hypoxic Cancer, Adv. Funct. Mater. 28 (2018) 1706375. https://doi.org/10.1002/adfm.201706375.

[34] D. Zheng, B. Li, L. Xu, Q.L. Zhang, J.X. Fan, C.X. Li, X.Z. Zhang, Normalizing Tumor Microenvironment Based on Photosynthetic Abiotic/Biotic Nanoparticles, ACS Nano. 12 (2018) 6218–6227. https://doi.org/10.1021/acsnano.8b02977.

[35] H. Chen, J. Tian, W. He, Z. Guo, H2O2-activatable and O2-evolving nanoparticles for highly efficient and selective photodynamic therapy against hypoxic tumor cells, J. Am. Chem. Soc. 137 (2015) 1539–1547. https://doi.org/10.1021/ja511420n.

[36] X. Song, J. Xu, C. Liang, Y. Chao, Q. Jin, C. Wang, M. Chen, Z. Liu, Self-Supplied Tumor Oxygenation through Separated Liposomal Delivery of H2O2 and Catalase for

Enhanced Radio-Immunotherapy of Cancer, Nano Lett. 18 (2018) 6360–6368. https://doi.org/10.1021/acs.nanolett.8b02720.

[37] W. Liu, T. Liu, M. Zou, W. Yu, C. Li, Z. He, M. Zhang, M. Liu, Z. Li, J. Feng, X. Zhang, Aggressive Man-Made Red Blood Cells for Hypoxia-Resistant Photodynamic Therapy, Adv. Mater. 30 (2018) 1802006. https://doi.org/10.1002/adma.201802006.

[38] P. Prasad, C.R. Gordijo, A.Z. Abbasi, A. Maeda, A. Ip, A.M. Rauth, R.S. Dacosta, X.Y. Wu, Multifunctional albumin-MnO2nanoparticles modulate solid tumor microenvironment by attenuating hypoxia, acidosis, vascular endothelial growth factor and enhance radiation response, ACS Nano. 8 (2014) 3202–3212. https://doi.org/10.1021/nn405773r.

[39] W. Fan, W. Bu, B. Shen, Q. He, Z. Cui, Y. Liu, X. Zheng, K. Zhao, J. Shi, Intelligent MnO $_2$Nanosheets Anchored with Upconversion Nanoprobes for Concurrent pH-/H $_2$O $_2$-Responsive UCL Imaging and Oxygen-Elevated Synergetic Therapy, Adv. Mater. 27 (2015) 4155–4161. https://doi.org/10.1002/adma.201405141.

[40] M. Song, T. Liu, C. Shi, X. Zhang, X. Chen, Bioconjugated manganese dioxide nanoparticles enhance chemotherapy response by priming tumor-Associated macrophages toward m1-like phenotype and attenuating tumor hypoxia, ACS Nano. 10 (2016) 633–647. https://doi.org/10.1021/acsnano.5b06779.

[41] C.R. Gordijo, A.Z. Abbasi, M.A. Amini, H.Y. Lip, A. Maeda, P. Cai, P.J. O'Brien, R.S. Dacosta, A.M. Rauth, X.Y. Wu, Design of hybrid MnO2-polymer-lipid nanoparticles with tunable oxygen generation rates and tumor accumulation for cancer treatment, Adv. Funct. Mater. 25 (2015) 1858–1872. https://doi.org/10.1002/adfm.201404511.

[42] T. Lin, X. Zhao, S. Zhao, H. Yu, W. Cao, W. Chen, H. Wei, H. Guo, O2-generating

MnO2nanoparticles for enhanced photodynamic therapy of bladder cancer by ameliorating hypoxia, Theranostics. 8 (2018) 990–1004. https://doi.org/10.7150/thno.22465.

[43] L. Chudal, N.K. Pandey, J. Phan, O. Johnson, X. Li, W. Chen, Investigation of PPIX-Lipo-MnO2 to enhance photodynamic therapy by improving tumor hypoxia, Mater. Sci. Eng. C. 104 (2019). https://doi.org/10.1016/j.msec.2019.109979.

[44] D.A. Bellnier, W.R. Greco, H. Nava, G.M. Loewen, A.R. Oseroff, T.J. Dougherty, Mild skin photosensitivity in cancer patients following injection of Photochlor (2-[1-hexyloxyethyl]-2-devinyl pyropheophorbide-a; HPPH) for photodynamic therapy, Cancer Chemother. Pharmacol. 57 (2006) 40–45. https://doi.org/10.1007/s00280-005-0015-6.

[45] G. Wagnieres, C. Hadjur, P. Grosjean, D. Braichotte, J.F. Savary, P. Monnier, H. Van Den Bergh, Clinical Evaluation of the Cutaneous Phototoxicity of 5,10,15,20-Tetra (m-hydroxyphenyl)chlorin, Photochem. Photobiol. 68 (1998) 382–387. https://doi.org/10.1111/j.1751-1097.1998.tb09696.x.

[46] R.S. Ray, S.F. Mujtaba, A. Dwivedi, N. Yadav, A. Verma, H.N. Kushwaha, S.K. Amar, S. Goel, D. Chopra, Singlet oxygen mediated DNA damage induced phototoxicity by ketoprofen resulting in mitochondrial depolarization and lysosomal destabilization, Toxicology. 314 (2013) 229–237. https://doi.org/10.1016/j.tox.2013.10.002.

[47] H.W. Lim, Mechanisms of phototoxicity in porphyria cutanea tarda and erythropoietic protoporphyria., Immunol. Ser. 46 (1989) 671–85. http://www.ncbi.nlm.nih.gov/pubmed/2488874 (accessed June 29, 2018).

[48] S.-I. Moriwaki, J. Misawa, Y. Yoshinari, I. Yamada, M. Takigawa, Y. Tokura, Analysis of photosensitivity in Japanese cancer-bearing patients receiving photodynamic therapy with

porfimer sodium (PhotofrinTM), Photodermatol. Photoimmunol. Photomed. 17 (2008) 241–243. https://doi.org/10.1111/j.1600-0781.2001.170507.x.

[49] H.C. Wolfsen, T.A. Woodward, M. Raimondo, Photodynamic therapy for dysplastic barrett esophagus and early esophageal adenocarcinoma, Mayo Clin. Proc. 77 (2002) 1176–1181. https://doi.org/10.4065/77.11.1176.

[50] P. Mlkvy, H. Messmann, J. Regula, M. Conio, M. Pauer, C.E. Millson, A.J. MacRobert, S.G. Bown, Photodynamic therapy for gastrointestinal tumors using three photosensitizers-ALA induced PPIX, photofrin® and MTPHC. A pilot study, Neoplasma. 45 (1998) 157–161.

[51] S. Khandpur, R.M. Porter, S.J. Boulton, A. Anstey, Drug-induced photosensitivity: new insights into pathomechanisms and clinical variation through basic and applied science, Br. J. Dermatol. 176 (2017) 902–909. https://doi.org/10.1111/bjd.14935.

[52] A. Boiy, R. Roelandts, J. Van Den Oord, P.A.M. De Witte, Photosensitizing activity of hypericin and hypericin acetate after topical application on normal mouse skin, Br. J. Dermatol. 158 (2008) 360–369. https://doi.org/10.1111/j.1365-2133.2007.08329.x.

[53] G. Cimino, Psoralens as Photoactive Probes of Nucleic Acid Structure and Function: Organic Chemistry, Photochemistry, and Biochemistry, Annu. Rev. Biochem. 54 (1985) 1151–1193. https://doi.org/10.1146/annurev.biochem.54.1.1151.

[54] Q. Zhang, X. Guo, Y. Cheng, L. Chudal, N.K. Pandey, J. Zhang, L. Ma, Q. Xi, G. Yang, Y. Chen, X. Ran, C. Wang, J. Zhao, Y. Li, L. Liu, Z. Yao, W. Chen, Y. Ran, R. Zhang, Use of copper-cysteamine nanoparticles to simultaneously enable radiotherapy, oxidative therapy and immunotherapy for melanoma treatment, Signal Transduct. Target. Ther. 5 (2020) 58. https://doi.org/10.1038/s41392-020-0156-4.

[55] L. Ma, W. Chen, G. Schatte, W. Wang, A.G. Joly, Y. Huang, R. Sammynaiken, M. Hossu, A new Cu-cysteamine complex: Structure and optical properties, J. Mater. Chem. C. 2 (2014) 4239–4246. https://doi.org/10.1039/c4tc00114a.

[56] L. Ma, X. Zou, W. Chen, A new x-ray activated nanoparticle photosensitizer for cancer treatment, J. Biomed. Nanotechnol. 10 (2014) 1501–1508. https://doi.org/10.1166/jbn.2014.1954.

[57] S. Shrestha, J. Wu, B. Sah, A. Vanasse, L.N. Cooper, L. Ma, G. Li, H. Zheng, W. Chen, M.P. Antosh, X-ray induced photodynamic therapy with copper-cysteamine nanoparticles in mice tumors, Proc. Natl. Acad. Sci. U. S. A. 116 (2019) 16823–16828. https://doi.org/10.1073/pnas.1900502116.

[58] B. Sah, J. Wu, A. Vanasse, N.K. Pandey, L. Chudal, Z. Huang, W. Song, H. Yu, L. Ma, W. Chen, M.P. Antosh, Effects of Nanoparticle Size and Radiation Energy on Copper-Cysteamine Nanoparticles for X-ray Induced Photodynamic Therapy, Nanomaterials. 10 (2020) 1087. https://doi.org/10.3390/nano10061087.

[59] N.K. Pandey, L. Chudal, J. Phan, L. Lin, O. Johnson, M. Xing, J.P. Liu, H. Li, X. Huang, Y. Shu, W. Chen, A facile method for the synthesis of copper-cysteamine nanoparticles and study of ROS production for cancer treatment, J. Mater. Chem. B. 7 (2019) 6630–6642. https://doi.org/10.1039/c9tb01566c.

[60] M. Yao, L. Ma, L. Li, J. Zhang, R.X. Lim, W. Chen, Y. Zhang, A new modality for cancer treatment-nanoparticle mediated microwave induced photodynamic therapy, J. Biomed. Nanotechnol. 12 (2016) 1835–1851. https://doi.org/10.1166/jbn.2016.2322.

[61] P. Wang, X. Wang, L. Ma, S. Sahi, L. Li, X. Wang, Q. Wang, Y. Chen, W. Chen, Q. Liu, Nanosonosensitization by Using Copper–Cysteamine Nanoparticles Augmented

Sonodynamic Cancer Treatment, Part. Part. Syst. Charact. 35 (2018) 1700378. https://doi.org/10.1002/ppsc.201700378.

[62] X. Huang, F. Wan, L. Ma, J.B. Phan, R.X. Lim, C. Li, J. Chen, J. Deng, Y. Li, W. Chen, M. He, Investigation of copper-cysteamine nanoparticles as a new photosensitizer for anti-hepatocellular carcinoma, Cancer Biol. Ther. 00 (2019) 0–14. https://doi.org/10.1080/15384047.2018.1564568.

[63] X. Zhen, L. Chudal, N.K. Pandey, J. Phan, X. Ran, E. Amandor, X. Huang, O. Johnson, Y. Ran, W. Chen, M.R. Hamblin, L. Huang, A powerful combination of copper-cysteamine nanoparticles with potassium iodide for bacterial destruction, Mater. Sci. Eng. C. 110 (2020) 110659. https://doi.org/10.1016/j.msec.2020.110659.

[64] L. Chudal, N.K. Pandey, J. Phan, O. Johnson, L. Lin, H. Yu, Y. Shu, Z. Huang, M. Xing, J.P. Liu, M.L. Chen, W. Chen, Copper-Cysteamine Nanoparticles as a Heterogeneous Fenton-Like Catalyst for Highly Selective Cancer Treatment, ACS Appl. Bio Mater. 3 (2020) 1804–1814. https://doi.org/10.1021/acsabm.0c00098.

[65] L. Zhou, H. Wang, Y. Li, Stimuli-responsive nanomedicines for overcoming cancer multidrug resistance, Theranostics. 8 (2018) 1059–1074. https://doi.org/10.7150/thno.22679.

[66] R. Mo, Z. Gu, Tumor microenvironment and intracellular signal-activated nanomaterials for anticancer drug delivery, Mater. Today. 19 (2016) 274–283. https://doi.org/10.1016/j.mattod.2015.11.025.

[67] R.A. Gatenby, R.J. Gillies, Why do cancers have high aerobic glycolysis?, Nat. Rev. Cancer. 4 (2004) 891–899. https://doi.org/10.1038/nrc1478.

[68] M.P. Gamcsik, M.S. Kasibhatla, S.D. Teeter, O.M. Colvin, Glutathione levels in human

tumors, Biomarkers. 17 (2012) 671–691. https://doi.org/10.3109/1354750X.2012.715672.

[69] J.A. Joyce, Therapeutic targeting of the tumor microenvironment, Cancer Cell. 7 (2005) 513–520. https://doi.org/10.1016/j.ccr.2005.05.024.

[70] R. Zhou, S. Zhu, L. Gong, Y. Fu, Z. Gu, Y. Zhao, Recent advances of stimuli-responsive systems based on transition metal dichalcogenides for smart cancer therapy, J. Mater. Chem. B. 7 (2019) 2588–2607. https://doi.org/10.1039/c8tb03240h.

[71] M.E. Davis, Z. Chen, D.M. Shin, Nanoparticle therapeutics: An emerging treatment modality for cancer, Nat. Rev. Drug Discov. 7 (2008) 771–782. https://doi.org/10.1038/nrd2614.

[72] S. Svenson, Clinical translation of nanomedicines, Curr. Opin. Solid State Mater. Sci. 16 (2012) 287–294. https://doi.org/10.1016/j.cossms.2012.10.001.

[73] S. Tran, P.-J. DeGiovanni, B. Piel, P. Rai, Cancer nanomedicine: a review of recent success in drug delivery, Clin. Transl. Med. 6 (2017). https://doi.org/10.1186/s40169-017-0175-0.

[74] X. Xu, W. Ho, X. Zhang, N. Bertrand, O. Farokhzad, Cancer nanomedicine: From targeted delivery to combination therapy, Trends Mol. Med. 21 (2015) 223–232. https://doi.org/10.1016/j.molmed.2015.01.001.

[75] O. Krasnovskaya, A. Naumov, D. Guk, P. Gorelkin, A. Erofeev, E. Beloglazkina, A. Majouga, Copper Coordination Compounds as Biologically Active Agents, Int. J. Mol. Sci. 21 (2020) 3965. https://doi.org/10.3390/ijms21113965.

[76] M. Arredondo, M.T. Núñez, Iron and copper metabolism, Mol. Aspects Med. 26 (2005) 313–327. https://doi.org/10.1016/j.mam.2005.07.010.

[77] R.A. Festa, D.J. Thiele, Copper: An essential metal in biology, 2011.

https://doi.org/10.1016/j.cub.2011.09.040.

[78] H.J.H. Fenton, LXXIII. - Oxidation of tartaric acid in presence of iron, J. Chem. Soc. Trans. 65 (1894) 899–910. https://doi.org/10.1039/CT8946500899.

[79] M.C. Pereira, L.C.A. Oliveira, E. Murad, Iron oxide catalysts: Fenton and Fentonlike reactions – a review, Clay Miner. 47 (2012) 285–302. https://doi.org/10.1180/claymin.2012.047.3.01.

[80] H. Ranji-Burachaloo, P.A. Gurr, D.E. Dunstan, G.G. Qiao, Cancer Treatment through Nanoparticle-Facilitated Fenton Reaction, ACS Nano. 12 (2018) 11819–11837. https://doi.org/10.1021/acsnano.8b07635.

[81] X. Qian, J. Zhang, Z. Gu, Y. Chen, Nanocatalysts-augmented Fenton chemical reaction for nanocatalytic tumor therapy, Biomaterials. 211 (2019) 1–13. https://doi.org/10.1016/j.biomaterials.2019.04.023.

[82] A.D. Bokare, W. Choi, Review of iron-free Fenton-like systems for activating H2O2 in advanced oxidation processes, J. Hazard. Mater. 275 (2014) 121–135. https://doi.org/10.1016/j.jhazmat.2014.04.054.

[83] A.N. Pham, G. Xing, C.J. Miller, T.D. Waite, Fenton-like copper redox chemistry revisited: Hydrogen peroxide and superoxide mediation of copper-catalyzed oxidant production, J. Catal. 301 (2013) 54–64. https://doi.org/10.1016/j.jcat.2013.01.025.

[84] H.C. Sutton, C.C. Winterbourn, On the participation of higher oxidation states of iron and copper in fenton reactions, 1989. https://doi.org/10.1016/0891-5849(89)90160-3.

[85] B. Ma, S. Wang, F. Liu, S. Zhang, J. Duan, Z. Li, Y. Kong, Y. Sang, H. Liu, W. Bu, L. Li, Self-Assembled Copper-Amino Acid Nanoparticles for in Situ Glutathione “aND” H 2 O 2 Sequentially Triggered Chemodynamic Therapy, J. Am. Chem. Soc. 141 (2019) 849–

857. https://doi.org/10.1021/jacs.8b08714.

[86] L. Sen Lin, T. Huang, J. Song, X.Y. Ou, Z. Wang, H. Deng, R. Tian, Y. Liu, J.F. Wang, Y. Liu, G. Yu, Z. Zhou, S. Wang, G. Niu, H.H. Yang, X. Chen, Synthesis of Copper Peroxide Nanodots for H2O2 Self-Supplying Chemodynamic Therapy, J. Am. Chem. Soc. 141 (2019) 9937–9945. https://doi.org/10.1021/jacs.9b03457.

[87] R. Hu, Y. Fang, M. Huo, H. Yao, C. Wang, Y. Chen, R. Wu, Ultrasmall Cu 2-x S nanodots as photothermal-enhanced Fenton nanocatalysts for synergistic tumor therapy at NIR-II biowindow, Biomaterials. 206 (2019) 101–114. https://doi.org/10.1016/j.biomaterials.2019.03.014.

[88] L. Ma, W. Chen, G. Schatte, W. Wang, A.G. Joly, Y. Huang, R. Sammynaiken, M. Hossu, A new Cu-cysteamine complex: Structure and optical properties, J. Mater. Chem. C. 2 (2014) 4239–4246. https://doi.org/10.1039/c4tc00114a.

[89] W. Zhu, Z. Dong, T. Fu, J. Liu, Q. Chen, Y. Li, R. Zhu, L. Xu, Z. Liu, Modulation of Hypoxia in Solid Tumor Microenvironment with MnO2Nanoparticles to Enhance Photodynamic Therapy, Adv. Funct. Mater. 26 (2016) 5490–5498. https://doi.org/10.1002/adfm.201600676.

[90] Q. Chen, L. Feng, J. Liu, W. Zhu, Z. Dong, Y. Wu, Z. Liu, Intelligent Albumin–MnO2Nanoparticles as pH-/H2O2-Responsive Dissociable Nanocarriers to Modulate Tumor Hypoxia for Effective Combination Therapy, Adv. Mater. 28 (2016) 7129–7136. https://doi.org/10.1002/adma.201601902.

[91] H. Fan, G. Yan, Z. Zhao, X. Hu, W. Zhang, H. Liu, X. Fu, T. Fu, X.-B.B. Zhang, W. Tan, A Smart Photosensitizer-Manganese Dioxide Nanosystem for Enhanced Photodynamic Therapy by Reducing Glutathione Levels in Cancer Cells., Angew. Chem. Int. Ed. Engl.

55 (2016) 5477–5482. https://doi.org/10.1002/anie.201510748.

[92] U. Sunar, D.J. Rohrbach, J. Morgan, N. Zeitouni, B.W. Henderson, Quantification of PpIX concentration in basal cell carcinoma and squamous cell carcinoma models using spatial frequency domain imaging., Biomed. Opt. Express. 4 (2013) 531–537. https://doi.org/10.1364/BOE.4.000531.

[93] L. Monsù Scolaro, M. Castriciano, A. Romeo, S. Patanè, E. Cefalì, M. Allegrini, Aggregation behavior of protoporphyrin IX in aqueous solutions: Clear evidence of vesicle formation, J. Phys. Chem. B. 106 (2002) 2453–2459. https://doi.org/10.1021/jp013155h.

[94] B. Bui, L. Liu, W. Chen, Latex carrier for improving protoporphyrin IX for photodynamic therapy, Photodiagnosis Photodyn. Ther. 14 (2016) 159–165. https://doi.org/10.1016/j.pdpdt.2016.03.007.

[95] C.S. Chen, J. Yao, R.A. Durst, Liposome encapsulation of fluorescent nanoparticles: Quantum dots and silica nanoparticles, J. Nanoparticle Res. 8 (2006) 1033–1038. https://doi.org/10.1007/s11051-006-9142-1.

[96] K.A. Carter, S. Shao, M.I. Hoopes, D. Luo, B. Ahsan, V.M. Grigoryants, W. Song, H. Huang, G. Zhang, R.K. Pandey, J. Geng, B.A. Pfeifer, C.P. Scholes, J. Ortega, M. Karttunen, J.F. Lovell, Porphyrin-phospholipid liposomes permeabilized by near-infrared light, Nat. Commun. 5 (2014). https://doi.org/10.1038/ncomms4546.

[97] M. Przybylo, D. Glogocka, J.W. Dobrucki, K. Fraczkowska, H. Podbielska, M. Kopaczynska, T. Borowik, M. Langner, The cellular internalization of liposome encapsulated protoporphyrin IX by HeLa cells, Eur. J. Pharm. Sci. 85 (2016) 39–46. https://doi.org/10.1016/J.EJPS.2016.01.028.

[98] C. Flors, M.J. Fryer, J. Waring, B. Reeder, U. Bechtold, P.M. Mullineaux, S. Nonell, M.T. Wilson, N.R. Baker, Imaging the production of singlet oxygen in vivo using a new fluorescent sensor, Singlet Oxygen Sensor Green®, J. Exp. Bot. 57 (2006) 1725–1734. https://doi.org/10.1093/jxb/erj181.

[99] S. Vemuri, C.. T. Rhodes, Preparation and characterization of liposomes as therapeutic delivery systems: a review, Pharm. Acta Helv. 70 (1995) 95–111. https://doi.org/10.1016/0031-6865(95)00010-7.

[100] T.M. qqAllen, P.R. Cullis, T.M. Allen, P.R. Cullis, T.M. qqAllen, P.R. Cullis, Liposomal drug delivery systems: From concept to clinical applications ☆, Adv. Drug Deliv. Rev. 65 (2013) 36–48. https://doi.org/10.1016/j.addr.2012.09.037.

[101] R.R. Sawant, V.P. Torchilin, Liposomes as'smart' pharmaceutical nanocarriers, Soft Matter. 6 (2010) 4026–4044. https://doi.org/10.1039/b923535n.

[102] P. Pradhan, J. Giri, F. Rieken, C. Koch, O. Mykhaylyk, M. D??blinger, R. Banerjee, D. Bahadur, C. Plank, Targeted temperature sensitive magnetic liposomes for thermo-chemotherapy, J. Control. Release. 142 (2010) 108–121. https://doi.org/10.1016/j.jconrel.2009.10.002.

[103] Y. Jin, X. Liang, Y. An, Z. Dai, Microwave-Triggered Smart Drug Release from Liposomes Co-encapsulating Doxorubicin and Salt for Local Combined Hyperthermia and Chemotherapy of Cancer, Bioconjug. Chem. 27 (2016) 2931–2942. https://doi.org/10.1021/acs.bioconjchem.6b00603.

[104] S. Bibi, E. Lattmann, A.R. Mohammed, Y. Perrie, Trigger release liposome systems: local and remote controlled delivery?, J. Microencapsul. 29 (2012) 262–276. https://doi.org/10.3109/02652048.2011.646330.

[105] J. Pan, Y. Wang, H. Pan, C. Zhang, X.X. Zhang, Y.Y. Fu, X.X. Zhang, C. Yu, S.K. Sun, X.P. Yan, Mimicking Drug–Substrate Interaction: A Smart Bioinspired Technology for the Fabrication of Theranostic Nanoprobes, Adv. Funct. Mater. 27 (2017) 1603440. https://doi.org/10.1002/adfm.201603440.

[106] D. Wu, P. Yotnda, Induction and Testing of Hypoxia in Cell Culture, J. Vis. Exp. 54 (2011). https://doi.org/10.3791/2899.

[107] M. Sachar, K.E. Anderson, X. Ma, Protoporphyrin IX: the Good, the Bad, and the Ugly, J. Pharmacol. Exp. Ther. . 356 (2016) 267–275. https://doi.org/10.1124/jpet.115.228130.

[108] F. Szoka, D. Papahadjopoulos, Comparative Properties and Methods of Preparation of Lipid Vesicles (Liposomes), Annu. Rev. Biophys. Bioeng. 9 (1980) 467–508. https://doi.org/10.1146/annurev.bb.09.060180.002343.

[109] W. Zhai, C. Wang, P. Yu, Y. Wang, L. Mao, Single-layer MnO2 nanosheets suppressed fluorescence of 7-hydroxycoumarin: Mechanistic study and application for sensitive sensing of ascorbic acid in vivo, Anal. Chem. 86 (2014) 12206–12213. https://doi.org/10.1021/ac503215z.

[110] D.M. Charbonneau, H.A. Tajmir-Riahi, Study on the interaction of cationic lipids with bovine serum albumin, J Phys Chem B. 114 (2010) 1148–1155. https://doi.org/10.1021/jp910077h.

[111] Y. Yokouchi, T. Tsunoda, T. Imura, H. Yamauchi, S. Yokoyama, H. Sakai, M. Abe, Effect of adsorption of bovine serum albumin on liposomal membrane characteristics, Colloids Surfaces B Biointerfaces. 20 (2001) 95–103. https://doi.org/10.1016/S0927-7765(00)00176-4.

[112] Y. Yuan, G. Hilliard, T. Ferguson, D.E. Millhorn, Cobalt inhibits the interaction between

hypoxia-inducible factor-$α$ and von Hippel-Lindau protein by direct binding to hypoxia-inducible factor-$α$, J. Biol. Chem. 278 (2003) 15911–15916. https://doi.org/10.1074/jbc.M300463200.

[113] M.S. Al Okail, Cobalt chloride, a chemical inducer of hypoxia-inducible factor-1ÃŽÂ± in U251 human glioblastoma cell line, JSCS. 14 (2008) 197–201. https://doi.org/10.1016/j.jscs.2010.02.005.

[114] Z.J. Dai, J. Gao, X. Bin Ma, K. Yan, X.X. Liu, H.F. Kang, Z.Z. Ji, H.T. Guan, X.J. Wang, Up-regulation of hypoxia inducible factor-1α by cobalt chloride correlates with proliferation and apoptosis in PC-2 cells, J. Exp. Clin. Cancer Res. 31 (2012) 28. https://doi.org/10.1186/1756-9966-31-28.

[115] S.R. McKeown, Defining normoxia, physoxia and hypoxia in tumours - Implications for treatment response, Br. J. Radiol. 87 (2014) 20130676. https://doi.org/10.1259/bjr.20130676.

[116] T.L. Whiteside, The tumor microenvironment and its role in promoting tumor growth., Oncogene. 27 (2008) 5904–5912. https://doi.org/10.1038/onc.2008.271.

[117] D.F. Quail, J.A. Joyce, Microenvironmental regulation of tumor progression and metastasis., Nat. Med. 19 (2013) 1423–37. https://doi.org/10.1038/nm.3394.

[118] S. Rockwell, I.T. Dobrucki, E.Y. Kim, S.T. Marrison, V.T. Vu, Hypoxia and radiation therapy: past history, ongoing research, and future promise., Curr. Mol. Med. 9 (2009) 442–58. http://www.ncbi.nlm.nih.gov/pubmed/19519402 (accessed March 24, 2019).

[119] M. Höckel, K. Schlenger, B. Aral, M. Mitze, U. Schäffer, P. Vaupel, Association between tumor hypoxia and malignant progression in advanced cancer of the uterine cervix, Cancer Res. 56 (1996) 4509–4515. https://doi.org/10.1056/NEJM199604183341606.

[120] Z. Huang, A review of progress in clinical photodynamic therapy, Technol. Cancer Res. Treat. 4 (2005) 283–293. https://doi.org/10.1177/153303460500400308.

[121] S. Choudhary, K. Nouri, M.L. Elsaie, Photodynamic therapy in dermatology: a review, Lasers Med. Sci. 24 (2009) 971–980. https://doi.org/10.1007/s10103-009-0716-x.

[122] C. Link, Current evidence and applications of photodynamic therapy in The Harvard community has made this article openly available . Current evidence and applications of photodynamic therapy in dermatology, Clin. Cosmet. Investig. Dermatol. (2017) 7–145. https://doi.org/10.2147/CCID.S35334.

[123] W. Chen, J. Zhang, Using nanoparticles to enable simultaneous radiation and photodynamic therapies for cancer treatment, J. Nanosci. Nanotechnol. 6 (2006) 1159–1166. https://doi.org/10.1166/jnn.2006.327.

[124] X. Chu, K. Li, H. Guo, H. Zheng, S. Shuda, X. Wang, J. Zhang, W. Chen, Y. Zhang, Exploration of Graphitic-C_3N_4 Quantum Dots for Microwave-Induced Photodynamic Therapy, ACS Biomater. Sci. Eng. 3 (2017) 1836–1844. https://doi.org/10.1021/acsbiomaterials.7b00110.

[125] F. Borgia, R. Giuffrida, E. Caradonna, M. Vaccaro, F. Guarneri, S.P. Cannavò, Early and late onset side effects of photodynamic therapy, Biomedicines. 6 (2018). https://doi.org/10.3390/biomedicines6010012.

[126] S. Mallidi, S. Anbil, S. Lee, D. Manstein, S. Elrington, G. Kositratna, D. Schoenfeld, B. Pogue, S.J. Davis, T. Hasan, Photosensitizer fluorescence and singlet oxygen luminescence as dosimetric predictors of topical 5-aminolevulinic acid photodynamic therapy induced clinical erythema., J. Biomed. Opt. 19 (2014) 28001. https://doi.org/10.1117/1.JBO.19.2.028001.

[127] R.R. Allison, G.H. Downie, R. Cuenca, X.H. Hu, C.J. Childs, C.H. Sibata, Photosensitizers in clinical PDT, Photodiagnosis Photodyn. Ther. 1 (2004) 27–42. https://doi.org/10.1016/S1572-1000(04)00007-9.

[128] S.-I. Moriwaki, J. Misawa, Y. Yoshinari, I. Yamada, M. Takigawa, Y. Tokura, Analysis of photosensitivity in Japanese cancer-bearing patients receiving photodynamic therapy with porfimer sodium (PhotofrinTM), Photodermatol. Photoimmunol. Photomed. 17 (2001) 241–243. https://doi.org/10.1034/j.1600-0781.2001.170507.x.

[129] photodynamic therapy of cancer, 9 (2014) 2339–2351.

[130] N. Bednarz, J. Zawacka-Pankau, A. Kowalska, Protoporphyrin IX induces apoptosis in HeLa cells prior to photodynamic treatment, 2007. http://www.if-pan.krakow.pl/pjp/pdf/2007/4_474.pdf (accessed March 8, 2019).

[131] S. Ibbotson, R. Stones, J. Bowling, S. Campbell, S. Kownacki, M. Sivaramakrishnan, R. Valentine, C.A. Morton, M. Sivaramakrishnan, S. Campbell, S. Ibbotson, J. Bowling, S. Kownacki, C.A. Morton, R. Stones, A consensus on the use of daylight photodynamic therapy in the UK, J. Dermatolog. Treat. 28 (2016) 360–367. https://doi.org/10.1080/09546634.2016.1240863.

[132] S. Goldstein, D. Meyerstein, G. Czapski, The Fenton reagents, Free Radic. Biol. Med. 15 (1993) 435–445. https://doi.org/10.1016/0891-5849(93)90043-T.

[133] K.T. Lee, Y.J. Lu, S.C. Chiu, W.C. Chang, E.Y. Chuang, S.Y. Lu, Heterogeneous Fenton Reaction Enabled Selective Colon Cancerous Cell Treatment, Sci. Rep. 8 (2018). https://doi.org/10.1038/s41598-018-34499-0.

[134] Q. An, C. Sun, D. Li, K. Xu, J. Guo, C. Wang, Peroxidase-like activity of Fe3O4@carbon nanoparticles enhances ascorbic acid-induced oxidative stress and selective damage to PC-

3 prostate cancer cells, ACS Appl. Mater. Interfaces. 5 (2013) 13248–13257. https://doi.org/10.1021/am4042367.

[135] H. Ranji-Burachaloo, F. Karimi, K. Xie, Q. Fu, P.A. Gurr, D.E. Dunstan, G.G. Qiao, MOF-mediated destruction of cancer using the cell's own hydrogen peroxide, ACS Appl. Mater. Interfaces. 9 (2017) 33599–33608. https://doi.org/10.1021/acsami.7b07981.

[136] C. Zhang, W. Bu, D. Ni, S. Zhang, Q. Li, Z. Yao, J. Zhang, H. Yao, Z. Wang, J. Shi, Synthesis of Iron Nanometallic Glasses and Their Application in Cancer Therapy by a Localized Fenton Reaction, Angew. Chemie Int. Ed. 55 (2016) 2101–2106. https://doi.org/10.1002/anie.201510031.

[137] J. Fu, Y. Shao, L. Wang, Y. Zhu, Lysosome-controlled efficient ROS overproduction against cancer cells with a high pH-responsive catalytic nanosystem, Nanoscale. 7 (2015) 7275–7283. https://doi.org/10.1039/c5nr00706b.

[138] Z. Chen, J.J. Yin, Y.T. Zhou, Y. Zhang, L. Song, M. Song, S. Hu, N. Gu, Dual enzyme-like activities of iron oxide nanoparticles and their implication for diminishing cytotoxicity, ACS Nano. 6 (2012) 4001–4012. https://doi.org/10.1021/nn300291r.

[139] S. Dinda, P.K. Das, Metal Ion (Fe^{2+} and Co^{2+}) Induced Morphological Transformation of Self-Aggregates of Cholesterol-Tethered Bipyridine Amphiphiles: Selective Cancer Cell Killing by Pro-Drug Activation, ACS Appl. Bio Mater. 2 (2019) 3737–3747. https://doi.org/10.1021/acsabm.9b00340.

[140] L. Ruan, M. Wang, M. Zhou, H. Lu, J. Zhang, J. Gao, J. Chen, Y. Hu, Doxorubicin–Metal Coordinated Micellar Nanoparticles for Intracellular Codelivery and Chemo/Chemodynamic Therapy in Vitro, ACS Appl. Bio Mater. 2 (2019) 4703–4707. https://doi.org/10.1021/acsabm.9b00879.

[141] H. Lee, H.J. Lee, D.L. Sedlak, C. Lee, PH-Dependent reactivity of oxidants formed by iron and copper-catalyzed decomposition of hydrogen peroxide, Chemosphere. 92 (2013) 652–658. https://doi.org/10.1016/j.chemosphere.2013.01.073.

[142] T.M. Florence, The production of hydroxyl radical from hydrogen peroxide, J. Inorg. Biochem. 22 (1984) 221–230. https://doi.org/10.1016/0162-0134(84)85007-2.

[143] S.K. Maji, A.K. Mandal, K.T. Nguyen, P. Borah, Y. Zhao, Cancer cell detection and therapeutics using peroxidase-active nanohybrid of gold nanoparticle-loaded mesoporous silica-coated graphene, ACS Appl. Mater. Interfaces. 7 (2015) 9807–9816. https://doi.org/10.1021/acsami.5b01758.

[144] H. Ranji-Burachaloo, Q. Fu, P.A. Gurr, D.E. Dunstan, G.G. Qiao, Improved Fenton Therapy Using Cancer Cell Hydrogen Peroxide, Aust. J. Chem. 71 (2018) 826. https://doi.org/10.1071/CH18281.

[145] T. Soltani, B.K. Lee, Enhanced formation of sulfate radicals by metal-doped BiFeO3 under visible light for improving photo-Fenton catalytic degradation of 2-chlorophenol, Chem. Eng. J. 313 (2017) 1258–1268. https://doi.org/10.1016/j.cej.2016.11.016.

[146] P.C. Nagajyothi, P. Muthuraman, T.V.M. Sreekanth, D.H. Kim, J. Shim, Green synthesis: In-vitro anticancer activity of copper oxide nanoparticles against human cervical carcinoma cells, Arab. J. Chem. 10 (2017) 215–225. https://doi.org/10.1016/j.arabjc.2016.01.011.

[147] L. Sen Lin, T. Huang, J. Song, X.Y. Ou, Z. Wang, H. Deng, R. Tian, Y. Liu, J.F. Wang, Y. Liu, G. Yu, Z. Zhou, S. Wang, G. Niu, H.H. Yang, X. Chen, Synthesis of Copper Peroxide Nanodots for H2O2 Self-Supplying Chemodynamic Therapy, J. Am. Chem. Soc. (2019). https://doi.org/10.1021/jacs.9b03457.

[148] S. Cao, J. Fan, W. Sun, F. Li, K. Li, X. Tai, X. Peng, A novel Mn-Cu bimetallic complex for enhanced chemodynamic therapy with simultaneous glutathione depletion, Chem. Commun. 55 (2019) 12956–12959. https://doi.org/10.1039/c9cc06040e.

[149] Z. Liu, L. Xiong, G. Ouyang, L. Ma, S. Sahi, K. Wang, L. Lin, H. Huang, X. Miao, W. Chen, Y. Wen, Investigation of Copper Cysteamine Nanoparticles as a New Type of Radiosensitiers for Colorectal Carcinoma Treatment, Sci. Rep. 7 (2017) 1–11. https://doi.org/10.1038/s41598-017-09375-y.

[150] X. Zhen, L. Chudal, N.K. Pandey, J. Phan, X. Ran, E. Amandor, X. Huang, O. Johnson, Y. Ran, W. Chen, M.R. Hamblin, L. Huang, A powerful combination of copper-cysteamine nanoparticles with potassium iodide for bacterial destruction, Mater. Sci. Eng. C. (2020) 110659. https://doi.org/10.1016/j.msec.2020.110659.

[151] G.M. Makrigiorgos, J. Baranowska-Kortylewicz, E. Bump, S.K. Sahu, R.M. Berman, A.I. Kassis, A Method for Detection of Hydroxyl Radicals in the Vicinity of Biomolecules Using Radiation-induced Fluorescence of Coumarin, Int. J. Radiat. Biol. 63 (1993) 445–458. https://doi.org/10.1080/09553009314550601.

[152] G. Louit, S. Foley, J. Cabillic, H. Coffigny, F. Taran, A. Valleix, J.P. Renault, S. Pin, The reaction of coumarin with the OH radical revisited: Hydroxylation product analysis determined by fluorescence and chromatography, Radiat. Phys. Chem. 72 (2005) 119–124. https://doi.org/10.1016/j.radphyschem.2004.09.007.

[153] T. Wen, F. Qu, N.B. Li, H.Q. Luo, A facile, sensitive, and rapid spectrophotometric method for copper(II) ion detection in aqueous media using polyethyleneimine, Arab. J. Chem. 10 (2017) S1680–S1685. https://doi.org/10.1016/j.arabjc.2013.06.013.

[154] H. Akafzade, S.C. Sharma, N. Hozhabri, W. Chen, L. Ma, Raman spectroscopy analysis

of new copper-cysteamine photosensitizer, J. Raman Spectrosc. 50 (2019) 522–527. https://doi.org/10.1002/jrs.5541.

[155] P.L. Moore, I.C. MacCoubrey, R.P. Haugland, A rapid,pH insensitive, two color fluorescence viability (cytotoxicity) assay, J. Cell. Biol. 111 (1990) 58a. https://ci.nii.ac.jp/naid/10008199972/ (accessed January 6, 2019).

[156] R. Gatti, S. Belletti, G. Orlandini, O. Bussolati, V. Dall'Asta, G.C. Gazzola, Comparison of annexin V and calcein-AM as early vital markers of apoptosis in adherent cells by confocal laser microscopy, 1998. https://doi.org/10.1177/002215549804600804.

[157] O. Bussolati, S. Belletti, J. Uggeri, R. Gatti, G. Orlandini, V. Dall'asta, G.C. Gazzola, Characterization of apoptotic phenomena induced by treatment with L-asparaginase in NIH3T3 cells, Exp. Cell Res. 220 (1995) 283–291. https://doi.org/10.1006/excr.1995.1317.

[158] A.H. Wyllie, J.F. Kerr, A.R. Currie, Cell death: the significance of apoptosis., Int. Rev. Cytol. 68 (1980) 251–306. http://www.ncbi.nlm.nih.gov/pubmed/7014501 (accessed March 5, 2019).

[159] K.J.W.A.C. AR, Apoptosis : a Basic Biological Phenomenon With Wide-, 1972. https://doi.org/10.1111/j.1365-2796.2005.01570.x.

[160] A.H. Wyllie, R.G. Morris, A.L. Smith, D. Dunlop, Chromatin cleavage in apoptosis: Association with condensed chromatin morphology and dependence on macromolecular synthesis, J. Pathol. 142 (1984) 67–77. https://doi.org/10.1002/path.1711420112.

[161] C.A. Schneider, W.S. Rasband, K.W. Eliceiri, NIH Image to ImageJ: 25 years of Image Analysis HHS Public Access, 2012. https://www.ncbi.nlm.nih.gov/pmc/articles/PMC5554542/pdf/nihms876304.pdf (accessed

March 2, 2019).

[162] Z. Tang, Y. Liu, M. He, W. Bu, Chemodynamic Therapy: Tumour Microenvironment-Mediated Fenton and Fenton-like Reactions, Angew. Chemie - Int. Ed. 58 (2019) 946–956. https://doi.org/10.1002/anie.201805664.

[163] V. Girish, A. Vijayalakshmi, Affordable image analysis using NIH Image/ImageJ., Indian J. Cancer. 41 (2004) 47. http://www.ncbi.nlm.nih.gov/pubmed/15105580 (accessed March 1, 2019).

[164] T.J. Collins, ImageJ for microscopy., Biotechniques. 43 (2007) S25–S30. https://doi.org/10.2144/000112505.